

Evaluating the Impact of Particulate Matter on the Vocal Fold Mucosa via a Novel Vocal Fold On-a-Chip

Patrick Thomas Coburn

Doctor of Philosophy

School of Communication Sciences and Disorders

McGill University

Montreal, Quebec, Canada

October 2023

A thesis submitted to McGill University in partial fulfilment
of the requirements for the degree of Doctor of Philosophy

Supervisory Committee:

Professor Nicole Y.K. Li-Jessen (Primary Supervisor)

Professor Susan Thibeault

Professor Xinyu Liu

Professor Linda Polka

© Patrick Thomas Coburn 2023

Acknowledgements

I must first express my gratitude to my principal supervisor, Professor Nicole Li-Jessen, whose support and guidance made this work possible. You have always challenged me to take my work above and beyond whilst also providing the tools and means to succeed. The dedication shown to your craft is truly remarkable and matched only by your commitment to developing the skillsets and professionalism of each member of your lab. You provided me with the ideal environment to thrive and grow as both a person and a scientist. It has been a privilege to work in your lab.

My sincere thanks to my committee members, Professors Susan Thibeault, Xinyu Liu, and Linda Polka. Your advice and input in conceptualizing, guiding, and refining this thesis were fundamental. Each discussion we had generated fresh ideas and solutions to overcome obstacles encountered. A special thanks also to Dr. Vlasta Lungova for her excellent guidance, advice, and training related to the cell culture work in this project including, most notably, iPSC research.

To past and present members of the Voice and Upper Airway Research Laboratory, it has been a pleasure to work alongside you and receive your perspectives on my research. A special thanks to my fellow wet lab personnel, Christian Moya-Garcia, Mika Brown, and Hideaki Okuyama, with whom I shared many illuminating discussions about experimental work.

My thanks also to Dr. Nicolas Audet, Head of the Imaging and Molecular Biology Platform at McGill University for the outstanding training and guidance related to qPCR. Further thanks to Johanne Ouellette, Chief Technician at the Facility for Electron Microscopy Research at McGill University for expertly performed sample preparation for transmission electron microscopy.

Most important of all, I want to thank my family for their constant love and support, which has underpinned everything that I have been able to achieve. To my parents, Julie and Tom, thank you for your endless patience and instilling me with such fierce spirit. Your belief and faith in me will always be a source of endless comfort. To my grandmas, Norah and Margaret, I look forward to reuniting with you and sharing a long overdue cup of tea.

My thanks to Cathy and Joe, whom welcomed me into their family with open arms. Words cannot express my gratitude for everything you have done for me down the years and all the

valuable advice you provided. To Ollie also, for the many delicious meals shared together and to the many more we hope to have.

Finally, to Lauren, you absolute legend. I will forever be grateful for the tremendous love, patience, and support you have shown me throughout the years. My excitement at finishing this journey pales in significance compared to my feelings about taking the next step in our lives together.

Thesis Organization

This thesis is written and presented in a manuscript-based style divided into the following chapters.

Chapter 1 provides a high-level introduction to the thesis and details the motivations, rationale, and philosophy behind the study design, including a summary of specific research aims.

Chapter 2 is a comprehensive review of literature related to upper airway organ-on-a-chip culture models including an examination of their emerging applications. The importance of design considerations and strategies are summarized. Future directions for expanding the applications of upper airway organ-on-a-chip models are proposed.

Chapter 3 is an original research manuscript for submission. The goal was to develop a novel VF mucosa organ-on-a-chip (VF-OOAC) via a systematic evaluation of small volume effects, 3D tissue architecture, perfusion, and fluidic shear in the microengineering of VF mucosa constructs.

Chapter 4 is an original research manuscript for submission. The goal was to investigate the VF-OOAC's capacity to evaluate environmental irritant toxicity. As a case study, the VF-OOAC was challenged with acute exposure to coarse particulate matter. Furthermore, induced pluripotent stem cell technology was integrated into the VF-OOAC to improve physiological relevance of the VF epithelium.

Chapter 5 provides a contextual discussion of the thesis, focusing on potential improvements and future opportunities related to the *in vitro* model presented.

Chapter 6 comprises concluding remarks for research findings of this thesis and recommendations for future work.

Contents

Acknowledgements	ii
Thesis Organization	iv
List of Figures	x
List of Tables	xiii
Acronym Glossary	xiv
Contribution to Original Knowledge	xv
Contribution of Authors	xvi
Abstract	xviii
Résumé.....	xx
Chapter 1. Introduction	1
Thesis Motivation.....	1
Thesis Rationale	2
Research Objectives & Hypotheses	3
Chapter 2. Organ-on-a-Chip: Time to Explore the Upper Airway?	4
Abstract	4
Introduction	4
Organ-on-a-Chip Technology	8
Utilizing Design Parameters of Organ-on-a-Chip Models.....	9
Microfluidic Device Parameters	10
Replicating Upper Airway Tissue Architecture	15
Modelling the Dynamic <i>In vivo</i> Microenvironment	17
Prospects & Future Outlook	20
Enhancing Culture Microenvironments.....	22

Real-time Monitoring & Paired Computational Modelling	23
Clinical Translation & Therapeutic Research	24
Conclusions	26
Author Contributions.....	26
Conflicts of Interest.....	26
Acknowledgements	27
References	27
Supporting Information.....	35
Preface to Chapter 3: Replicating Vocal Fold Mucosa Anatomy <i>In Vitro</i>	36
Human Vocal Fold Mucosa.....	36
Vocal Fold Epithelium.....	37
Lamina Propria	38
<i>In Vitro</i> Vocal Fold Mucosa Models.....	38
Organ-on-a-Chip Platforms.....	39
Chapter 3. Investigating the Impact of Dimensionality, Physiological Scaling, Perfusion, and Fluidic Shear for Microengineering Vocal Fold Mucosae in Microfluidic Culturing Platforms .	40
Abstract	40
Introduction	41
Materials & Methods.....	44
Cell Culture Maintenance	46
Transwell Experimental Set-up	47
VF-OOAC Experimental Culture.....	49
Immunocytochemistry	52
Immunohistochemistry	54
Transmission Electron Microscopy	54

Gene Expression	55
Statistical Analysis	56
Results & Discussion	56
Microscale culture supported functional gene upregulation.....	56
Increased dimensionality improved tissue functionality	60
Perfusion stimulated basal epithelium activity	62
Fluidic shear induced mechanosensitive gene upregulation.....	65
Limitations & Future Prospects.....	68
Conclusion.....	69
Author Contributions.....	69
Conflicts of interest	69
Acknowledgements	69
References	69
Supporting Information.....	77
RNA Quantity & Quality	77
Impact of Fluidic Shear in Perfused 2D VF-OOAC Culture	78
Preface to Chapter 4: Air Pollution Threat to the Vocal Fold Mucosa.....	80
Air Pollution.....	80
Particulate Matter	80
Association between Voice Disorders & Coarse Particulate Matter.....	81
Chapter 4. Evaluating the Resilience of the Vocal Fold Mucosa to Acute Exposure to Coarse Particulate Matter Pollutants – An Organ-on-a-Chip Analysis	83
Abstract	83
Introduction	84
Materials & Methods.....	87

Cell Culture Maintenance	87
VF Basal Progenitor Cell Differentiation	88
Particulate Matter Preparation	89
VF-OOAC Culture	89
PM ₁₀ Exposure Experiments	91
Immunocytochemistry Characterization.....	93
Immunohistochemistry	94
Gene Expression Characterization.....	94
Enzyme-linked Immunosorbent Assays	95
Statistical Analysis	96
Results & Discussion	96
PM ₁₀ Induces Cytotoxicity in VF Cell Monocultures	96
VF-OOAC _{ILEC} Demonstrates High Resilience to PM ₁₀	97
VF-OOAC _{iPSC} Increased Tissue Functionality versus Transwell Controls	101
Minimal impact of epithelial cell source on high resilience displayed by VF-OOAC to PM ₁₀ challenge	104
Limitations, Future Prospects, & Conclusion	106
Author Contributions.....	107
Conflicts of interest	107
Acknowledgements	108
References	108
Supporting Information.....	115
PM ₁₀ Composition	115
Culture Vessel Parameters.....	116
Chapter 5. Discussion	118

Microfluidic Chip Configuration	118
Particulate Matter Toxicity & Exposure	119
iPSC Applications for Health & Disease Modelling.....	120
Future Directions	121
Chapter 6. Conclusions	123
References	125

List of Figures

Figure 2.1. Comparison of 2D and 3D cell culture.....	6
Figure 2.2. Upper airway organ-on-a-chip models provide a range of parameters that can be manipulated to improve the mimicry of the native tissue microenvironment. The influence of each specific parameter may vary across different tissues and hence requires optimizing for each model.....	10
Figure 2.3. Microfluidic device configurations applicable to upper airway OOAC models. (A) A single microchannel is separated from a compartment by a porous membrane. The compartment permits 3D co-culture of epithelial and stromal cells whilst the microchannel can be used for endothelial cell culture under perfused conditions. (B) Double-channel configurations can be used for barrier studies exploring epithelial-endothelial or epithelial-stromal interfaces. Each microchannel can be used for dynamic fluid flow, including perfusion for endothelial cells and airflow for epithelial cells. (C) Multi-compartment configurations allow the 3D culture of stromal cells but also enable dynamic flow through neighbouring microchannels, permitting dual dynamic flow found in double-channel models to culture epithelial and endothelial cells in physiologically relevant conditions.....	12
Figure 2.4. Areas of significant interest for upper airway research to exploit to fully harness the potential of OOAC culture models.....	21
Figure 3.1. Human VF anatomy and cellular composition. (A) Anatomical location of the larynx. (B) Position of true VFs within the larynx. (C) Layered structure of true VFs in coronal section. (D) Arrangement of epithelial cells and fibroblasts within the VF mucosa.....	37
Figure 4.1. Study design overview. The influence of multiple culture parameters on structural and functional development of VF mucosae was systematically evaluated. (A) The effect on tissue development of cultivating VF mucosae in microscale systems was assessed in 2D and 3D setups. (B) Prospective static VF-OOAC culture systems were compared to determine how dimensionality influences VF mucosa growth. (C) Perfusion was integrated in the 3D VF-OOAC to determine tissue culture benefits. (D) By incorporating fluidic shear into the 3D VF-OOAC setup, the effect of mechanical stimulation on tissue development was examined.....	45
Figure 4.2. Perfusion-based culture system. (A) The setup enabled continuous perfusion of 3D VF-OOAC whilst maintaining sterility within a biological safety cabinet. (B) During operation, the peristaltic pump pulls media from media reservoirs, through the microchannel of the chips before dispensing waste media into effluent collectors. (C) Cultures are stored in a humidified, 37 °C, 5% CO ₂ incubator. (D) Comparison of vessels applied for (I) transwell, (II) 2D VF-OOAC, (III) 3D VF-OOAC culture. Centimetre ruler for scale.....	52
Figure 4.3. The effect of physiological scaling on VF mucosa culture in static VF-OOAC and transwell setups. (A) H&E [a-d], K5, [e-h], K14 [i-l], E-Cad [m-p], and LAMA5 [q-t] evaluated morphological features. Samples were counterstained with DAPI (blue) to indicate cell nuclei. H&E magnification 40×, scale bar = 15 µm. Immunostaining magnification 20×, scale bar = 30 µm. (B) Relative gene expression in 2D transwell, static 2D VF-OOAC, 3D transwell, static 3D VF-OOAC setups. All data presented as the fold change relative to 2D transwell. Significant	

differences for 2D transwell vs 2D VF-OOAC, and 3D transwell vs 3D VF-OOAC are denoted by * and # respectively.57

Figure 4.4. The impact of dimensionality on the culture of VF mucosae in VF-OOAC models. (A) Heatmap of relative gene expression in static 2D VF-OOAC and static 3D VF-OOAC setups. Data displayed as the fold change relative to static 2D VF-OOAC. (B) Dimensionality dictates pVFF morphology in each respective VF-OOAC model as seen by vimentin (green) and DAPI (blue) staining. pVFFs in static 2D VF-OOAC adhere to the collagen-coated membrane as a monolayer, restricting their capacity for cell-cell and cell-ECM interactions (I). pVFFs embedded in collagen gels in static 3D VF-OOAC spread and engage in more complex biological activity than possible in 2D culture (II). Magnification 20 \times , scale bar = 30 μ m.....61

Figure 4.5. The effect of perfusion on VF mucosa culture in 3D VF-OOAC. (A) H&E [I], K5, [II], K14 [III], E-Cad [IV], and LAMA5 [V] were evaluated using confocal microscopy to assess epithelial morphological features. Samples counterstained with DAPI (blue) to indicate cell nuclei. H&E magnification 40 \times , scale bar = 15 μ m. Immunostaining magnification 20 \times , scale bar = 30 μ m. (B) Relative gene expression in perfused 3D VF-OOAC versus static 3D VF-OOAC. Data displayed as the fold change relative to static 3D VF-OOAC.....64

Figure 4.6. The effect of fluidic shear presence on the culture of VF mucosae in perfused 3D VF-OOAC. (A) H&E [I], K5, [II], K14 [III], E-Cad [IV], and LAMA5 [V] evaluated morphological features. Samples counterstained with DAPI (blue) to indicate cell nuclei. H&E magnification 40 \times , scale bar = 15 μ m. Immunostaining magnification 20 \times , scale bar = 30 μ m. (B) Relative gene expression in perfused 3D VF-OOAC cultures with or without fluidic shear. Data displayed as the fold change relative to perfused 3D VF-OOAC without fluidic shear. (C) Vimentin staining showed fluidic shear induced fibroblast alignment in the direction of fluid flow (40 μ L/h) under perfused conditions versus static controls. Magnification 20 \times , scale bar = 50 μ m.....66

Figure 4.7. Transmission electron micrograph of the epithelium present in 3D VF-OOAC with fluidic shear present. (A) The cells of the epithelium near the superficial layer have a flattened morphology. (B) Cells in the deeper suprabasal layers display more square-like morphology. (C) Intercellular junctions present between neighbouring cells of the epithelium. (D) The basal cell layer is anchored to the basement membrane.....67

Figure 6.1. Evaluating the VF mucosa response to PM₁₀. (A) PM₁₀ toxicity screening was performed for pVFF and iLEC monocultures by applying a range of PM₁₀ concentrations (0-1600 μ g/mL) to cells for 24 hr. (B) VF-OOAC_{iLEC} were challenged with a PM₁₀ dose-response series (0, 50, 100, 400 μ g/mL) for 24 hr, with structural, functional, and inflammatory changes evaluated. (C) A VF-OOAC_{iPSC} was developed using iPSC-derived VF epithelial cells before challenging it with 100 μ g/mL PM₁₀ for 24 hr.....92

Figure 6.2. Effect of 24 hr exposure to PM₁₀ on the viability of iLEC and pVFF monocultures. (A) Cell viability of pVFF and iLEC cultures. Significant difference in cell viability versus respective 0 μ g/mL controls indicated by # (iLEC) or * (pVFF). (B) LIVE/DEAD assays indicated live (green) and dead (red) cells. Red-bordered images represent the lowest PM₁₀ dose that induced significant cell death in each respective cell type. Scale bar = 50 μ m.....97

Figure 6.3. Dose response study of 24 hr PM₁₀ exposure. (A) Transmitted light visualized PM₁₀ distribution at the epithelium surface (black particles). Yellow arrows indicate the basement

membrane. Red arrows indicate PM₁₀ particles. (B) Morphological features of VF-OOAC_{iLEC} cultures. K5, K13, K14, and E-Cad evaluated epithelium structure. LAMA5 assessed basement membrane. Vimentin and α SMA evaluated epithelial-to-mesenchymal transition presence. Samples counterstained with DAPI (blue). Magnification 20x, scale bar = 30 μ m. (C) Functional and structural gene expression. (D) Inflammatory gene expression. All gene expression data displayed relative to transwell_{iLEC} (0 μ g/mL) controls. (E) Average inflammatory cytokine secretion and standard deviation in response to PM₁₀. Data normalized to total protein content.....100

Figure 6.4. VF-OOAC_{iPSC} model development and response to 24 hr exposure to 100 μ g/mL PM₁₀. (A) Morphological features of VF-OOAC_{iPSC}. H&E, K13 (green) and DAPI (blue) assessed epithelial stratification and cell distribution, whilst LAMA5 (orange) evaluated the basement membrane. (B) Corresponding transwell controls. Scale bars: H&E = 15 μ m, Immunostaining = 30 μ m. (C) Structural and functional gene expression. (D) Inflammatory gene expression. All gene expression data presented as fold-change relative to transwell_{iPSC} (0 μ g/mL). Significant differences ($p < .05$) between VF-OOAC_{iPSC} and transwell_{iPSC} (0 μ g/mL) indicated by #. Significant differences ($p < .05$) induced by 100 μ g/mL PM₁₀ within VF-OOAC group indicated by *.....103

Figure 6.5. Average gene expression and standard deviation for VF-OOAC_{iLEC} and VF-OOAC_{iPSC} cultures challenged with 100 μ g/mL PM₁₀ for 24 hr. Significant interaction effects indicated by * ($p < .05$).....106

Figure S4.1. Bioanalyzer results for perfused 3D VF-OOAC samples with fluidic shear. All samples tested had a RIN >7, indicating no significant RNA degradation occurred during sample storage or processing.....77

Figure S4.2. The effect of perfusion and fluidic shear on the culture of VF mucosae in 2D VF-OOAC. During perfusion of the lower channel, the pVFF monolayer experiences fluidic shear. (A) H&E [I], K5, [II], K14 [III], E-Cad [IV], and LAMA5 [V] were evaluated using confocal microscopy to assess epithelial morphological features. Samples were counterstained with DAPI (blue) to indicate cell nuclei. Magnification 20x, scale bar = 30 μ m. (B) Heatmap of relative gene expression in perfused 2D VF-OOAC with fluidic shear compared to static 2D VF-OOAC. Data displayed as the fold change relative to static 2D VF-OOAC. (C) Overhead imaging of the epithelial layer using K5 staining demonstrated that despite the absence of an ALI, the epithelial cells still formed a fully confluent layer with strong basal cytokeratin expression in both static 2D VF-OOAC and perfused 2D VF-OOAC with fluidic shear. Perfusion Magnification 10x, scale bar = 50 μ m.....78

Figure S6.1. Particle size distribution (in vol. %) present in ERM-CZ PM₁₀-like dust.....116

Figure S6.2. Dose response to 24 hr PM₁₀ exposure for transwell_{iLEC}. Transmitted light visualized PM₁₀ distribution at the epithelium surface (black particles). K5, K14, and E-Cad evaluated epithelium structure. LAMA5 assessed basement membrane. Vimentin and α SMA evaluated epithelial-to-mesenchymal transition presence. Samples counterstained with DAPI (blue). Magnification 20x, scale bar = 30 μ m.....117

List of Tables

Table 2.1. Comparison of biological culture parameters across different upper airway in vitro models.....	7
Table 2.2. Comparison of characteristics related to the culture of immortalized, primary, or iPSC-derived cells in upper airway OOACs.....	15
Table 2.3. Human cell sources used in transwell co-culture models of the vocal fold mucosa.....	16
Table 4.1. Six unique setups in total were applied. Physiological scaling was examined in the context of 2D or 3D culture by comparing two different VF-OOAC designs with relevant transwell controls. Dimensionality was inspected by comparing both VF-OOAC designs. Perfusion was integrated into the VF-OOAC design that provided the greatest tissue development up to this point. Finally, fluidic shear was added to the perfused model.....	45
Table 4.2. Comparison of the two microfluidic chip devices used for investigating the impact of different culture parameters on VF mucosae in VF-OOAC setups.....	49
Table 4.3. Antibodies applied for immunocytochemistry evaluation of VF mucosae. AF = Alexa Fluor, K5 = Cytokeratin 5, K14 = Cytokeratin 14, LAMA5 = Laminin alpha 5, E-Cad = E-Cadherin.....	53
Table 4.4. TaqMan assays for qPCR evaluation of VF mucosae.....	56
Table 6.1. Summary of antibodies applied for immunocytochemistry.....	93
Table 6.2. TaqMan assays used for qPCR.....	95
Table 6.3. Comparison of functional and inflammatory gene expression in VF-OOAC _{iLEC} and VF-OOAC _{iPSC} challenged with 100 µg/mL PM ₁₀ for 24 hr. Significant differences (* p < .05) and effect size are displayed compared to negative controls (0 µg/mL) within each model group. ↑ = upregulated. ↓ = downregulated. N.S. = Non-significant.....	104
Table S2.1. Upper airway organ on-a-chip models.....	35
Table S6.1. Certified fraction values present in ERM-CZ PM ₁₀ -like dust.....	115
Table S6.2. Parameters of the VF-OOAC and transwell controls used for VF mucosa culture...	116

Acronym Glossary

ALI	Air-liquid Interface
ECM	Extracellular Matrix
ELISA	Enzyme Linked Immunosorbent Assay
iLEC	Immortalized Laryngeal Epithelial Cell
iPSC	Induced Pluripotent Stem Cell
OOAC	Organ-On-A-Chip
PAH	Polycyclic Aromatic Hydrocarbon
PM	Particulate Matter
PM _{2.5}	Fine Particulate Matter
PM ₁₀	Coarse Particulate Matter
qPCR	Quantitative Polymerase Chain Reaction
ROS	Reactive Oxygen Species
TEM	Transmission Electron Microscopy
VF	Vocal Fold
pVFF	Primary Vocal Fold Fibroblast
VF-OOAC	Vocal Fold Mucosa Organ-on-a-Chip
VF-OOAC _{iLEC}	Vocal Fold Mucosa Organ-on-a-Chip with immortalized epithelium
VF-OOAC _{iPSC}	Vocal Fold Mucosa Organ-on-a-Chip with stem cell-derived epithelium

Contribution to Original Knowledge

This thesis included several novelties related to the microengineering of a 3D vocal fold (VF) mucosa construct using microfluidic technology, i.e., *vocal-fold-organ-on-a-chip* (VF-OOAC), as a reliable *in vitro* experimental model.

The first original research paper presented focused on developing a novel VF-OOAC and evaluating culture parameters related to its structural and functional architecture. This VF mucosa model represents the first example of a perfused microfluidic 3D co-culture relevant to the upper airway, replicating cellular components of the mucosa's epithelial (immortalized laryngeal epithelial cells) and lamina propria (primary vocal fold fibroblasts) regions.

Through harnessing microfluidic technology, this microengineered VF mucosa model is unique in its capacity to integrate physiological scaling, 3D co-culture, perfusion, and fluidic shear into a single *in vitro* platform, offering a significant advantage over conventional platforms. This study contributed to understanding the influence of culture parameters on VF mucosa tissue development. The findings will aid future design of VF mucosa *in vitro* models and provide a foundation for implementing microfluidic culturing technology in VF research.

The second original research paper focused on the utility evaluation of the VF-OOAC by challenging the system with coarse particulate matter (PM₁₀), a global environmental irritant with clinical relevance to the VFs. The findings showed the VF-OOAC had a high resistance to all PM₁₀ doses tested. To validate the findings, the first instance of using induced pluripotent stem cell (iPSC) technology in an upper airway organ-on-a-chip model was also reported. This iPSC model similarly demonstrated robust VF mucosa resilience to PM₁₀, confirming the defensive mechanisms of stratified squamous epithelium are sufficient to protect the vulnerable lamina propria from acute irritant exposure. To the best of my knowledge, no *in vitro* model had replicated *in vivo* VF mucosa resilience to ambient environmental irritant acute exposure.

This thesis demonstrated the capacity of the proposed VF-OOAC to replicate *in vivo* behaviour when exposed to environmental irritants. Overall, this novel *in vitro* platform may accelerate basic and clinical research focused on deciphering the role of ambient irritants in voice disorder pathophysiology. This may help advance scientific understanding for related therapeutics development.

Contribution of Authors

Manuscripts included in this Thesis

1. **Coburn, P.T.**, Liu, X., Thibeault, S. L., Li-Jessen N. Y. K., *Organ-on-a-Chip: Time to Explore the Upper Airway?* – Perspective Review Paper, presented in Chapter 2

P. Coburn (first author) was responsible for the conceptualization, literature review, writing original draft, reviewing, and editing of the manuscript. X. Liu, S. Thibeault were responsible for conceptualization, reviewing, and editing. N. Li-Jessen was responsible for the conceptualization, writing original draft, reviewing and editing, supervision, and funding acquisition.

This work is in preparation for journal submission.

2. **Coburn, P.T.**, Lungova, V., Liu, X., Thibeault, S. L., Li-Jessen N. Y. K., *Investigating the Impact of Dimensionality, Physiological Scaling, Perfusion, and Fluidic Shear for Microengineering Vocal Fold Mucosae in Microfluidic Culturing Platforms* – Original Research Paper, presented in Chapter 3

P. Coburn (first author) was responsible for the conceptualization, experimental planning, data acquisition and characterization, data analysis, writing original draft, reviewing, and editing the manuscript. V. Lungova, X. Liu, S. Thibeault were responsible for conceptualization, reviewing, and editing. N. Li-Jessen was responsible for conceptualization, writing original draft, reviewing, editing, supervision, and funding acquisition.

This work is in preparation for journal submission.

3. **Coburn, P.T.**, Lungova, V., Chen, C., Durcan, T., Liu, X., Thibeault, S. L., Li-Jessen N. Y. K., *Evaluating the Resilience of the Vocal Fold Mucosa to Acute Exposure to Coarse Particulate Matter Pollutants – An Organ-on-a-Chip Analysis* – Original Research Paper, presented in Chapter 4

P. Coburn (first author) was responsible for the conceptualization, experimental planning, data acquisition and characterization, data analysis, writing original draft, reviewing, and editing the manuscript. V. Lungova, C. Chen, T. Durcan, X. Liu, S. Thibeault were responsible for conceptualization, reviewing, and editing. N. Li-Jessen was responsible for conceptualization, writing original draft, reviewing, editing, supervision, and funding acquisition.

This work is in preparation for Journal submission.

Published Refereed Articles not included in this Thesis

1. Landry, V., **Coburn, P. T.**, Kost, K., Liu, X. & Li-Jessen, N. Y. K. Diagnostic Accuracy of Liquid Biomarkers in Airway Diseases: Toward Point-of-Care Applications. *Frontiers in Medicine*, 9, (2022)

2. **Coburn, P. T.** (first author), Li, X., Li, J., Kishimoto, Y. & Li-Jessen, N. Y. K. Progress in Vocal Fold Regenerative Biomaterials: An Immunological Perspective. *Advanced NanoBiomed Research*, 2(2), (2021)
3. **Coburn, P. T.** (first author), Herbay, A. C., Berrini, M. & Li-Jessen, N. Y. K. An in vitro assessment of the response of THP-1 macrophages to varying stiffness of a glycol-chitosan hydrogel for vocal fold tissue engineering applications. *Journal of Biomedical Research Part A*, 109(8), 1337-1352, (2020)

Conference Papers & Abstracts

1. **Coburn, P.T.**, Lungova, V., Liu, X., Thibeault, S. L., Li-Jessen N. Y. K. Evaluating the Impact of Air Pollution on Voice and Upper Airway Health using an iPSC-derived Vocal Fold Mucosa Organ-on-a-Chip. TERMIS AP Conference October 16th-19th 2023 (Oral Presentation)
2. **Coburn, P.T.**, Lungova, V., Liu, X., Thibeault, S. L., Li-Jessen N. Y. K. Evaluating the Impact of Air Pollution on the Vocal Fold Mucosa Using a Bioengineered Microfluidic Cell Culture Device. 6th Congress of European ORL-HNS. Milan, Italy, October 29th-November 2nd 2022 (Poster)
3. **Coburn, P.T.**, Lungova, V., Liu, X., Thibeault, S. L., Li-Jessen N. Y. K. Development of a vocal fold microfluidic device to assess the impact of air pollution on vocal health. 16th Meeting of the International Association of Phonosurgery. Kyoto, Japan, October 13th-14th 2022 (Oral Presentation)
4. Yu, G. **Coburn, P.T.**, Berrini, M., Li-Jessen, N. Computer simulation of cell-material interaction: the interplay of macrophages and fibroblasts in a glycol-chitosan hydrogel. 11th World Biomaterials Congress. Virtual, December 11th-15th 2020 (Poster)
5. **Coburn, P. T.**, Li-Jessen, N. Y. K. Development of a vocal fold on-a-chip to assess the impact of air pollution on the vocal fold mucosa. 2020 Till & McCulloch Meetings. Vancouver (Virtual), Canada, October 26th-28th 2020 (Poster)
6. **Coburn, P. T.**, Herbay, A. C., Li-Jessen, N. Y. K. Immunological profiling of vocal fold hydrogel scaffolds. 13th International Conference on Advances in Quantitative Laryngology, Voice, and Speech Research. Montréal, Canada, June 2nd-4th 2019 (Poster)
7. **Coburn, P. T.**, Li-Jessen, N. Y. K. Influence of human vocal fold fibroblasts on macrophages in a glycol-chitosan hydrogel in vitro co-culture system. 11th East Asian Conference on Phonosurgery. Busan, South Korea, November 23rd-24th 2018 (Oral Presentation)
8. **Coburn, P. T.**, Li-Jessen, N. Y. K. An In Vitro Testing Platform of Macrophage Polarization in Hydrogel Scaffolds 5th TERMIS World Congress. Kyoto, Japan, September 4th-7th 2018 (Poster)
9. **Coburn, P. T.**, Li-Jessen, N. Y. K. Investigation of the Macrophage Response to Chitosan-Glycol Hydrogel. 12th International Conference on Advances in Quantitative Laryngology, Voice, and Speech Research. Hong Kong, October 17th-21st 2017 (Oral Presentation)

Abstract

Human vocal folds (VFs) are layered, functional tissues of the larynx that are responsible for voice production. Environmental irritants, such as ambient air pollutants, can induce inflammation in the VF mucosa, with epidemiological data associating them with voice disorders including vocal cord dysfunction, chronic laryngitis, and laryngeal cancer. Elucidating the mechanisms controlling the interaction between the VF mucosa and environmental irritants may therefore provide molecular targets for future therapeutics to treat VF or laryngeal inflammation.

In vitro culture models represent an initial platform for disease modelling and therapeutic assessment. However, conventional cell culture cannot fully recapitulate the microenvironmental complexity found *in vivo*, including biomechanical cues or paracrine signalling efficacy. This mismatch can produce inaccurate simulations of clinical observations. Developing an *in vitro* system that integrates further microenvironmental factors of native tissue could improve its physiological relevance to help reveal how environmental irritants contribute to voice disorder pathophysiology.

This thesis harnessed an advanced *in vitro* technology, organ-on-a-chip (OOAC), to microengineer a VF mucosa construct. OOAC models are biomimetic, microfluidic culture systems that can replicate structural and functional features of tissues and organs including tissue-tissue interfaces, mechanical stimulation, fluid flow, and biochemical gradients. By integrating these critical microenvironment elements, OOAC systems offer improved modelling efficacy to reproduce clinical responses at a level not possible using conventional techniques.

Firstly, we propose a strategy to cultivate the epithelial, basement membrane, and lamina propria components of the VF mucosa using organ-on-a-chip techniques (VF-OOAC). This model investigated co-cultures of immortalized laryngeal epithelial cells and primary VF fibroblasts using commercialized single- or double-microchannel microfluidic devices. Culture parameters including small-volume effects, three-dimensional architecture, perfused culture, and fluidic shear, were systematically evaluated to quantify their influence on tissue development. We demonstrated our VF-OOAC model displayed structural and functional tissue development exceeding that of conventional transwell culture controls.

Next, we performed a utility evaluation of the VF-OOAC. Animal studies have reported significant VF epithelial resilience when challenged with short-term exposure to ambient irritants but this has yet to be replicated with existing *in vitro* models. In this study, the VF-OOAC was subjected to a dose-response series of a global air pollutant, coarse particulate matter (PM₁₀) for 24 hr. The VF-OOAC was found to replicate the high resilience shown *in vivo* by the VF mucosa to short-term exposure to environmental irritants.

Lastly, immortalized laryngeal epithelial cells were replaced by induced pluripotent stem cell (iPSC)-derived VF epithelial cells to improve epithelial functionality and physiological relevance. Compared to transwell controls, the VF-OOAC had increased epithelial functionality, confirming the benefits of microfluidic culture observed for immortalized experiments were translatable to iPSC-derived cultures. When challenged with PM₁₀, the iPSC-derived epithelium also replicated the robust protection of the lamina propria observed in previous experiments, with no significant inflammatory activity detected.

Overall, the proposed VF-OOAC model supported improved tissue development compared to conventional transwell culture. The inclusion of an iPSC-derived epithelium in the VF-OOAC provides an *in vitro* platform to help advance the personalized medicine initiative in VF research. Furthermore, VF-OOAC models replicated the resilience of native VF epithelium to acute environmental irritant challenges, demonstrating the system's potential application as an early preclinical tool in therapeutic and toxicant screening.

Résumé

Les cordes vocales humaines sont des tissus fonctionnels en couches du larynx qui sont responsables de la production vocale. Les irritants environnementaux, tels que les polluants de l'air ambiant, peuvent conduire à une inflammation dans la muqueuse des cordes vocales, les données épidémiologiques les associant à des troubles de la voix, y compris la dysfonction du cordon vocal, la laryngite chronique et le cancer du larynx. L'élucidation des mécanismes contrôlant l'interaction entre la muqueuse de la corde vocale et les irritants environnementaux peut donc fournir des cibles moléculaires pour les futurs traitements visant à traiter la FV ou l'inflammation du larynx.

Les modèles *in vitro* représentent une plateforme initiale pour la modélisation des maladies et l'évaluation thérapeutique. Cependant, la culture cellulaire conventionnelle ne peut pas récapituler complètement la complexité microenvironnementale trouvée *in vivo*, y compris les indices biomécaniques ou l'efficacité de la signalisation paracrine. Ce décalage peut produire des simulations inexacts des observations cliniques. La mise au point d'un système *in vitro* qui intègre d'autres facteurs microenvironnementaux des tissus indigènes pourrait améliorer sa pertinence physiologique pour aider à révéler comment les irritants environnementaux contribuent à la pathophysiologie des troubles de la voix.

À cette fin, cette thèse a utilisé une technologie *in vitro* avancée, organe sur puce (OSP), pour micro-ingénier une construction de muqueuse des cordes vocales. Les modèles OSP sont des systèmes de cultures biomimétiques qui peuvent reproduire les caractéristiques structurelles et fonctionnelles des tissus et des organes, y compris les interfaces tissu-tissu, la stimulation mécanique, l'écoulement des fluides et les gradients biochimiques. En intégrant ces éléments critiques du microenvironnement, les systèmes OSP offrent une meilleure efficacité de modélisation pour reproduire les réponses cliniques à un niveau impossible en utilisant des techniques conventionnelles.

Dans un premier temps, nous proposons une stratégie pour cultiver les composants épithéliaux, de la membrane basale et de la *lamina propria* de la muqueuse des cordes vocales en utilisant des techniques d'organe sur puce (cordes vocales OSP). Ce modèle a étudié les co-cultures de cellules épithéliales laryngées immortalisées et de fibroblastes de cordes vocales primaires à

l'aide de dispositifs microfluidiques à microcanaux simples ou doubles commercialisés. Les paramètres de culture, y compris les effets de petit volume, l'architecture tridimensionnelle, la culture perfusée et le cisaillement fluide, ont été évalués pour quantifier leur influence sur le développement des tissus. Nous avons démontré que notre modèle cordes vocales OSP présentait un développement tissulaire structurel et fonctionnel supérieur à celui des contrôles conventionnels en culture Transwell.

Ensuite, nous avons effectué une évaluation de l'utilité des cordes vocales OSP. Des études sur des animaux ont fait état d'une résilience épithéliale importante de la corde vocale lorsqu'elle est confrontée à une exposition à court terme à des irritants ambiants, mais cette résilience n'a pas encore été reproduite avec les modèles *in vitro* existants. Dans cette étude, la corde vocale OSP a été soumise à une série dose-réponse d'un polluant atmosphérique global, une matière particulaire grossière (PM₁₀) pendant 24 hr. La corde vocale OSP a été utilisée pour reproduire la haute résilience montrée *in vivo* par la muqueuse de corde vocale à l'exposition à court terme aux irritants environnementaux.

Enfin, les cellules épithéliales laryngées immortalisées ont été remplacées par des cellules épithéliales corde vocales dérivées de cellules souches pluripotentes induites (CSPi) pour améliorer la fonctionnalité épithéliale et la pertinence physiologique. Par rapport aux témoins Transwell, la corde vocale OSP avait une fonctionnalité épithéliale accrue, confirmant que les avantages de la culture microfluidique observés pour les expériences immortalisées étaient traduisibles en cultures dérivées d'CSPi. Lorsqu'il a été confronté à des PM₁₀, l'épithélium dérivé de l'CSPi a également reproduit la protection robuste de la *lamina propria* observée dans des expériences précédentes, sans activité inflammatoire significative détectée.

Dans l'ensemble, le modèle de corde vocale OSP proposé a permis d'améliorer le développement des tissus par rapport à la culture Transwell conventionnelle. L'inclusion d'un épithélium dérivé de l'CSPi dans la corde vocale OSP fournit une plateforme *in vitro* pour aider à faire avancer l'initiative de médecine personnalisée dans la recherche sur la corde vocale. De plus, les modèles de corde vocale OSP ont reproduit la résilience de l'épithélium natif aux irritants environnementaux aigus, démontrant l'application potentielle du système en tant qu'outil préclinique précoce dans la modélisation thérapeutique et toxique.

Chapter 1. Introduction

Thesis Motivation

The human VF mucosa is a biomechanically active, multicellular 3D structure responsible for normal voice production. Dysfunction in VF mucosa tissue is a principal cause of voice disorders, which have an estimated lifetime prevalence of 30% and incurred annual health costs exceeding \$11 billion in the United States alone.¹⁻³

Existing *in vitro* models, including dishes, transwells, and bioreactors, often use culture setups with a static microenvironment or a single cell type. In addition, these macroscale models can suffer inhibited paracrine signalling efficacy, due to the diffusion distances and dilution effects present in the culture.

Effective *in vitro* recapitulation of the VF mucosa microenvironment requires modelling its principal components, i.e., epithelium, lamina propria, and basement membrane. Existing models have achieved this by co-culturing the two major cell populations of the mucosa – epithelial cells and fibroblasts – in transwell systems. Replicating the structure and functional native VF mucosa tissue in preclinical *in vitro* models is of imminent significance in addressing the ongoing healthcare and societal challenges posed by voice disorders.

Innovations in microfluidic technology have led to the rise of organ-on-a-chip (OOAC) platforms. These microphysiological culture systems can exert mechanical stimulation on cells and provide perfused conditions to simulate vascular and interstitial fluid flow. Fundamentally, microfluidic culture provides opportunities to initiate greater biological complexity into VF mucosa tissue constructs to stimulate superior tissue development.

An outstanding challenge for VF *in vitro* modelling is the need to reliably imitate clinical responses of native VF tissue. To help achieve this, microenvironmental parameters that regulate and dictate tissue activities should be integrated into VF *in vitro* platforms. These parameters include translatable media volumes, dynamic metabolite exchange, and mechanical stimulation. For instance, introducing perfusion and small-volume effects into VF mucosa cultures provides biomechanical cues, controlled concentration gradients, and enhanced paracrine signalling efficacy. A VF mucosa organ-on-a-chip (VF-OOAC) could assemble these features into a single *in vitro* testing platform to attain a more accurate representation of native VF tissue behaviour.

Such a model could improve the capacity to quantify the relationship between environmental irritants and vocal pathophysiology, advancing scientific understanding for related therapeutics development. However, the use of OOAC methods for cultivating the VF mucosa has yet to be validated and thus the potential benefits over conventional culture techniques are unknown.

Coarse particulate matter (PM₁₀) is an environmental irritant that represents an ideal exploratory case study for validating the VF-OOAC's tissue structure and functionality. PM₁₀ poses a direct threat to upper airway health and may contribute to voice disorders including VF fibrosis, chronic laryngitis, and laryngeal cancer.⁴⁻⁶

Thesis Rationale

To achieve the goal of developing a VF-OOAC, a bottom-up approach will first be adopted to deconstruct design elements important for *in vitro* VF mucosa culture, and build a platform optimized for structural and functional tissue growth. As opposed to primary VF epithelial cells, immortalized laryngeal epithelial cells (iLECs) were initially used as their culture longevity and expansion capacity benefited platform optimization and refinement. Conversely, the greater compatibility of primary VF fibroblasts (pVFFs) with cell culture and their critical role in regulating VF epithelium development via cellular crosstalk made them an ideal fibroblast cell source.⁷

It has been posited VF stratified squamous epithelium is sufficiently robust to withstand acute exposure (≤ 24 hr) to environmental irritants *in vivo*, although this has yet to be effectively replicated using *in vitro* cell culture.⁸ As such, model validation was enacted by challenging the VF-OOAC with PM₁₀ for 24 hr to assess its capacity for replicating *in vivo* behaviour.

To further authenticate the VF-OOAC, induced pluripotent stem cell (iPSC) technology was integrated into the platform. Immortalized airway epithelial cells have been associated with restricted differentiation and inhibited barrier capacity compared to native tissue cells.^{9,10} The use of iPSC-derived VF epithelial cells may overcome these limitations due to their capacity for recapitulating tissue functional and producing *in vivo*-level cellular responses. This could enhance the predictive efficacy and physiological relevance of the VF-OOAC and improve the clinical translation of generated datasets.^{11,12}

Research Objectives & Hypotheses

The overall goal of this thesis was to develop a VF-OOAC platform and test its applicability for studying the response to environmental challenges. To achieve this, we integrated principles of cell biology and microfluidic science to: (1) manipulate microenvironmental culture parameters to microengineer an *in vitro* platform of the VF mucosa; (2) assess the platform's capacity to replicate *in vivo* behaviour when challenged with acute exposure to environmental irritants; (3) integrate iPSC technology into the platform to enhance the clinical relevance of *in vitro* observations.

Aim 1. Engineer an *in vitro* VF-OOAC Model

We hypothesized: (1) microscale culture would increase structural and functional tissue development; (2) 3D culture would enhance cell polarization; (3) perfusion would stimulate differentiation and proliferation; (4) fluidic shear would promote mechanosensitive gene expression. The combined influence of these parameters was predicted to microengineer a VF mucosa exhibiting tissue development surpassing that of transwell controls.

Aim 2a. Assess VF mucosa's Response to PM₁₀ for VF-OOAC Utility Evaluation

This experimental series served to assess the capacity of the VF-OOAC to replicate *in vivo* VF mucosa resilience to short-term environmental irritant challenges. This strategy relied on challenging the VF-OOAC with PM₁₀ for 24 hr and examining the outcome on structural, functional, and inflammatory characteristics of the tissue. We hypothesized the VF-OOAC would display high resilience to PM₁₀ and incur no dose response due to the protective mechanisms provided by stratified squamous epithelium.

Aim 2b. Strengthen Clinical Relevance of VF-OOAC Testing Platform

To improve VF mucosa tissue functionality and enhance clinical relevance of the platform, we proposed integrating an iPSC-derived VF epithelium into our VF-OOAC and used a 24 hr PM₁₀ challenge to evaluate its resilience via similar outcome measurements to Aim 2a. We hypothesized iPSC-derived VF epithelial cells would improve recapitulation of native VF epithelium's defensive mechanisms, including its barrier capacity and tissue functionality, leading to greater resilience to irritants compared to iLECs.

Chapter 2. Organ-on-a-Chip: Time to Explore the Upper Airway?

Patrick T. Coburn^a, Xinyu Liu^b, Susan L. Thibeault^c, Nicole Y. K. Li-Jessen^{a,d,e,f,†}

a. School of Communication Sciences and Disorders, McGill University, Canada

b. Department of Mechanical Engineering, University of Toronto, Canada

c. Department of Surgery, Division of Otolaryngology – Head and Neck Surgery, University of Wisconsin, Madison, WI, USA

d. Department of Biomedical Engineering, McGill University, Canada

e. Department of Otolaryngology – Head & Neck Surgery, McGill University, Canada

f. Research Institute of McGill University Health Centre, Canada

† Corresponding author

Abstract

The upper airway has critical roles in respiration, swallowing, and speech. In addition, it serves as a filter to prevent inhaled and ingested matter from penetrating the tissues of the lower airway. Hinderance of these functions can be life-threatening or significantly impair patient quality-of-life. Access to effective preclinical models is essential for furthering our understanding of the biological mechanisms involved in upper airway disease modelling, therapeutics development, and precision medicine. With continued debate surrounding the practicality and ethics of animal models, the need for biomimetic *in vitro* systems, such as organ-on-a-chip, is growing to replicate more aspects of the native tissue microenvironment compared to conventional techniques. With organ-on-a-chip technology successfully, and widely, applied in other organ research fields, now is the time for upper airway researchers to harness this advanced technology and create preclinical *in vitro* platforms with enhanced efficacy and fidelity.

This perspective paper examines the design principles of organ-on-a-chip models utilized to produce upper airway microtissues. Following this, an assessment of opportunities and future perspectives is presented as a guide to stimulate the advancement of organ-on-a-chip use in upper airway culture models.

Introduction

The upper respiratory tract extends from the nose to the top of the trachea and has major functions in respiration, swallowing, and communication. Each organ of the upper airway

possesses a specialized tissue composition and functionality. For example, the human vocal folds (VFs) undergo constant microtrauma during phonation.¹ To compensate for this, VFs are covered by a multilayered, non-keratinized stratified squamous epithelium which, as a highly robust epithelia of the internal organs, provides structural support and resilience against excessive injury. Conversely, the more delicate pseudostratified columnar epithelium of the nasal cavity has an abundant population of ciliated cells for filtration of inhaled air and removal of trapped particulates via mucociliary clearance.²

Epithelial tissue is one component of the upper airway mucosa which, alongside the basement membrane and lamina propria, serves to provide humidification and protection to the local tissue environment.³ All upper airway mucosae contain a rich cellular architecture that includes various epithelial, stromal, immune, and endothelial cells. The specific size and composition of airway mucosa varies between different regions. For example, the average reported thickness for nasal and oropharyngeal mucosae is 3.5 mm and 9.9 mm respectively.⁴

Although animal models remain the ‘gold standard’ of preclinical research, continued scientific and ethical advances have intensified debate around the efficacy and application of their use.^{5,6} Physiological differences between species lead to animal models frequently failing to predict pathophysiological responses at a clinical level.^{7–10} Moreover, the high cost of breeding, housing, and performing lengthy protocols restricts animal model availability.¹¹ The United States Food and Drug Administration has identified a need to enact the 3Rs (replacement, refinement, reduction) of animal research through developing alternative models.¹² One proposed method to achieve this is creating biomimetic *in vitro* systems to use for environmental and drug toxicology screening.

Conventional *in vitro* models based on 2D cell culture display limited physiological relevance. Cultivating cells in 2D impacts many *in vivo* cellular processes including differentiation, proliferation, apoptosis, and mechano-responses (**Figure 2.1**).¹³ Specifically, 2D culture restricts polarity and adhesion distribution, limiting the capacity of cells to interact with the local environment.¹⁴ Furthermore, proliferation rates in 2D culture are typically higher than *in vivo* due to the absence of structural architecture, such as intercellular junctions, that helps regulate apoptosis mechanisms in epithelial cells.^{15–18}

2D vs 3D Cell Culture

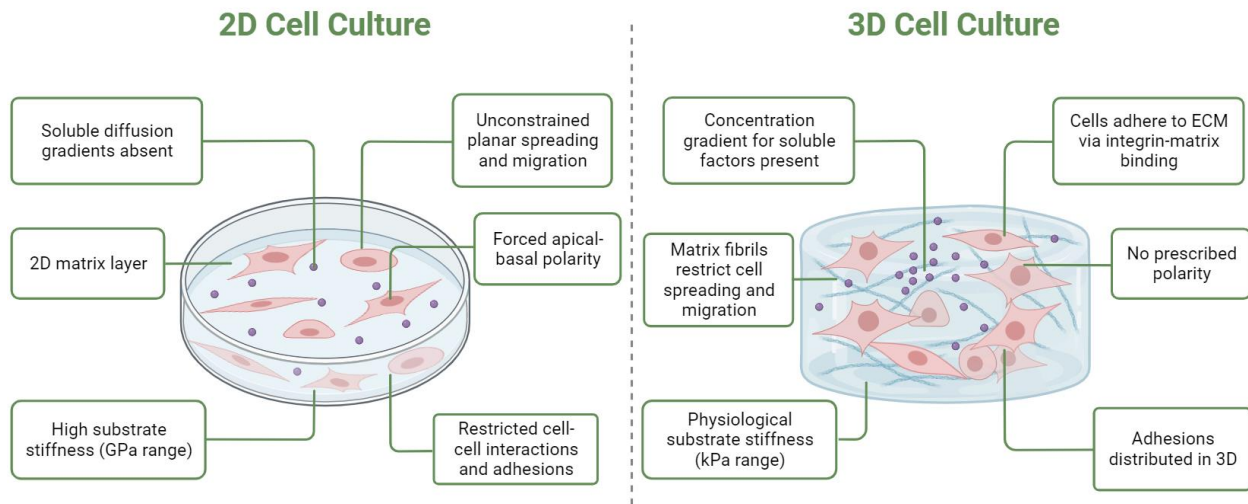


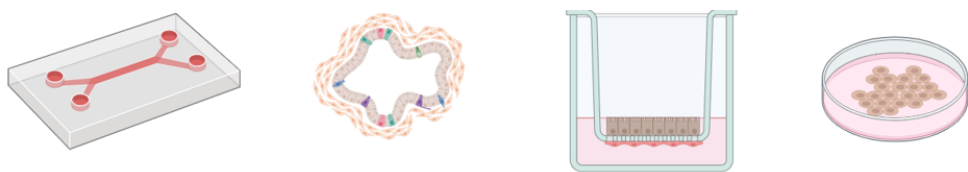
Figure 2.1. Comparison of 2D and 3D cell culture. Created with BioRender.com.

To obtain an improved representation of the complex, multicellular architecture found *in vivo*, 3D culture systems have been utilized. The provision of a 3D cellular microenvironment better replicates *in vivo* behaviour, including extracellular matrix (ECM) synthesis, apoptosis, migration, proliferation, and differentiation.¹⁹ In addition, 3D cellular environments can replicate signalling cascades not found in 2D culture, such the interaction between β 1-integrin and epidermal growth factor receptors.²⁰ A common approach for 3D culture setups uses transwell inserts that has several advantages for cultivating upper airway tissues, including the use of an air-liquid interface (ALI) and 3D co-culture (**Table 2.1**). ALI culture is particularly important for mimicking *in vivo* conditions of the luminal airway when cultivating upper airway epithelial cells. For instance, ALI culture was found necessary for the differentiation and development of a multilayered nasal epithelium *in vitro*.²¹ Similarly, using co-culture setups is also significant as it introduces cellular crosstalk and multicellular responses that underpin upper airway functionality and immunology.²²

Despite improvements over 2D culture, transwell 3D co-culture retains some significant limitations. The static microenvironment restricts metabolite diffusion speed, which can produce cellular morphology and proliferation rates divergent from those *in vivo*.²³ Moreover, the cell-media ratio is unrepresentative of native tissues, which can lead to mischaracterizing irritant or

drug responses versus clinical observations.^{24,25} More complex 3D culture models such as nasal organoids have been developed using patient-derived epithelial cells and have displayed characteristic structures of native tissues including cilia, mucins, and tight junctions.²⁶ However, ALI absence in organoid models restricts epithelium differentiation and negates the possibility of delivering aerosolized therapeutics or irritants to mimic *in vivo* exposure routes.²¹ In addition, necrosis at the centre of tissue constructs due to mass transport limitations alongside the absence of mechanical stimulation present further challenges for organoid cultures.²⁷

Table 2.1. Comparison of biological culture parameters across different upper airway *in vitro* models.



	Organ on-a-chip	Organoid	Transwell Co-Culture	2D Monoculture
Physiological cell-media ratio	Yes	No	No	No
3D tissue architecture	Yes	Yes	Yes	No
Air-liquid interface	Yes	No	Yes	No
Perfusion	Yes	Yes	No	No
Circulating immune cells	Yes	No	No	No
Mechanical Stimulation	High	Medium	Low	Low

Organ-on-a-chip (OOAC) is an alternative, biomimetic platform that uses microfluidic devices containing chambers inhabited by living cells to simulate tissue- and organ-level physiology.²⁷ OOACs, also known as microphysiological systems, are specifically designed to model features of human biology using microscale culture setups with an increased capacity to replicate *in vivo* behaviour.²⁸ For instance, cultivating cells in microchannels provides an inherent

compatibility with dynamic air or culture medium flow to recapitulate breathing or perfusion motions found *in vivo*.

This perspective review aims to inform researchers on the applications and advantages of OOAC technology in upper airway research for modelling nasal, pharyngeal, and laryngeal tissues. The versatility of OOAC approaches enables them to be tailored to replicate tissue architecture and dynamism of the native microenvironment, which is vital for improving physiological relevance of *in vitro* models. Here, key design considerations for upper airway OOAC models are identified, including both physical and biological parameters. Following this, notable research topics of interest are highlighted, with a specific focus on the role of OOAC technology in advancing personalized medicine and clinical translation of *in vitro* modelling.

Organ-on-a-Chip Technology

Modern OOAC technology originated from efforts in the electronics industry to develop miniaturized total chemical analysis systems in the latter half of the twentieth century.²⁹ These later became ‘lab-on-a-chip’ tools incorporating fluidic microsystems into a single platform for performing multiple steps of a chemical assay.³⁰ Further advances led to the fabrication of microscale fluidic channels for the addition of living cells.³¹ In particular, improvements in polymer science and microfabrication techniques facilitated the development of increasingly complex devices to model organ-level functions.^{27,32–34} Microchannels with large surface areas and high mass transfer rates enabled the use of micro- or nano-volumes, rapid mixing speeds/responses, and precision control over physical and chemical properties.^{34–38} For non-upper airway tissues (lung^{39,40}, kidney⁴¹, gut⁴² etc.), OOAC technology has already been successfully applied to create perfused microsystems recapitulating tissue-tissue interfaces, mechanical stimulation, and biochemical gradients found *in vivo*.^{39,40,43}

From January 2014 to August 2023, only eight microphysiological systems were published that modelled functional upper airway biology (**Table S2.1**). Each of these was specifically purposed for nasal tissue with no studies reported for other upper airway tissues such as the VFs or epiglottis. Of note, a range of microfluidic platforms have also been developed for head and neck cancer.^{44–47} However, whilst cancer models are an excellent resource, they offer limited insight into healthy tissue homeostasis and cannot be applied to study therapeutics and

pathophysiology related to non-cancerous disorders such as pharyngitis, laryngitis, or vocal fold scarring, or reactive upper airway dysfunction syndrome. As such, a major research gap exists for developing OOAC models related to functional laryngeal and pharyngeal tissues in particular.

Utilizing Design Parameters of Organ-on-a-Chip Models

A principal goal of OOAC models is to minimize the degree of complexity needed to represent a specific biological application and avoid introducing unnecessary factors that complicate the system's use or analysis.²⁸ Hence, selecting the approach for forming functional tissues within an OOAC is a significant initial consideration. For bottom-up approaches described in this review, immortalized, primary, or stem-cell derived cells are cultivated in microfluidic devices that support the development and formation of functional tissues. The tissue culture strategy will influence the design of the microfluidic device due to its role in organizing and supporting cells in specific configurations and routing fluids – such as culture medium or air – through specific tissue channels or compartments.²⁸ Whilst many OOAC designs are possible, a multitude of microfluidic device and biological parameters have a significant influence on OOAC functionality. Here, we explore their importance in creating physiologically relevant upper airway OOACs.

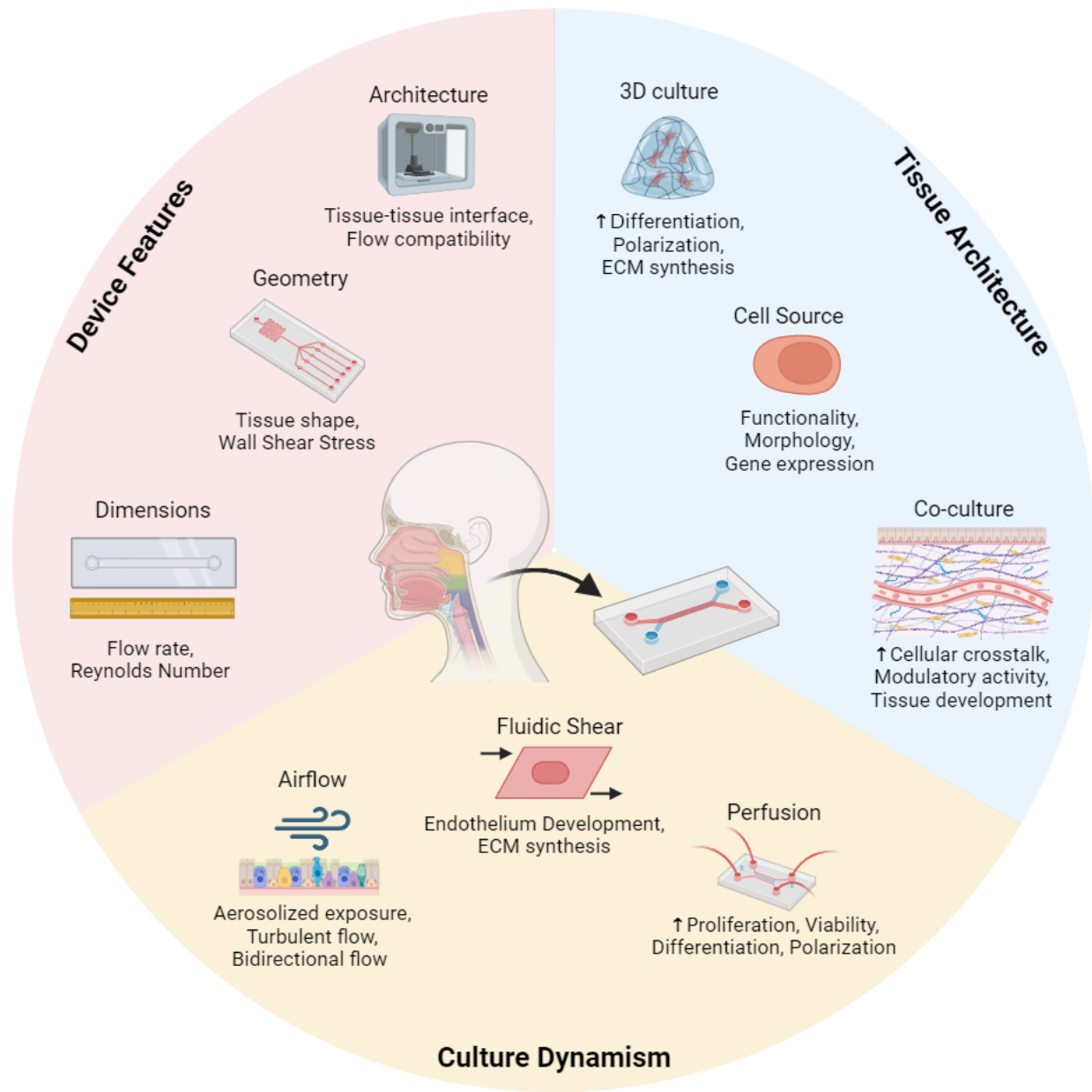


Figure 2.2. Upper airway organ-on-a-chip models have a range of parameters that can be manipulated to improve the mimicry of the native tissue microenvironment. The influence of each specific parameter may vary across different tissues and hence requires optimizing for each model. Created with BioRender.com.

Microfluidic Device Parameters

Conceptualization & Configuration

OOAC models have been stated to broadly fit into two major groups: solid organ chips or barrier tissue chips.²⁸ Solid organ chip cultures create 3D tissues with the capacity to interact with

each other and surrounding culture media. This setup has most commonly been used in non-airway models such as for liver, cardiac, and adipose OOACs. Barrier tissue chips are designed to support the formation of cellular barriers between fluid compartments to study selective transport processes. These systems have been utilized in airway OOACs to mimic the epithelial-endothelial barrier of lung tissues such as alveoli and small airways.^{39,40,48}

Within each overarching group, OOAC models can be further specified by their device configuration. Although no standardized design is universally applicable for all OOACs, notable setups for upper airway modelling include double-, or multi-channel/compartment setups (**Figure 2.3**). Each setup is compatible with ALI culture, which is crucial in the formation and differentiation of functional upper airway epithelium.²¹ However, the specific microchannel/compartment arrangement can vary significantly across OOAC platforms. For instance, a common approach in upper airway research has relied on a modified snapwell or transwell separated from a microchannel by a porous membrane (**Figure 2.3A**).^{49–51} This setup has the advantage of perfusion compatibility and also enables 3D culture, which has particular relevance for stromal cells that require increased spatial and chemical complexity to form *in vivo* tissue structures.⁵² For the membrane separating the channel and compartment, pore size and density can be tuned to control nutrient/waste exchange, paracrine signalling, and cell migration. A drawback of this model is that epithelial cells are generally cultivated at a static ALI only, although a more dynamic ALI is potentially obtainable using exposure technology (e.g. Cultex® or Vitrocell®).^{53,54}

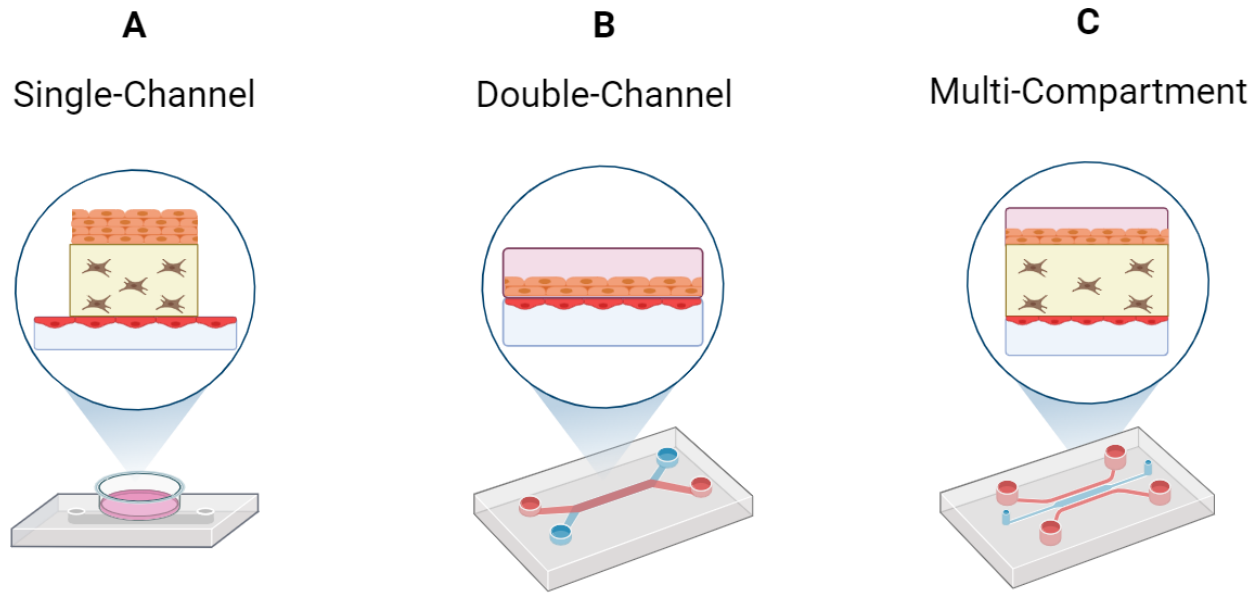


Figure 2.3. Microfluidic device configurations applicable to upper airway OOAC models. (A) A single microchannel is separated from a compartment by a porous membrane. The compartment permits 3D co-culture of epithelial and stromal cells whilst the microchannel can be used for endothelial cell culture under perfused conditions. (B) Double-channel configurations can be used for barrier studies exploring epithelial-endothelial or epithelial-stromal interfaces. Each microchannel can be used for dynamic fluid flow, including medium perfusion for endothelial cells and airflow for epithelial cells. (C) Multi-compartment configurations allow 3D culture of stromal cells but also enable dynamic flow through neighbouring microchannels, permitting dual dynamic flow found in double-channel models to culture epithelial and endothelial cells in physiologically relevant conditions.

Double-channel designs consist of two overlapping microchannels separated by a porous membrane in a sandwich or parallel configuration (**Figure 2.3B**). This design is useful for creating a dynamic ALI, whereupon the endothelial channel is perfused with culture medium whilst an airflow is passed through the epithelial channel.³³ This example would produce a 2D co-culture useful for studying basic cellular responses, such as the impact of drugs or irritants on barrier permeability.^{55–57}

Multi-channel/compartment systems build on the double-channel model and are typically designed with at least three distinct cell culture regions (**Figure 2.3C**). This design is advantageous for better replicating the biological complexity of native upper airway mucosae due to its compatibility with perfused 3D culture and a dynamic ALI, combining advantages from the simpler designs. An example configuration of this would be a device with two microchannels either side of a central compartment used for 3D hydrogel culture.⁵⁸ This setup ensures epithelial, stromal, and endothelial cells are cultivated in physiologically relevant surroundings, namely a dynamic ALI, 3D environment, and perfused conditions respectively. One limitation of this

approach occurs if porous plastic membranes are used to separate each compartment as this creates an inorganic physical barrier between the lamina propria and epithelial tissue regions. However, this could potentially be offset by adjusting membrane pore size to permit cell migration ($\geq 3 \mu\text{m}$).

Dimensions & Geometry

An inherent advantage of OOACs over conventional models is the increasingly relevant physiological scaling they provide due to the cell-media ratios used being more representative of native tissue. Compared to macroscale models, cultivating tissues at the microscale enhances paracrine signalling efficacy via small volume effects.^{27,59,60} Microscale culture also inherently provides decreased diffusion distances and increases the speed of cellular responses by minimizing metabolite heterogeneity and dilution.⁶⁰ Fundamentally, this permits tissue development in OOACs to proceed at rates more closely aligned with those *in vivo*. For example, a nasal OOAC was able to replicate gland-like structures observed in native tissues but never previously obtained with conventional culture.⁶¹

In addition to the general advantages of microscale culture, the specific dimensions and geometry of the channels/compartments in OOACs can exert significant influence over the functionality of cultivated tissues and, particularly for perfused cultures, operational efficiency of the OOAC system.⁶² Microchannel dimensions can be adjusted to reflect the size of the luminal airways or vasculature found *in vivo*. Altering microchannel size also has important implications for the associated flow profile when culture medium or air is passed through the channel. Notably, this includes wall shear stress and shear stress exerted on cells. For example, computational simulations of a nasal OOAC revealed enlarging microchannel height from 0.275 mm to 4 mm increased the Reynold's Number beyond the laminar flow threshold (>2000).^{51,63} Modelling turbulent flow is important for replicating physiological airflow of the upper airway, which exerts considerable shear stress on local cells. Using microchannel dimensions to control flow profiles is a useful strategy for replicating flow-induced mechanical stimulation found *in vivo*.

Similarly, microchannel geometry can be controlled to produce airflow patterns characteristic of those found in the upper airway. In one case, the geometry of a nasal OOAC was developed based on the Carlton-Civic Standardized Nasal Model to replicate anatomical structures of the nasal cavity including recirculation zones and winding streamlines.⁶⁴ This enabled a flow

pathway through the microfluidic device more representative of airflow streamlines *in vivo*. Similar techniques could be adapted for the laryngeal and pharyngeal cavities to cultivate tissues able to experience relevant airflow patterns and physiological shear stresses.

Materials & Fabrication

The materials used in a microfluidic device are influential factors for cell attachment, biocompatibility, microfabrication compatibility, and intended characterization. OOACs can be constructed with various material combinations, particularly for devices containing multiple culture compartments. Common materials used in device assembly include poly(dimethylsiloxane) (PDMS), thermoplastics such as polystyrene, poly(methyl methacrylate), polycarbonate, or cyclic olefin copolymer, and glass. Each distinct material has associated advantages and disadvantages. For example, PDMS offers ease-of-manipulation, high gas permeability, optical clarity for high-quality microscopy read-outs, and biocompatibility.^{27,65} However, PDMS devices are susceptible to fluid evaporation and leaching of uncured oligomers. In addition, PDMS suffers from non-specific hydrophobic molecule adsorption, which renders it unsuitable for preclinical models examining hydrophobic drugs.^{43,66–71} Alternatively, thermoplastic devices have high temperature and pressure resistance, physical and chemical stability, and hydrophilic surfaces for improved cell attachment.^{72,73} Notably, they have high compatibility with low-cost, mass production, which has helped facilitate their growing commercial availability. Drawbacks to thermoplastic devices include their limited gas permeability and reduced optical clarity compared to PDMS.^{72,74,75}

Ultimately, material selection is a compromise between desired functionality and the availability of fabrication facilities. For example, thermoplastics (polycarbonate, polystyrene etc.) are often used as porous membranes in OOACs due to their established biocompatibility, cell attachment properties, and commercial availability as thin ($\leq 10\ \mu\text{m}$), porous sheets. Depending on the tissue modelled, material mechanical properties can be a key factor. For instance, the high elasticity of PDMS has been exploited in lung OOAC models to allow mechanical stretching to exert physiological strain on cells.⁴⁰

To fabricate the microfluidic device, a variety of microfabrication techniques are available including soft lithography, injection moulding, 3D printing, and hot embossing.^{72,76} Whilst fabrication methods are closely associated with the choice of material, experimental purpose is

also an important consideration. Although thermoplastic polymers can be readily manipulated using injection moulding, this technique is unsuitable for producing devices with complex designs or operational features such as stretching. Alternatively, 3D printing can rapidly produce complex, intricate prototypes but is limited by poor optical clarity and resin biocompatibility issues. Ultimately, as microfabrication techniques continue to advance, expanding design possibilities and device complexity will help spearhead efforts to recreate the complex architecture of the upper airway *in vitro*.

Replicating Upper Airway Tissue Architecture

Cell Source

Assembling the biological elements of an OOAC is a crucial step in defining the model's recapitulation capacity. Consideration should be given to cell sources, tissue compositions, and culture dimensionality, which all contribute to OOAC functionality. OOACs are often designed to replicate specific physiological characteristics of tissues, such as epithelial or endothelial barrier functionality, and thus may require a specific cell source to achieve this (**Table 2.2**). For example, many immortalized cell lines and even certain induced pluripotent stem cell (iPSC)-derived cells often express only a fraction of the functional capacity of primary cells found in native tissues.⁷⁷ In addition, the accumulation of karyotypic abnormalities in immortalized cell lines can produce drug or toxicant responses divergent from native tissue.

Table 2.2. Characteristics related to the culture of immortalized, primary, or iPSC-derived upper airway cells.

Characteristic	Cell Source		
	Immortalized	Primary	iPSC-derived
Ease-of-culture	Simple	Moderate	Complex
Cost	Low	Medium	High
Senescence	Long-term self-renewal	Limited self-renewal	Long-term self-renewal
Replicability	High	Donor variability	Donor variability
Morphology	Polarity loss, absence of morphological features	Healthy morphology (initially)	Healthy morphology (maturity varies)
Phenotype	Changes in phenotype, functional alterations	Maintain native phenotype for limited number of passages	Display native phenotype
Genome	Altered genomic content	Genetically stable	Undifferentiated iPSCs can display genetic instability
Contamination risk	Low	Medium	High
<i>In vivo</i> relevance	Low	High (initially)	High

Whilst primary cells may initially possess functional and metabolic properties similar to those *in vivo*, they suffer protein and gene expression alterations within a few days of culture, frequently display donor-specific behaviour, and have limited availability.⁷⁸ This can limit the time window of the upper airway OOAC, especially for long-term studies. This has notable relevance for certain upper airway primary cells that do not grow well *in vitro* such as VF epithelial cells, which have a limited culture capacity before senescence occurs.⁷⁹ Specifically for transwell co-cultures modelling the VF mucosa, this technical challenge has inspired the use of various alternative epithelial cell sources (**Table 2.3**). Of these cell sources, iPSCs are of notable interest for OOAC applications as they can be used to create patient-specific models without the availability and purity concerns associated with primary cells.^{80,81} To fully realize this potential, improvements in long-term efficacy, upscaled production, and reproducibility of iPSC-derived tissues remain ongoing research challenges.

Table 2.3. Human cell sources used in transwell co-culture models of the vocal fold mucosa.

Epithelial Cells	Vocal Fold Fibroblasts	Reference
Embryonic stem cell-derived VF	Primary	Leydon et al. (2013) ⁸²
Primary VF	Primary	Ling et al. (2015) ⁸³
Primary bronchial/tracheal	Immortalized	Walimbe et al. (2016) ⁸⁴
Induced pluripotent stem cell-derived VF	Primary	Lungova et al. (2019) ⁸⁵ , (2022) ⁸⁶
Immortalized VF	Primary	Xia et al. (2021) ⁷⁹
Primary buccal	Immortalized	Grossman et al. (2023) ⁸⁷

Tissue Types

The intended purpose of an OOAC will dictate the tissue composition cultivated within it. For instance, the mucus-producing epithelium lining the luminal airway is a crucial tissue in innate immunity and as a chemical and physical barrier to inhaled and ingested irritants, pathogens, or allergens. Culturing tissue-specific epithelial cells in OOAC models provides a platform to study the consequences of epithelial barrier disruption or altered mucus production for upper airway health and functionality.^{88–90}

Incorporating subepithelial ECM and matrix-embedded stromal cells such as fibroblasts, smooth muscle cells, or mesenchymal progenitor cells, alongside epithelial cells can significantly improve mimicry of organ-level upper airway pathophysiology.⁹¹ In particular, fibroblasts have a prominent role in tissue homeostasis, regulating proliferation, migration, and differentiation of

local cells via the synthesis of ECM components.^{14,92,93} Indeed, for culturing some airway epithelia *in vitro*, most notably VF epithelium, fibroblast presence is critical for inducing differentiation and structural development of a multilayered epithelium.⁸² In addition to their role in supporting tissue development, the stromal environment of tissues is of essential importance in disease due to it being dramatically altered, particularly in systemic conditions such as fibrosis or cancer. As such, integrating stromal cells in upper airway OOACs is key to producing disease models with greater predictive efficacy.

Integrating endothelial tissue is another target for upper airway OOACs. As a vital component of tissue homeostasis, endothelial barrier integrity regulates metabolite transfer and immune cell migration.⁹⁴ Incorporating vasculature into upper airway OOACs can enable dynamic permeability studies of therapeutics and toxicants.

Modelling the Dynamic *In vivo* Microenvironment

Perfusion Culture

In vivo, extensive vascular and interstitial networks throughout upper airway mucosae provide constant nutrient renewal to maintain tissue viability and functionality whilst simultaneously preventing the build-up of acidic waste products.^{95,96} One method to replicate this dynamic environment *in vitro* is to use perfusion culture, which can improve tissue viability⁹⁷⁻⁹⁹, polarization¹⁰⁰, morphology¹⁰⁰, differentiation¹⁰¹, and ECM synthesis¹⁰¹. Perfusion is an integral feature of OOAC technology, functioning as an *in vitro* circulatory system that maintains concentration gradients for nutrient and waste convective transport.^{28,102}

OOACs can be connected to either a passive or active pumping system such as a peristaltic pump, syringe pump, gravity, or surface tension. Although passive systems are typically more straightforward to implement and operate, active systems afford much greater control over the flow profile.¹⁰³ That said, culture length is a determining factor in the choice of pump used. For example, as syringe pumps can only deliver a set volume of media loaded in the syringe, they may be unsuitable for longer-term cultures requiring large volumes of perfused media. Furthermore, the higher costs and technical complexity involved in assembling active pump systems can present accessibility issues.

Overall, the degree of automation and flow control provided by the pumping system are primary considerations for mimicking *in vivo* flow conditions, which can vary significantly between different vessels. For instance, whilst capillary flow ranges from 0.5-1.5 mm/s, interstitial fluid velocities in the ECM of upper airway mucosae are an order of magnitude slower (~ 0.1 -4.0 $\mu\text{m/s}$).¹⁰⁴⁻¹⁰⁷ The combined effect of fluid velocity and vessel diameter creates distinct shear stress levels and controls the mass transport regime of soluble factors in the culture.²⁸

Shear stress is an influential factor in OOAC cultures given its impact is tissue-dependent and varies substantially. For example, high levels of shear stress ($>8 \text{ dyn/cm}^2$) in endothelial tissue are thought to have protective effects on the endothelium and contribute to homeostasis and functionality.¹⁰⁸ Conversely, fibroblasts are significantly influenced by much lower shear stress values, with 0.1 - 0.3 dyn/cm^2 inducing cellular alignment and 1 - 3 dyn/cm^2 associated with fibroblast-myofibroblast transition.¹⁰⁹

Overall, perfusion-based culture represents a critically understudied area for upper airway OOACs. The only model to use a perfused setup was a nasal OOAC, which supplied RPMI 2650 cells via a syringe pump set to flow media through the device at $200 \mu\text{L/h}$.⁵⁰ As more complex models are developed that incorporate additional stromal and endothelial components, harnessing the benefits of perfusion will be key in facilitating greater tissue development.

Airflow

In addition to mimicking vascular or interstitial fluid flow, upper airway OOACs can also replicate air movement across the luminal airway surface. Physiological airflow can be modelled in OOAC microchannels, with a number of methods available to produce this phenomenon. In pressurized systems, a compressed air source can be connected to an OOAC, with airflow velocity carefully regulated via a mass flow controller.¹¹⁰ In such setups, airflow must be filtered in-line prior to entering the microfluidic device to minimize contamination risk. Furthermore, to mimic physiological conditions, air reaching epithelial cells must be warmed and humidified. One method to achieve this is by heating the tubing connected to the OOAC inlet and maintaining relative humidity of the air at $\sim 95\%$ via a bubbler-type humidifier.¹¹⁰ To prevent condensation forming in tubing lines, the entire airflow system can be kept in a $5\% \text{ CO}_2$ incubator.

In vivo, airflow exerts mechanical stimulation on epithelial cells in the form of fluidic shear. Airflow characteristics can be modified to replicate the velocity and direction found in the upper airway. For example, bidirectional airflow can be applied through microchannels to mimic the passage of air during breathing. This was utilized in a nasal model to better replicate fluidic shear levels found in the native nasal cavity, with results suggesting increasing wall shear stress from 0.1 to 1.0 dyne/cm² triggers increased mucus production.⁵¹ Fluidic shear is an important regulator of other epithelial barrier functions too, with a different nasal model reporting decreased cell viability and impeded barrier integrity when shear stress was increased from 0.23 Pa to 0.78 Pa.⁵⁶

Airflow in OOACs is also valuable for studying exposure and barrier transport of therapeutics or toxins. Aerosolized doses better replicate *in vivo* exposure experienced by cells compared to submerged exposure techniques classically used in conventional culture.¹¹¹ For example, cilia beat frequency intensified over 1 hr in a nasal model exposed to 1.0 mg/m³ of gaseous formaldehyde.⁴⁹

Mechanical Stimulation

Cells of the upper airway reside in a diverse biomechanical environment subject to a variety of tissue-specific mechanical stimulation. During breathing, fluidic shear is exerted on epithelial cells which also undergo minute amounts of expansion and contraction.¹¹² Stromal cells also experience fluidic shear via interstitial fluid movement through connective tissues.¹¹³ VF cells in particular are subject to significant biomechanical forces during phonation when high frequency vibrations (100-300 Hz) expose fibroblasts to tensile and shear deformations.^{114–118} Similarly, the VF vascular network must also withstand this biomechanical activity. However, even when the VFs are at rest, endothelial tissue experiences pulsatile stretch, fluidic shear, and hydrostatic pressure during homeostasis maintenance.¹¹⁹ Replicating this biomechanically active microenvironment is difficult using conventional *in vitro* techniques as such static culture systems cannot replicate the dynamism of native tissues.

Prospects & Future Outlook

Although it remains in relative infancy within the field, the application of microfluidic culture for upper airway research continues to demonstrate encouraging progress. The incoming development wave should build on the foundations already provided to introduce increasingly complex tissue models to better mimic the *in vivo* microenvironment. Here, we propose strategies to exploit OOAC technology for enhancing cell microenvironments, incorporating real-time culture monitoring, constructing advanced disease models, strengthening predictive power via paired *in silico* models, and advancing personalized medicine (**Figure 2.4**).

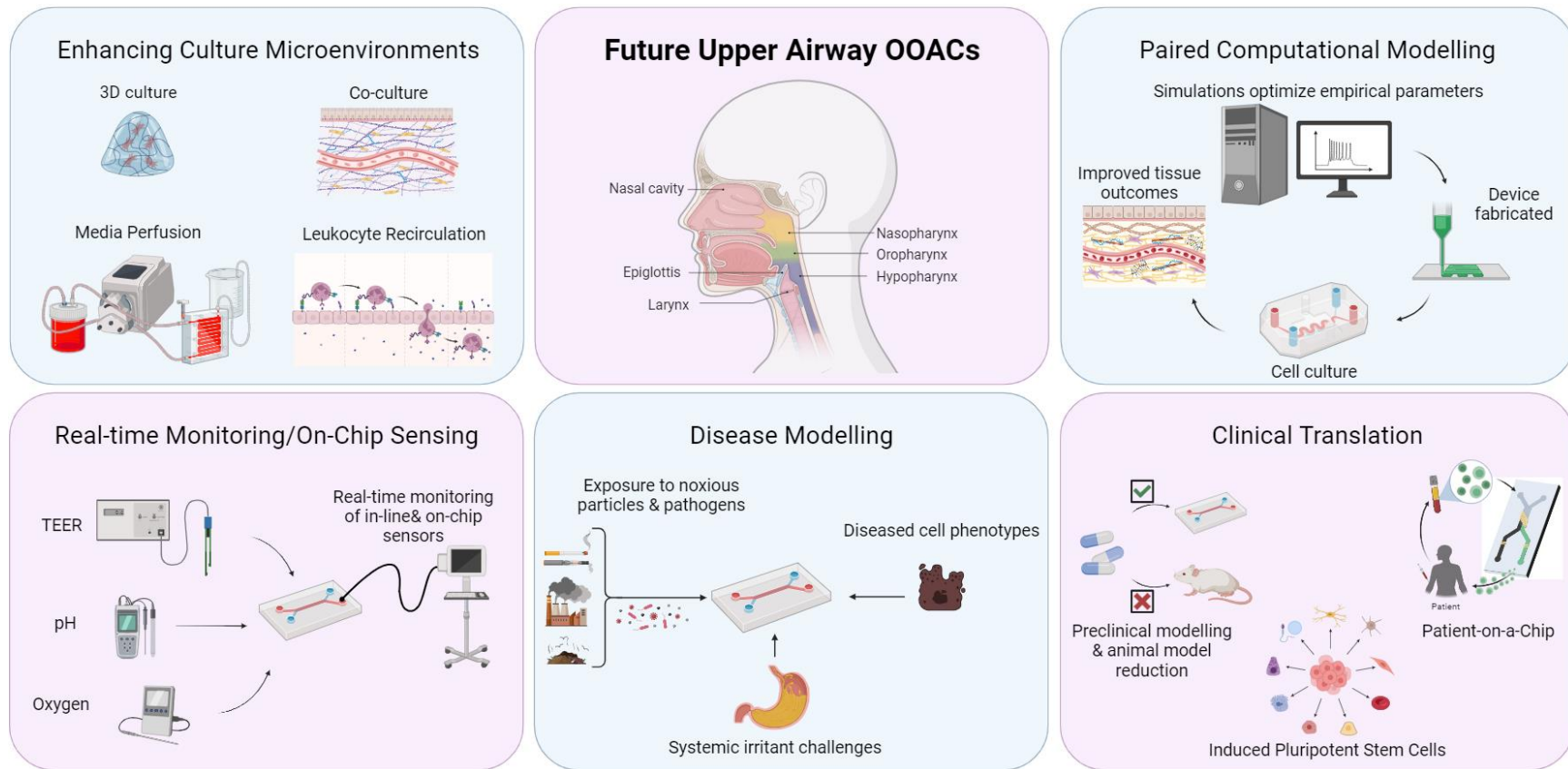


Figure 2.4. Areas of significant interest for upper airway research to fully exploit the potential of OOAC culture models. Created with BioRender.com.

Enhancing Culture Microenvironments

Microsystems proposed for the upper airway have been dominated by epithelial cell monocultures based on static media exchange. However, perfusion culture facilitates dynamic media replenishment and is crucial for supporting higher order biological processes including mimicking drug pharmacokinetics and supporting multiorgan coupling by fluidically linking separate tissue components.¹²⁰ Modelling perfusion and other complex biological factors in OOACs, such as 3D co-culture or mechanical stimulation, requires overcoming associated technical challenges related to their implementation. Integrating these microenvironmental parameters should be a key research focus given their importance to obtaining greater physiological relevance and predictive efficacy of upper airway models.

From a perfusion perspective, using a pump and tubing setup can be demanding to assemble aseptically. Furthermore, perfusion systems must be carefully monitored, as single-pass circuits can diminish localized signalling molecule concentrations whilst recirculating setups require a regular input of fresh medium. Failure to monitor these factors can inhibit tissue development and decrease cell viability. A further challenge for microfluidic culture is air bubble formation within the device or tubing lines, which can create significant stress on cells and alter their functionality, causing a loss of adherence and cell death.¹²¹ Finally, performing 3D co-culture requires optimizing biological conditions such as the use of a universal medium conducive to tissue development, and adapting the microfluidic device configuration. Inappropriate medium will restrict cell proliferation and differentiation whilst an unsuitable device configuration can cause 3D co-culture incompatibility.^{13,19}

Innovations in other research fields offer valuable insight for improving microenvironment recapitulation in upper airway OOACs.^{28,33,122,123} For example, one approach combining perfused microfluidic and organoid culture technologies found fluidic shear exerted on kidney microtissues increased tissue vascularization and maturation.¹²⁴ Elsewhere, an established technique to avoid air bubble introduction into cultures is to outfit perfusion systems with bubble traps.¹²⁵ Moreover, hydrogel-based setups can address the need for 3D co-culture OOACs and are particularly useful for modelling parenchymal tissues such as the lamina propria of upper airway mucosae.³³

Ultimately, fully replicating the multicellular environment and ECM structure of native upper airway tissues is not simple. The VF mucosa alone contains epithelial cells, fibroblasts,

myofibroblasts, Langerhans cells, and macrophages, along with highly specialized ECM architecture.^{92,126} Co-culturing that many cell types is unrealistic, as is incorporating all mechanical forces experienced *in vivo* by cells and ECM fibres. Instead, a more obtainable goal is for researchers to prioritize the specific biological architecture required for investigating their defined research questions.

Real-time Monitoring & Paired Computational Modelling

Given the progressive application and complexity of OOAC platforms, there is an expanding need for approaches integrating sensing systems to monitor microenvironmental changes in real-time.^{25,127} Access to a range of *in situ* data related to cell functions and microenvironmental parameters provides vital information for characterizing toxicant or pharmaceutical compound responses in a dynamic, non-invasive manner.¹²⁵ OOACs can be outfitted with sensors (e.g. electric, electrochemical, mechanical, optical) to probe tissue functionality, oxygen concentration, pH level, and molecular transport.^{128–131} Each sensor type has associated benefits and limitations. For instance, electrochemical sensors provide direct and rapid detection of biological events via an electrical signal and can quantify metabolites in a culture. In addition, the non-destructive assessment of epithelial and endothelial barrier integrity offered by electrochemical sensors is of critical interest for drug permeability studies. This was recently exploited in a nasal model that used a carbon nanofiber electrode for real-time monitoring of drug permeation across the epithelial barrier.^{55,56} In other research fields, optical sensors have gained notable popularity for use in OOAC systems due to their high sensitivity, miniaturization capacity, and reliable performance under a range of flow rates.¹³²

Despite the importance of long-term *in situ* evaluation of biochemical and biophysical parameters, effectively integrating sensors into OOAC systems remains a challenge. For example, electrochemical sensor reliability can be compromised by electrode position, size, biofouling, or biocompatibility.⁸¹ Meanwhile, optical sensors relying on dyes can influence cell metabolism, whilst serial measurement can induce photobleaching and phototoxicity.¹³³ Moreover, multiplexing with optical sensors is inherently limited by spectral overlap.¹³⁴ However, the difficulty of integrating multiple sensors is not restricted to optical sensing techniques. Fundamentally, the small fluid volumes of OOAC systems means interference between different sensors presents a significant design challenge.¹²⁷

Overall, integrating biosensors in an OOAC platform offers the opportunity to significantly increase the system throughput and complement conventional off-chip analytics such as immunostaining, histology, protein assays, and gene expression. A major benefit of access to expanded datasets is that they can be input into *in silico* models, which are powerful tools with several key advantages over empirical *in vitro* approaches. This includes the capacity to incorporate a wider range of experimental parameters, simulate long-term biological processes, and perform a large number of replicates over a much shorter timeframe.^{135,136} Using a combined approach of *in silico* and *in vitro* methods has been gaining momentum in upper airway research, principally as a method to study fluid flow interactions and patterns through OOAC setups to help optimize flow patterns and shear stress profiles.^{50,51,64} Fundamentally, increasing *in vitro* data output via the use of biosensors can strengthen the fidelity of projected tissue responses *in silico*. However, this also highlights a restriction of the approach as the complexity of the *in vitro* system is a limiting factor in the predictive power and physiological relevance of *in silico* models.

Future approaches combining *in silico* and *in vitro* methods could be applied to model the *in vivo* exposure route from the point of inhalation to cellular uptake.¹³⁷ For example, computing flow patterns of aerosolized drugs or airborne irritants within the upper airway could provide valuable insight into their adsorption and deposition profiles related to specific airway tract size and breathing rate.^{138–140} In turn, this could be used to inform an *in vitro* OOAC laryngeal model of the appropriate exposure dose.

Clinical Translation & Therapeutic Research

The capacity of OOACs to recapitulate upper airway tissue microenvironments holds considerable potential for patient-specific research on drug development for rare diseases and clinical experiments.^{123,141} For example, prospective therapies could be trialled in OOAC models using patient-specific cells to evaluate treatment efficacy prior to prescription. This approach may involve exploiting iPSC technology to derive almost any cell type via reprogramming a patient's own cells or, alternatively, culturing biopsies and pathogenic cells to create individual diseased tissue models.¹⁴² However, it should be noted whilst several weeks of culture is possible in OOAC models, there is a functional time window related to iPSC differentiation, which typically require at least 2-3 weeks of differentiation to mature into specific cell lineages.²⁸ As such, OOACs utilizing iPSC-derived cells should be carefully planned to be compatible with longer-term culture,

particularly if further iPSC differentiation and maturation is required after cell seeding in the device.

The application of OOAC technology for disease modelling in upper airway research has been dominated by head and neck cancer models thus far.^{44–47} However, non-cancerous disorders including laryngopharyngeal reflux, laryngitis, pharyngeal mucositis, VF scarring, allergic rhinitis, sinusitis, chronic cough, obstructive sleep apnoea, and reactive upper airway dysfunction syndrome represent just a few conditions possible to model in OOACs.^{143–148} An expanded repertoire of OOAC disease models could help elucidate the mechanisms related to the pathophysiology of upper airway disorders.¹⁴⁹

OOAC models offer the opportunity to overcome limitations associated with conventional disease models such as a static microenvironment or inaccurate dosages. Firstly, perfusion culture would improve tissue viability and is necessary for accurately mimicking compound toxicity and drug responses *in vivo*.¹²³ In addition, the provision of self-replenishing, perfused conditions enables OOAC cultures to be maintained for up to several weeks, allowing longer-term exposure studies.^{150–153} Notably, the study of ‘true’ chronic exposure (months to years) is beyond the current capabilities of OOAC technology. Such investigations remain reliant on epidemiological studies and animal experimentation. That said, implementing dynamic airflow in OOAC models grants compatibility with aerosolized therapeutic or irritant exposure, increasing the clinical relevance of the dose applied. This is of significant interest for airway research as nebulized drugs are the most common delivery format for inhalable therapeutics.¹⁵⁴

The benefits of OOAC technology in disease modelling applications has been effectively demonstrated in lower airway research. For instance, a lung-alveolus OOAC model was able to mimic lung pathogen-induced inflammation, including neutrophil migration and endothelium permeability.⁴⁰ Furthermore, a lung-airway OOAC model successfully simulated the cytokine hypersecretion of COPD patients in response to pathogens and cigarette smoke.^{39,48} These successes in lower airway OOACs demonstrate techniques applicable to upper airway models. For example, recirculating leukocytes through endothelial cell-lined microchannels would provide the prospect of studying diapedesis in response to pathogens or environmental irritants.

Multiorgan OOACs offer a powerful tool for studying the absorption, distribution, metabolism and excretion studies of pharmaceutical compounds, which could help streamline the

early phases of preclinical modelling reduce the quantity of statistically insignificant animal trials.¹²³ This is notable considering the exorbitant costs associated with drug development, with recent 2020 figures suggesting the cost of bringing a drug to market can reach \$2.8 billion USD.¹⁵⁵ Developing a multiorgan OOAC of the full respiratory airway tract (i.e. from nasal cavity to alveoli) would offer potential for studying initial exposure through to biological effect for inhalable nanomedicines targeting respiratory diseases such as pneumonia, lung cancer, and asthma.^{137,154} To better understand drug toxicity, this prospective multiorgan model could be extended to include liver and kidney tissues to incorporate their key functions in drug metabolism and excretion.^{41,123,156–158} Multiorgan approaches represent a growing research area that has seen as many as 10 coupled tissue components modelled.¹⁵⁹ Ultimately, multiorgan systems will play a prominent role in future upper airway OOAC research due to their impressive mimicry of complex physiological and pathophysiological responses.¹²³

Conclusions

OOAC models constitute a growing form of *in vitro* human experimentation providing physiologically relevant testing platforms for studying pathophysiological and pharmacological responses. This emerging technology offers a wealth of opportunities for significantly improving upon the repertoire of existing upper airway *in vitro* models applied for disease modeling, therapeutics development, and precision medicine. Areas of interest in the immediate future will likely address the scarcity of laryngeal and pharyngeal models, in addition to introducing greater automation and tissue complexity to current platforms, such as through perfusion and 3D co-culture respectively. Longer-term prospects should seek to combine multiple innovations, such as iPSC technology and real-time microenvironmental monitoring, into OOAC platforms to drive the expansion of personalized medicine approaches in the upper airway research field.

Author Contributions

PTC: Conceptualization, writing-original draft, reviewing and editing. NLJ: Conceptualization, writing-original draft, reviewing and editing, supervision, funding acquisition. XL, ST: Conceptualization, reviewing and editing.

Conflicts of Interest

The authors have no conflicts of interest to declare.

Acknowledgements

The authors acknowledge research grants from the National Sciences and Engineering Research Council of Canada (RGPIN-2018-03843 and ALLRP 548623-19), Canada Research Chair research stipend (NLJ), and by the National Institutes of Health (grant R01 DC-018577-01A1). The presented content is solely the responsibility of the authors and does not necessarily represent the official views of the above funding agencies.

References

1. Titze, I. R. Mechanical stress in phonation. *J. Voice* **8**, 99–105 (1994).
2. Sahin-Yilmaz, A. & Naclerio, R. M. Anatomy and physiology of the upper airway. *Proc. Am. Thorac. Soc.* **8**, 31–39 (2011).
3. Strohl, K. P., Butler, J. P. & Malhotra, A. Mechanical Properties of the Upper Airway. in *Comprehensive Physiology* vol. 2 1853–1872 (Wiley, 2012).
4. Kairaitis, K. *et al.* Pharyngeal mucosal wall folds in subjects with obstructive sleep apnea. *J. Appl. Physiol.* **118**, 707–715 (2015).
5. Horejs, C. Organ chips, organoids and the animal testing conundrum. *Nat. Rev. Mater.* **6**, 372–373 (2021).
6. Doke, S. K. & Dhawale, S. C. Alternatives to animal testing: A review. *Saudi Pharm. J.* **23**, 223–229 (2015).
7. Fricker, M., Deane, A. & Hansbro, P. M. Animal models of chronic obstructive pulmonary disease. *Expert Opin. Drug Discov.* **9**, 629–645 (2014).
8. Zeitels, S. M. *et al.* Vocal Fold Injection of Absorbable Materials: A Histologic Analysis With Clinical Ramifications. *Ann. Otol. Rhinol. Laryngol.* **128**, 71S–81S (2019).
9. Coburn, P. T., Li, X., Li, J., Kishimoto, Y. & Li-Jessen, N. Y. K. Progress in Vocal Fold Regenerative Biomaterials: An Immunological Perspective. *Adv. NanoBiomed Res.* **2100119**, (2021).
10. Alipour, F. & Jaiswal, S. Phonatory characteristics of excised pig, sheep, and cow larynges. *J. Acoust. Soc. Am.* **123**, 4572–4581 (2008).
11. Balls, M. Replacement of animal procedures: Alternatives in research, education and testing. *Lab. Anim.* **28**, 193–211 (1994).
12. Administration, U. S. F. & D. *FDA's Predictive Toxicology Roadmap*. <https://www.fda.gov/downloads/ScienceResearch/SpecialTopics/RegulatoryScience/UCM587831.pdf> (2020).
13. Duval, K. *et al.* Modeling Physiological Events in 2D vs. 3D Cell Culture. *Physiology* **32**, 266–277 (2017).
14. Catten, M., Gray, S. D., Hammond, T. H., Zhou, R. & Hammond, E. Analysis of cellular location and concentration in vocal fold lamina propria. *Otolaryngol. - Head Neck Surg.* **118**, 663–667 (1998).
15. Stockinger, A., Eger, A., Wolf, J., Beug, H. & Foisner, R. E-cadherin regulates cell growth by modulating proliferation-dependent β -catenin transcriptional activity. *J. Cell Biol.* **154**, 1185–1196 (2001).
16. Chen, X. & Thibeault, S. L. Biocompatibility of a synthetic extracellular matrix on immortalized vocal fold fibroblasts in 3D culture. *Acta Biomater.* **6**, 2940–2948 (2010).
17. Page, H., Flood, P. & Reynaud, E. G. Three-dimensional tissue cultures: Current trends and beyond. *Cell Tissue Res.* **352**, 123–131 (2013).
18. McCaffrey, L. M. & Macara, I. G. Epithelial organization, cell polarity and tumorigenesis.

- Trends Cell Biol.* **21**, 727–735 (2011).
19. Baker, B. M. & Chen, C. S. Deconstructing the third dimension-how 3D culture microenvironments alter cellular cues. *J. Cell Sci.* **125**, 3015–3024 (2012).
 20. Wang, F. *et al.* Reciprocal interactions between β 1-integrin and epidermal growth factor receptor in three-dimensional basement membrane breast cultures: A different perspective in epithelial biology. *Proc. Natl. Acad. Sci. U. S. A.* **95**, 14821–14826 (1998).
 21. Lee, M. K. *et al.* Air-liquid interface culture of serially passaged human nasal epithelial cell monolayer for in vitro drug transport studies. *Drug Deliv. J. Deliv. Target. Ther. Agents* **12**, 305–311 (2005).
 22. Ball, S. L., Mann, D. A., Wilson, J. A. & Fisher, A. J. The role of the fibroblast in inflammatory upper airway conditions. *Am. J. Pathol.* **186**, 225–233 (2016).
 23. Kieninger, J., Weltin, A., Flamm, H. & Urban, G. A. Microsensor systems for cell metabolism-from 2D culture to organ-on-chip. *Lab Chip* **18**, 1274–1291 (2018).
 24. Cooper, M., Charest, J. L. & Coppeta, J. Design principles for dynamic microphysiological systems. in *Microfluidic Cell Culture Systems* 1–29 (Elsevier, 2019).
 25. Wikswo, J. P. *et al.* Scaling and systems biology for integrating multiple organs-on-a-chip. *Lab Chip* **13**, 3496–3511 (2013).
 26. Liu, Z. *et al.* Human nasal epithelial organoids for therapeutic development in cystic fibrosis. *Genes (Basel)*. **11**, 1–17 (2020).
 27. Bhatia, S. N. & Ingber, D. E. Microfluidic organs-on-chips. *Nat. Biotechnol.* **32**, 760–772 (2014).
 28. Leung, C. M. *et al.* A guide to the organ-on-a-chip. *Nat. Rev. Methods Prim.* **2**, (2022).
 29. Manz, A., Graber, N. & Widmer, H. M. Miniaturized total chemical analysis systems: A novel concept for chemical sensing. *Sensors Actuators B Chem.* **1**, 244–248 (1990).
 30. Kopp, M. U., De Mello, A. J. & Manz, A. Chemical amplification: Continuous-flow PCR on a chip. *Science (80-.)*. **280**, 1046–1048 (1998).
 31. Duffy, D. C., McDonald, J. C., Schueller, O. J. A. & Whitesides, G. M. Rapid prototyping of microfluidic systems in poly(dimethylsiloxane). *Anal. Chem.* **70**, 4974–4984 (1998).
 32. Ingber, D. E. Developmentally inspired human ‘organs on chips’. *Development* **145**, dev156125 (2018).
 33. Bennet, T. J., Randhawa, A., Hua, J. & Cheung, K. C. Airway-On-A-Chip: Designs and Applications for Lung Repair and Disease. *Cells* **10**, 1602 (2021).
 34. Wu, Q. *et al.* Organ-on-a-chip: Recent breakthroughs and future prospects. *Biomed. Eng. Online* **19**, 1–19 (2020).
 35. Figeys, D. & Pinto, D. Lab-on-a-Chip: A Revolution in Biological and Medical Sciences. *Anal. Chem.* **72**, 330 A–335 A (2000).
 36. Haeberle, S. & Zengerle, R. Microfluidic platforms for lab-on-a-chip applications. *Lab Chip* **7**, 1094–1110 (2007).
 37. Whitesides, G. M. The origins and the future of microfluidics. *Nature* **442**, 368–373 (2006).
 38. Sosa-Hernández, J. E. *et al.* Organs-on-a-chip module: A review from the development and applications perspective. *Micromachines* **9**, (2018).
 39. Benam, K. H. *et al.* Small airway-on-a-chip enables analysis of human lung inflammation and drug responses in vitro. *Nat. Methods* **13**, 151–157 (2016).
 40. Huh, D. *et al.* Reconstituting Organ-Level Lung Functions on a Chip. *Science (80-.)*. **328**, 1662–1669 (2010).
 41. Wilmer, M. J. *et al.* Kidney-on-a-Chip Technology for Drug-Induced Nephrotoxicity

- Screening. *Trends Biotechnol.* **34**, 156–170 (2016).
42. Kim, H. J., Huh, D., Hamilton, G. & Ingber, D. E. Human gut-on-a-chip inhabited by microbial flora that experiences intestinal peristalsis-like motions and flow. *Lab Chip* **12**, 2165–2174 (2012).
 43. Huh, D., Hamilton, G. A. & Ingber, D. E. From 3D cell culture to organs-on-chips. *Trends Cell Biol.* **21**, 745–754 (2011).
 44. Yang, Q. *et al.* Design of organ-on-a-chip to improve cell capture efficiency. *Int. J. Mech. Sci.* **209**, 106705 (2021).
 45. Tanweer, F., Louise Green, V., David Stafford, N. & Greenman, J. Application of microfluidic systems in management of head and neck squamous cell carcinoma. *Head Neck* **35**, 756–763 (2013).
 46. Moya-Garcia, C. R. *et al.* In vitro models for head and neck cancer: Current status and future perspective. *Front. Oncol.* **12**, 1–26 (2022).
 47. Pillai, S., Kwan, J. C., Yaziji, F., Yu, H. & Tran, S. D. Mapping the Potential of Microfluidics in Early Diagnosis and Personalized Treatment of Head and Neck Cancers. *Cancers (Basel)*. **15**, 3894 (2023).
 48. Benam, K. H. *et al.* Matched-Comparative Modeling of Normal and Diseased Human Airway Responses Using a Microengineered Breathing Lung Chip. *Cell Syst.* **3**, 456–466 (2016).
 49. Wang, W. *et al.* Live human nasal epithelial cells (hNECs) on chip for in vitro testing of gaseous formaldehyde toxicity via airway delivery. *Lab Chip* **14**, 677–680 (2014).
 50. Shrestha, J. *et al.* A 3D-printed microfluidic platform for simulating the effects of CPAP on the nasal epithelium. *Biofabrication* **13**, (2021).
 51. Brooks, Z. *et al.* 3D printed transwell-integrated nose-on-chip model to evaluate effects of air flow-induced mechanical stresses on mucous secretion. *Biomed. Microdevices* **24**, 1–11 (2022).
 52. Li, Z. & Cui, Z. Three-dimensional perfused cell culture. *Biotechnol. Adv.* **32**, 243–254 (2014).
 53. Fröhlich, E. *et al.* Comparison of two in vitro systems to assess cellular effects of nanoparticles-containing aerosols. *Toxicol. Vitro.* **27**, 409–417 (2013).
 54. Polk, W. W., Sharma, M., Sayes, C. M., Hotchkiss, J. A. & Clippinger, A. J. Aerosol generation and characterization of multi-walled carbon nanotubes exposed to cells cultured at the air-liquid interface. *Part. Fibre Toxicol.* **13**, 1–12 (2016).
 55. Gholizadeh, H. *et al.* Real-time quantitative monitoring of in vitro nasal drug delivery by a nasal epithelial mucosa-on-a-chip model. *Expert Opin. Drug Deliv.* **18**, 803–818 (2021).
 56. Gholizadeh, H. *et al.* In vitro interactions of aerosol formulations with human nasal epithelium using real-time monitoring of drug transport in a nasal mucosa-on-a-chip. *Biosens. Bioelectron.* **223**, 115010 (2023).
 57. Byun, J. *et al.* Identification of urban particulate matter-induced disruption of human respiratory mucosa integrity using whole transcriptome analysis and organ-on-a chip. *J. Biol. Eng.* **13**, 88 (2019).
 58. Synvivo. SynALI 3D Lung Model Using Idealized Microvascular Network. *Technical protocol* www.synvivobio.com.
 59. Mehling, M. & Tay, S. Microfluidic cell culture. *Curr. Opin. Biotechnol.* **25**, 95–102 (2014).
 60. Young, E. W. K. K. & Beebe, D. J. Fundamentals of microfluidic cell culture in controlled microenvironments. *Chem. Soc. Rev.* **39**, 1036 (2010).

61. Na, K., Lee, M., Shin, H.-W. & Chung, S. In vitro nasal mucosa gland-like structure formation on a chip. *Lab Chip* **17**, 1578–1584 (2017).
62. Tajeddin, A. & Mustafaoglu, N. Design and Fabrication of Organ-on-Chips: Promises and Challenges. *Micromachines* **12**, 1443 (2021).
63. Brooks, Z. Mechanical Stresses On Nasal Mucosa Using Nose-On-Chip Model. *Master of Science Thesis; B.S.B.E., Wright State University* (2018).
64. Nof, E. *et al.* Human Multi-Compartment Airways-on-Chip Platform for Emulating Respiratory Airborne Transmission: From Nose to Pulmonary Acini. *Front. Physiol.* **13**, 1–18 (2022).
65. Halldorsson, S., Lucumi, E., Gómez-sjöberg, R. & Fleming, R. M. T. T. Advantages and challenges of microfluidic cell culture in polydimethylsiloxane devices. *Biosens. Bioelectron.* **63**, 218–231 (2015).
66. Yun, S. H. *et al.* Characterization and resolution of evaporation-mediated osmolality shifts that constrain microfluidic cell culture in poly(dimethylsiloxane) devices. *Anal. Chem.* **79**, 1126–1134 (2007).
67. Torino, S., Corrado, B., Iodice, M. & Coppola, G. PDMS-Based Microfluidic Devices for Cell Culture. *Inventions* **3**, 65 (2018).
68. Toepke, M. W. & Beebe, D. J. PDMS absorption of small molecules and consequences in microfluidic applications. *Lab Chip* **6**, 1484–1486 (2006).
69. Oomen, P. E., Skolimowski, M. D. & Verpoorte, E. Implementing oxygen control in chip-based cell and tissue culture systems. *Lab Chip* **16**, 3394–3414 (2016).
70. Regehr, K. J. *et al.* Biological implications of polydimethylsiloxane-based microfluidic cell culture. *Lab Chip* **9**, 2132–2139 (2009).
71. Lee, J. N., Jiang, X., Ryan, D. & Whitesides, G. M. Compatibility of mammalian cells on surfaces of poly(dimethylsiloxane). *Langmuir* **20**, 11684–11691 (2004).
72. Gencturk, E., Mutlu, S. & Ulgen, K. O. Advances in microfluidic devices made from thermoplastics used in cell biology and analyses. *Biomicrofluidics* **11**, (2017).
73. Kricka, L. J. *et al.* Fabrication of plastic microchips by hot embossing. *Lab Chip* **2**, 1–4 (2002).
74. Kim, M. Y., Li, D. J., Pham, L. K., Wong, B. G. & Hui, E. E. Microfabrication of high-resolution porous membranes for cell culture. *J. Memb. Sci.* **452**, 460–469 (2014).
75. Jabarin, S. A. & Lofgren, E. A. Thermal stability of polyethylene terephthalate. *Polym. Eng. Sci.* **24**, 1056–1063 (1984).
76. Xia, Y. & Whitesides, G. M. Soft Lithography. *Annu. Rev. Mater. Sci.* **28**, 153–184 (1998).
77. Diederichs, S. & Tuan, R. S. Functional Comparison of Human-Induced Pluripotent Stem Cell-Derived Mesenchymal Cells and Bone Marrow-Derived Mesenchymal Stromal Cells from the Same Donor. *Stem Cells Dev.* **23**, 1594–1610 (2014).
78. Howard, D., Buttery, L. D., Shakesheff, K. M. & Roberts, S. J. Tissue engineering: Strategies, stem cells and scaffolds. *J. Anat.* **213**, 66–72 (2008).
79. Chen, X. *et al.* Novel immortalized human vocal fold epithelial cell line: In vitro tool for mucosal biology. *FASEB J.* **35**, 1–16 (2021).
80. Shi, Y., Inoue, H., Wu, J. C. & Yamanaka, S. Induced pluripotent stem cell technology: A decade of progress. *Nat. Rev. Drug Discov.* **16**, 115–130 (2017).
81. Ahadian, S. *et al.* Organ-On-A-Chip Platforms: A Convergence of Advanced Materials, Cells, and Microscale Technologies. *Adv. Healthc. Mater.* **7**, 1700506 (2018).
82. Leydon, C., Selekmán, J. A., Palecek, S. & Thibeault, S. L. Human Embryonic Stem Cell-

- Derived Epithelial Cells in a Novel In Vitro Model of Vocal Mucosa. *Tissue Eng. Part A* **19**, 2233–2241 (2013).
83. Ling, C. *et al.* Bioengineered vocal fold mucosa for voice restoration. *Sci. Transl. Med.* **7**, (2015).
 84. Walimbe, T., Panitch, A. & Sivasankar, M. P. An in vitro scaffold-free epithelial-fibroblast coculture model for the larynx. *Laryngoscope* **127**, (2017).
 85. Lungova, V., Chen, X., Wang, Z., Kendzierski, C. & Thibeault, S. L. Human induced pluripotent stem cell-derived vocal fold mucosa mimics development and responses to smoke exposure. *Nat. Commun.* **10**, 4161 (2019).
 86. Lungova, V., Wendt, K. & Thibeault, S. L. Exposure to e-cigarette vapor extract induces vocal fold epithelial injury and triggers intense mucosal remodeling. *Dis. Model. Mech.* **15**, (2022).
 87. Grossmann, T. *et al.* Introducing a new type of alternative laryngeal mucosa model. *PLoS One* **18**, e0287634 (2023).
 88. Leydon, C., Imaizumi, M., Yang, D., Thibeault, S. L. & Fried, M. P. Structural and functional vocal fold epithelial integrity following injury. *Laryngoscope* **124**, 2764–2769 (2014).
 89. Samitas, K., Carter, A., Kariyawasam, H. H. & Xanthou, G. Upper and lower airway remodelling mechanisms in asthma, allergic rhinitis and chronic rhinosinusitis: The one airway concept revisited. *Allergy* **73**, 993–1002 (2018).
 90. Knight, D. A. & Holgate, S. T. The airway epithelium: Structural and functional properties in health and disease. *Respirology* **8**, 432–446 (2003).
 91. Benam, K. H. Disrupting Experimental Strategies for Inhalation Toxicology: The Emergence of Microengineered Breathing-Smoking Human Lung-on-a-Chip. *Appl. Vitro. Toxicol.* **4**, 107–114 (2018).
 92. Gray, S. D. Cellular physiology of the vocal folds. *Otolaryngol. Clin. North Am.* **33**, 679–697 (2000).
 93. Chen, X. & Thibeault, S. L. Characteristics of Age-Related Changes in Cultured Human Vocal Fold Fibroblasts. *Laryngoscope* **118**, 1700–1704 (2008).
 94. Azzi, S., Hebda, J. K. & Gavard, J. Vascular Permeability and Drug Delivery in Cancers. *Front. Oncol.* **3**, 1–14 (2013).
 95. Sato, K. Blood Vessels of the Larynx and Vocal Fold. in *Functional Histoanatomy of the Human Larynx* 287–303 (Springer Singapore, 2018).
 96. Tao, C., Jiang, J. J. & Czerwonka, L. Liquid Accumulation in Vibrating Vocal Fold Tissue: A Simplified Model Based on a Fluid-Saturated Porous Solid Theory. *J. Voice* **24**, 260–269 (2010).
 97. Latifi, N. *et al.* A Flow Perfusion Bioreactor System for Vocal Fold Tissue Engineering Applications. *Tissue Eng. Part C Methods* **22**, 823–838 (2016).
 98. Cartmell, S. H., Porter, B. D., García, A. J. & Guldberg, R. E. Effects of Medium Perfusion Rate on Cell-Seeded Three-Dimensional Bone Constructs in Vitro. *Tissue Eng.* **9**, 1197–1203 (2003).
 99. Domansky, K. *et al.* Perfused multiwell plate for 3D liver tissue engineering. *Lab Chip* **10**, 51–58 (2010).
 100. Pusch, J. *et al.* The physiological performance of a three-dimensional model that mimics the microenvironment of the small intestine. *Biomaterials* **32**, 7469–7478 (2011).
 101. Van Den Dolder, J. *et al.* Flow perfusion culture of marrow stromal osteoblasts in titanium

- fiber mesh. *J. Biomed. Mater. Res. - Part A* **64**, 235–241 (2003).
102. Cukierman, E., Pankov, R., Stevens, D. R. & Yamada, K. M. Taking Cell-Matrix Adhesions to the Third Dimension. *Science* (80-.). **294**, 1708–1712 (2001).
 103. Byun, C. K., Abi-Samra, K., Cho, Y. K. & Takayama, S. Pumps for microfluidic cell culture. *Electrophoresis* **35**, 245–257 (2014).
 104. Wei, F. *et al.* Changes in interstitial fluid flow, mass transport and the bone cell response in microgravity and normogravity. *Bone Res.* **10**, (2022).
 105. Chary, S. R. & Jain, R. K. Direct measurement of interstitial convection and diffusion of albumin in normal and neoplastic tissues by fluorescence photobleaching. *Proc. Natl. Acad. Sci. U. S. A.* **86**, 5385–5389 (1989).
 106. Polacheck, W. J., Charest, J. L. & Kamm, R. D. Interstitial flow influences direction of tumor cell migration through competing mechanisms. *Proc. Natl. Acad. Sci.* **108**, 11115–11120 (2011).
 107. Ivanov, K. P., Kalinina, M. K. & Levkovich, Y. I. Flow Velocity in Capillaries of Brain and Muscles Physiological Significance. *Microvasc. Res.* **22**, 143–155 (1981).
 108. Meng, F. *et al.* In vitro fluidic systems: Applying shear stress on endothelial cells. *Med. Nov. Technol. Devices* **15**, 100143 (2022).
 109. Ng, C. P., Hinz, B. & Swartz, M. A. Interstitial fluid flow induces myofibroblast differentiation and collagen alignment in vitro. *J. Cell Sci.* **118**, 4731–4739 (2005).
 110. Park, S. & Young, E. W. K. E-FLOAT: Extractable Floating Liquid Gel-Based Organ-on-a-Chip for Airway Tissue Modeling under Airflow. *Adv. Mater. Technol.* **6**, 2100828 (2021).
 111. Smyth, T. & Georas, S. N. Effects of ozone and particulate matter on airway epithelial barrier structure and function: a review of in vitro and in vivo studies. *Inhal. Toxicol.* **33**, 177–192 (2021).
 112. Savla, U., Sporn, P. H. S. & Waters, C. M. Cyclic stretch of airway epithelium inhibits prostanoid synthesis. *Am. J. Physiol.* **273**, 1013–1019 (1997).
 113. Shi, Z. D. & Tarbell, J. M. Fluid flow mechanotransduction in vascular smooth muscle cells and fibroblasts. *Ann. Biomed. Eng.* **39**, 1608–1619 (2011).
 114. Brown, W. S., Morris, R. J., Hollien, H. & Howell, E. Speaking fundamental frequency characteristics as a function of age and professional singing. *J. Voice* **5**, 310–315 (1991).
 115. Titze, I. R. On the relation between subglottal pressure and fundamental frequency in phonation. *J. Acoust. Soc. Am.* **85**, 901–906 (1989).
 116. Titze, I. R. *et al.* Design and validation of a bioreactor for engineering vocal fold tissues under combined tensile and vibrational stresses. *J. Biomech.* **37**, 1521–1529 (2004).
 117. Kutty, J. K. & Webb, K. Tissue engineering therapies for the vocal fold lamina propria. *Tissue Eng. Part B* **15**, (2009).
 118. Hirano, M., Kakita, Y., Ohmaru, K. & Kurita, S. *Structure and Mechanical Properties of the Vocal Fold*. *Speech and Language* vol. 7 (ACADEMIC PRESS, INC., 1982).
 119. Liu, M.-C. *et al.* Electrofluidic pressure sensor embedded microfluidic device: a study of endothelial cells under hydrostatic pressure and shear stress combinations. *Lab Chip* **13**, 1743 (2013).
 120. Ingber, D. E. Is it Time for Reviewer 3 to Request Human Organ Chip Experiments Instead of Animal Validation Studies? *Adv. Sci.* **7**, 1–15 (2020).
 121. Wang, Y. *et al.* Systematic prevention of bubble formation and accumulation for long-term culture of pancreatic islet cells in microfluidic device. *Biomed. Microdevices* **14**, 419–426

- (2012).
122. Low, L. A., Mummery, C., Berridge, B. R., Austin, C. P. & Tagle, D. A. Organs-on-chips: into the next decade. *Nat. Rev. Drug Discov.* **20**, 345–361 (2021).
 123. Ingber, D. E. Human organs-on-chips for disease modelling, drug development and personalized medicine. *Nat. Rev. Genet.* **23**, 467–491 (2022).
 124. Homan, K. A. *et al.* Flow-enhanced vascularization and maturation of kidney organoids in vitro. *Nat. Methods* **16**, 255–262 (2019).
 125. Zhang, Y. S. *et al.* Multisensor-integrated organs-on-chips platform for automated and continual in situ monitoring of organoid behaviors. *Proc. Natl. Acad. Sci. U. S. A.* **114**, E2293–E2302 (2017).
 126. Thompson, A. C. & Griffin, N. R. Langerhans cells in normal and pathological vocal cord mucosa. *Acta Otolaryngol.* **115**, 830–832 (1995).
 127. Wikswo, J. P. *et al.* Engineering Challenges for Instrumenting and Controlling Integrated Organ-on-Chip Systems. *IEEE Trans. Biomed. Eng.* **60**, 682–690 (2013).
 128. Jalili-Firoozinezhad, S. *et al.* A complex human gut microbiome cultured in an anaerobic intestine-on-a-chip. *Nat. Biomed. Eng.* **3**, 520–531 (2019).
 129. Li, X., George, S. M., Verneti, L., Gough, A. H. & Taylor, D. L. A glass-based, continuously zonated and vascularized human liver acinus microphysiological system (vLAMPS) designed for experimental modeling of diseases and ADME/TOX. *Lab Chip* **18**, 2614–2631 (2018).
 130. Henry, O. Y. F. *et al.* Organs-on-chips with integrated electrodes for trans-epithelial electrical resistance (TEER) measurements of human epithelial barrier function. *Lab Chip* **17**, 2264–2271 (2017).
 131. Maoz, B. M. *et al.* Organs-on-Chips with combined multi-electrode array and transepithelial electrical resistance measurement capabilities. *Lab Chip* **17**, 2294–2302 (2017).
 132. Shaegh, S. A. M. *et al.* A microfluidic optical platform for real-time monitoring of pH and oxygen in microfluidic bioreactors and organ-on-chip devices. *Biomicrofluidics* **10**, (2016).
 133. Wikswo, J. P. The relevance and potential roles of microphysiological systems in biology and medicine. *Exp. Biol. Med.* **239**, 1061–1072 (2014).
 134. Eklund, S. E. *et al.* Multianalyte microphysiometry as a tool in metabolomics and systems biology. *J. Electroanal. Chem.* **587**, 333–339 (2006).
 135. Even-Tzur, N., Kloog, Y., Wolf, M. & Elad, D. Mucus secretion and cytoskeletal modifications in cultured nasal epithelial cells exposed to wall shear stresses. *Biophys. J.* **95**, 2998–3008 (2008).
 136. Zhao, K. & Jiang, J. What is normal nasal airflow? A computational study of 22 healthy adults. *Int. Forum Allergy Rhinol.* **4**, 435–446 (2014).
 137. EPA. Exposure Assessment Tools by Routes - Inhalation. *US Environmental Protection Agency* <https://www.epa.gov/expobox/exposure-assessment-tools-routes-inhalation> (2023).
 138. Zhang, Z. & Kleinstreuer, C. Airflow structures and nano-particle deposition in a human upper airway model. *J. Comput. Phys.* **198**, 178–210 (2004).
 139. Zhang, T., Gao, B., Zhou, Z. & Chang, Y. The movement and deposition of PM_{2.5} in the upper respiratory tract for the patients with heart failure: an elementary CFD study. *Biomed. Eng. Online* **15**, 138 (2016).
 140. Hinderliter, P. M. *et al.* ISDD: A computational model of particle sedimentation, diffusion and target cell dosimetry for in vitro toxicity studies. *Part. Fibre Toxicol.* **7**, 36 (2010).

141. Park, S. E., Georgescu, A. & Huh, D. Organoids-on-a-chip. *Science* (80-.). **364**, 960–965 (2019).
142. Jodat, Y. A. *et al.* Human-Derived Organ-on-a-Chip for Personalized Drug Development. *Curr. Pharm. Des.* **24**, 5471–5486 (2019).
143. Shusterman, D. The Effects of Air Pollutants and Irritants on the Upper Airway. *Proc. Am. Thorac. Soc.* **8**, 101–105 (2011).
144. Park, M., Lee, J. S. & Park, M. K. The Effects of Air Pollutants on the Prevalence of Common Ear, Nose, and Throat Diseases in South Korea: A National Population-Based Study. *Clin. Exp. Otorhinolaryngol.* **12**, 294–300 (2019).
145. Schwarzbach, H. L., Mady, L. J. & Lee, S. E. What is the Role of Air Pollution in Chronic Rhinosinusitis? *Immunol. Allergy Clin. North Am.* **40**, 215–222 (2020).
146. Liu, D., Qian, T., Sun, S. & Jiang, J. J. Laryngopharyngeal reflux and inflammatory responses in mucosal barrier dysfunction of the upper aerodigestive tract. *J. Inflamm. Res.* **13**, 1291–1304 (2020).
147. Meggs, W. J. Rads and Ruds the Toxic Induction of Asthma and Rhinitis. *J. Toxicol. Clin. Toxicol.* **32**, 487–501 (1994).
148. Perkner, J. J. *et al.* Irritant-Associated Vocal Cord Dysfunction. *J. Occup. Environ. Med.* **40**, 136–143 (1998).
149. Shrestha, J. *et al.* Lung-on-a-chip: the future of respiratory disease models and pharmacological studies. *Crit. Rev. Biotechnol.* **40**, 213–230 (2020).
150. Deinhardt-Emmer, S. *et al.* SARS-CoV-2 Causes Severe Epithelial Inflammation and Barrier Dysfunction. *J. Virol.* **95**, (2021).
151. Nawroth, J. C. *et al.* A Microengineered Airway Lung Chip Models Key Features of Viral-induced Exacerbation of Asthma. *Am. J. Respir. Cell Mol. Biol.* **63**, 591–600 (2020).
152. Xiao, S. *et al.* A microfluidic culture model of the human reproductive tract and 28-day menstrual cycle. *Nat. Commun.* **8**, (2017).
153. Chou, D. B. *et al.* On-chip recapitulation of clinical bone marrow toxicities and patient-specific pathophysiology. *Nat. Biomed. Eng.* **4**, 394–406 (2020).
154. Yue, L. *et al.* Inhaled drug delivery: Past, present, and future. *Nano Today* **52**, 101942 (2023).
155. Wouters, O. J., McKee, M. & Luyten, J. Estimated Research and Development Investment Needed to Bring a New Medicine to Market, 2009-2018. *JAMA - J. Am. Med. Assoc.* **323**, 844–853 (2020).
156. Ronaldson-Bouchard, K. & Vunjak-Novakovic, G. Organs-on-a-Chip: A Fast Track for Engineered Human Tissues in Drug Development. *Cell Stem Cell* **22**, 310–324 (2018).
157. Ramme, A. P. *et al.* Autologous induced pluripotent stem cell-derived four-organ-chip. *Futur. Sci. OA* **5**, (2019).
158. Chang, S.-Y. *et al.* Human liver-kidney model elucidates the mechanisms of aristolochic acid nephrotoxicity. *JCI Insight* **2**, 1–14 (2017).
159. Edington, C. D. *et al.* Interconnected Microphysiological Systems for Quantitative Biology and Pharmacology Studies. *Sci. Rep.* **8**, 1–18 (2018).

Supporting Information

Table S2.1. Upper airway microphysiological systems.

Application	Culture	Cell Type	Culture Dimensionality	ALI	Airflow	Culture length	Perfusion Culture	Mechanical Stimulation	Innovation	Reference
Formaldehyde toxicity	Monoculture	Nasal epithelial stem cells	2D	Yes	Syringe pump: 200 μ L/min ^b	35 days	N/A	N/A	Gaseous irritant	Wang et al. (2014) ⁴⁹
Allergic rhinitis / Chronic sinusitis	Co-culture	Nasal epithelial cells Vascular endothelial cells	2D	Yes	N/A	4 days	N/A	Hydrostatic pressure: 46.8 Pa	Tissue-tissue interface	Na et al. (2017) ⁶¹
Particulate matter toxicity	Tri-culture	Nasal epithelial cells Lung fibroblasts ^a Vascular endothelial cells	2D	No	N/A	4 days	N/A	N/A	Stromal tissue	Byun et al. (2019) ⁵⁷
Drug transport	Monoculture	Nasal epithelial cell line (RPMI 2650)	2D	Yes	N/A	21 days	N/A ^c	N/A ^c	On-chip sensing	Gholizadeh et al. (2021) ⁵⁵
					Nebulizer: 0.5 L/min, 1.7 L/min	14 days	N/A	Shear stress (airflow): 0.23 Pa, 0.78 Pa		Gholizadeh et al. (2023) ⁵⁶
Sleep apnea	Monoculture	Nasal epithelial cell line (RPMI 2650)	2D	Yes	Pressure controller: 5-20 cm H ₂ O	11 days	Syringe pump: 200 μ L/h	Shear stress (airflow): Not reported	Turbulent airflow	Shrestha et al. (2021) ⁵⁰
Nasal physiology	Monoculture	Nasal epithelial cell line (RPMI 2650)	2D	Yes	Mass flow controller: 4L/min	5-7 days	N/A	Shear stress (airflow): 1.0 dyn/cm ²	Bidirectional airflow	Brooks et al. (2022) ⁵¹
Respiratory infection	Tri-culture	Nasal epithelial cell line (RPMI 2650) Bronchial epithelial cell line (Calu-3) Alveolar epithelial cell line (hAELVi)	2D	Yes	Peristaltic pump: 0.2-6.5 mL/min	21-28 days	N/A	Shear stress (airflow): Not reported	Multi-organ system	Nof et al. (2022) ⁶⁴

^aUsed lung fibroblast cell line (WI-38) prior to primary lung fibroblasts

^bAirflow applied only during formaldehyde exposure

^cPhosphate buffer was perfused through non-cellular device compartment at 0.5 mL/min during ibuprofen challenge only and generated a wall shear stress of 0.04 dyn/cm²

Preface to Chapter 3: Replicating Vocal Fold Mucosa Anatomy *In Vitro*

Human communication is an essential component of our social wellbeing and quality of life. Voice disorders pose a growing global health problem due to their detrimental effect on individual health, occupational function, and societal productivity. They affect nearly 30% of the general population and 80% of occupational voice users worldwide.^{1,13–15} For instance, between 2004 and 2008, dysphonia reportedly impacted over 500,000 patients in a United States medical claims database.¹⁶ The financial burden of voice disorders is substantial, with incurred healthcare and workplace productivity costs estimated to exceed \$11 billion in the United States alone.^{1–3}

The overwhelming majority of voice disorders are attributed to detrimental changes in the VF mucosa caused either by physical injury or inflammatory activity related to environmental challenges.¹⁷ Improved understanding of the molecular mechanisms underlying pathological changes in the VF mucosa will facilitate the development of the next generation of therapeutics for voice disorders.

Human Vocal Fold Mucosa

The human vocal fold (VF) mucosa is a layered structure composed of three distinct regions, namely, the epithelium, basement membrane, and lamina propria (**Figure 3.1**).¹⁸ Mucosal tissue forms the principal vibratory portion of the VFs and is thus fundamental to voice production.

Maintaining a homeostatic local microenvironment is key to preserving VF health and function. In particular, protection of the vulnerable lamina propria is essential as disruption to its tissue architecture can have serious consequences for the phonatory capacity of the VFs.

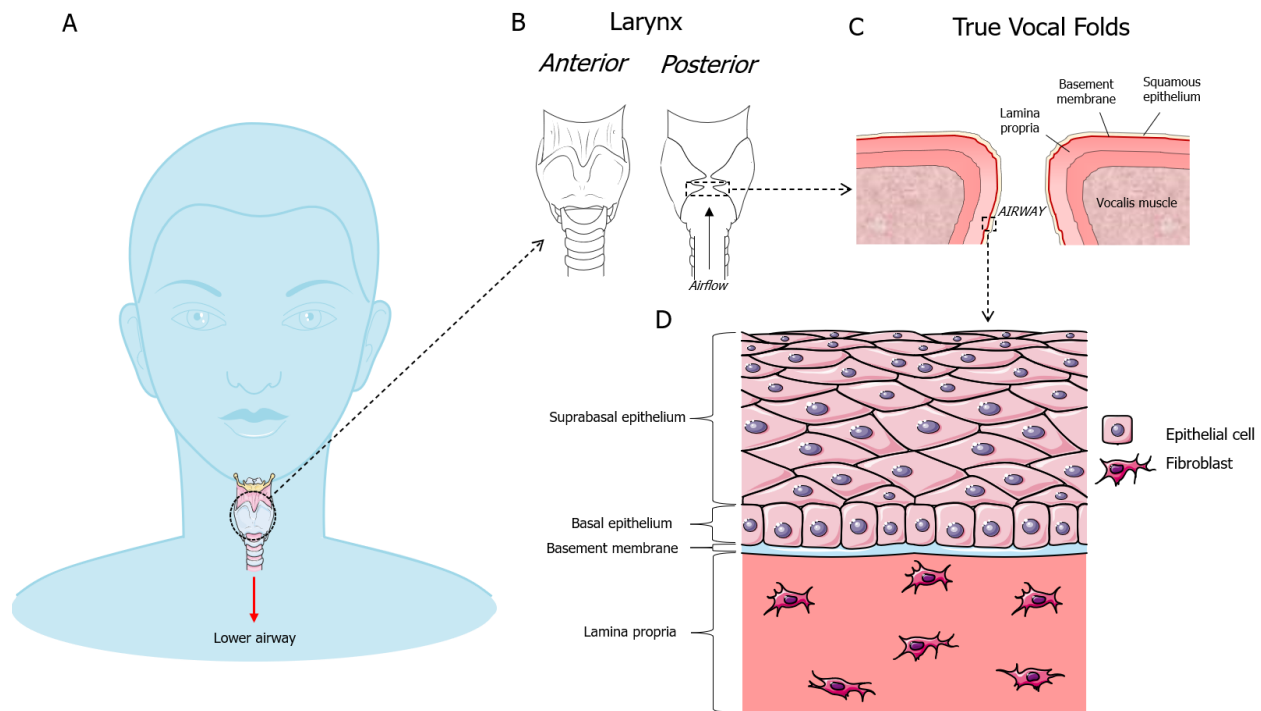


Figure 3.1. Human VF anatomy and cellular composition. (A) Anatomical position of the larynx. (B) Location of true VFs within the larynx. (C) Layered structure of true VFs in coronal section. (D) Arrangement of epithelial cells and fibroblasts within the VF mucosa. Figure adapted from ¹⁹ and made using Servier Medical Art templates, which are licensed under a Creative Commons Attribution 3.0 Unported License.

Vocal Fold Epithelium

The multilayered VF epithelium provides a protective barrier for the deeper VF tissue layers against potential hazards.^{20,21} These can take many forms, primarily including environmental challenges (e.g., irritants, allergens, pathogens), or systemic challenges (e.g. drying, acid reflux).⁸ VF epithelium comprises an underlying basal layer supporting 5-10 suprabasal layers of stratified, squamous cells (**Figure 3.1D**).^{8,22,23} The basement membrane lies below the basal epithelium and is a thin, sheet-like layer of proteins connecting the epithelium and lamina propria via collagenous structures.^{20,24,25} Upon injury to the VF epithelium, pores traversing the basement membrane enable immune cell migration to facilitate debris clearance and tissue repair.^{24,26,27}

The luminal surface of the epithelium is covered by microvilli to increase surface area and retain mucus to help maintain hydration and promote normal voice quality.^{20,28–30} Epithelial cell junctions, including tight, anchoring, and communicating junctions, control cell-cell and cell-basement membrane adherence.^{8,27,31} These cell junctions are crucial in operating the transcellular

and paracellular signalling pathways of the epithelium, which respectively regulate ion transport and barrier integrity.³²

Lamina Propria

Located under the basement membrane, the lamina propria confers tensile strength, elasticity, and compressibility to VF tissue and contains polysaccharides, collagens, minerals, and water.^{20,33–35} Whilst the lamina propria contains a more diverse cell population than the VF epithelium, cellular distribution is sparse. The most prevalent cells are VF fibroblasts, which maintain tissue homeostasis and regulate proliferation, migration, and differentiation of local cells via synthesis of glycosaminoglycans, proteoglycans, elastin, and collagen.^{20,36,37} When activated, VF fibroblasts undergo a transition to myofibroblasts that engage in wound contracture, scar tissue formation, and fibrosis.^{20,38}

The spatial arrangement of extracellular matrix (ECM) proteins in the lamina propria underpins the highly specialized biomechanical properties of the VFs. Prominent ECM components include collagen, elastin, and hyaluronic acid (HA), which impart tensile strength, elasticity, and viscoelasticity to the VFs.^{34,39,40}

In Vitro Vocal Fold Mucosa Models

In vitro models are a preclinical tool for investigating VF mucosa biology in health and disease. Whilst animal models remain the ‘gold standard’, anatomical, economic, and ethical obstacles persist regarding their use and efficacy in VF research.^{19,41–45} Conversely, *in vitro* models offer an inexpensive alternate with the capacity to incorporate patient-specific cells and high-throughput techniques.

A significant challenge for *in vitro* VF mucosa models is mimicking the native tissue microenvironment. The simplest methods use VF fibroblast monocultures plated on plastic or glass surfaces coated with collagen to improve cell attachment.⁴⁶ 2D cell culture provides a rapid, user-friendly method for quantifying cellular responses but is a substantial oversimplification of *in vivo* conditions including cell signalling, concentration gradients, and biomechanical cues.⁴⁷

3D co-culture in transwell inserts provides an alternative *in vitro* VF mucosa model. Typically, VF fibroblasts are embedded in a collagen gel with epithelial cells seeded atop the gel.

After several days of co-culture, media is removed from the insert to initiate an air-liquid interface (ALI) to stimulate epithelium differentiation. The introduction of paracellular signalling between epithelial cells and fibroblasts stimulates tissue development and homeostasis regulation in cultivated VF mucosae.^{7,48} Furthermore, culturing cells in 3D provides chemical and spatial complexity that better regulates cellular processes including apoptosis, migration, proliferation, polarization and differentiation.⁴⁹

Despite their uses, transwell models have several inherent design limitations. Firstly, the fluid volumes used significantly exceed those found *in vivo* causing inaccurate physiological scaling that can contribute to erroneous simulations of drug or toxins responses.^{50,51} Secondly, transwell VF mucosa models are incompatible with media perfusion. This creates a static microenvironment with unstable concentration gradients and restricted mass transport, which constrains tissue development.⁵² Finally, the absence of mechanical stimulation in transwell models is unrepresentative of the biomechanically active native VF mucosa microenvironment.

Organ-on-a-Chip Platforms

Advances in microfluidic science and microfabrication technology have led to the creation of *in vitro* models known as organ-on-a-chip (OOAC), which are biomimetic culture systems housed in a microfluidic device. OOACs offer superior performance and clinical relevance versus conventional methods due to better recapitulating the dynamism of the *in vivo* microenvironment. This includes relevant cell-media ratios, perfusion-based media exchange, and mechanical stimulation.⁵³

Thus far, OOAC technology has not been applied for cultivating the VF mucosa. However, the successful development of OOACs modelling lower airway tissues (alveoli, lung, bronchi, trachea) suggests the technology holds considerable potential for use in VF research.⁵⁴ The assembly of a VF mucosa OOAC (VF-OOAC) could provide a preclinical testing platform with improved *in vivo* mimicry at cell, tissue, and organ levels than current VF mucosa *in vitro* systems. Successful development of a VF-OOAC would provide the field of laryngology with a valuable tool for disease modeling, therapeutics development, and precision medicine.⁵⁵

Chapter 3. Investigating the Impact of Dimensionality, Physiological Scaling, Perfusion, and Fluidic Shear for Microengineering Vocal Fold Mucosae in Microfluidic Culturing Platforms

Patrick T. Coburn^a, Vlasta Lungova^b, Xinyu Liu^c, Susan L. Thibeault^b, Nicole Y. K. Li-Jessen^{a,d,e,f,†}

a. School of Communication Sciences and Disorders, McGill University, Canada

b. Department of Surgery, Division of Otolaryngology – Head and Neck Surgery, University of Wisconsin, Madison, WI, USA

c. Department of Mechanical Engineering, University of Toronto, Canada

d. Department of Biomedical Engineering, McGill University, Canada

e. Department of Otolaryngology – Head & Neck Surgery, McGill University, Canada

f. Research Institute of McGill University Health Centre, Canada

† Corresponding author

Abstract

The primary goal of this study was to engineer a human vocal fold mucosa organ-on-a-chip (VF-OOAC) and identify culture parameters key to the microtissue's growth. Innovations in microfluidic technology have led to biomimetic OOAC culture systems that can reproduce aspects of the native tissue microenvironment such as interstitial flow, paracrine signalling and concentration gradients. OOAC design parameters including physiological scaling, dimensionality, perfusion, and fluidic shear, require specifying when emulating individual organs.

This study performed a comprehensive VF-OOAC design evaluation by varying culture dimensionality, controlling microfluidic flow in cell-lined microchannels, and contrasting tissue growth against conventional transwell models. Primary vocal fold fibroblasts and immortalized laryngeal epithelial cells were co-cultured in individual systems for up to 15 days. Immunohistochemistry, immunocytochemistry, qPCR, and TEM were applied for characterizing the structure and functionality of derived vocal fold mucosae.

Compared to transwell controls, microfluidic cultures had higher functional gene expression related to gap junctions and hyaluronic acid synthesis. Microfluidic 3D cultures also expressed elevated tight junction and mucin expression whilst supporting greater epithelial polarization. Perfusion importance in stimulating basal epithelia activity was also noted. Fibroblast morphological changes and upregulation of mechanosensitive genes were observed in response to

fluidic shear. Using advanced microfluidic technology, this study identified culturing parameters fundamental to engineering VF mucosa microtissue. The proposed platform offers a versatile tool for future use in basic research related to VF mucosa health and disease.

Introduction

Located in the larynx, human vocal folds (VFs) regulate multiple vital daily functions including speaking, breathing and swallowing. VFs have a layered mucosal structure with distinctive cell populations and extracellular matrix (ECM) constituents. VF mucosa consists of squamous epithelium and lamina propria connected by a basement membrane.¹ The squamous epithelium is stratified and composed of 5-10 layers of epithelial cells that provide a protective barrier for the underlying lamina propria.^{2,3} The basal epithelial layer is anchored to the basement membrane that connects the epithelium and lamina propria via collagenous structures.⁴ Within the lamina propria, VF fibroblasts are the most abundant cell population and control tissue homeostasis, synthesize ECM, and modulate local inflammatory activity.⁵⁻⁷ Collagen, elastin, and hyaluronic acid (HA) are found throughout the ECM to confer tensile strength and elasticity to the tissue.⁸

Pre-clinical studies, including animal and cell culture models, have been the primary experimentation method in both basic and clinical research. However, animal models provide limited information applicable to human tissues due to significant physiological differences.⁹⁻¹¹ Moreover, the high cost of breeding, housing, and performing lengthy protocols limits animal model availability.¹² Ethical concerns also persist, with organizations such as the National Centre for the Replacement, Refinement, and Reduction of Animals in Research emphasizing the need to develop biomimetic culture platforms.^{13,14}

Developing biomimetic *in vitro* models is a growing area in VF biology and pre-clinical research.¹⁵ Bioengineering the human VF mucosa necessitates, at the minimum, cultivating its two dominant cell populations, epithelial cells and fibroblasts.¹⁶ Previous VF mucosa models using these cell types have relied on transwell systems that have shown particular promise for simulating human responses to irritants.¹⁷⁻¹⁹ For instance, Lungova et al. developed a co-culture model of the VF mucosa with morphological and genetic similarities to native VF tissue.¹⁸ This mucosa

demonstrated a clinically relevant inflammatory response to cigarette smoke extract, including IL6/IL8 upregulation and increased mucus production.

However, transwell models have a limited capacity for mimicking physiological tissue microenvironments. They use unrepresentative cell-media ratios that provide cells with fluid volumes that can exceed native tissue by up to 1000 times.²⁰ This inaccurate physiological scaling contributes to transwell models mischaracterizing irritant or drug responses versus clinical observations.²¹ The static microenvironment of transwell cultures also restricts metabolite diffusion speed, leading to cellular morphology and proliferation rates that may diverge from native tissue.²²

Bioreactors²³ and magnetic nanoparticles²⁴ have been proposed to engineer 3D VF constructs but have yet to advance beyond VF fibroblast monocultures. Innovations in microsystems engineering have led to organ on-a-chip (OOAC) platforms, which are biomimetic culture systems housed in a microfluidic chip.^{25–27} OOAC models have been proposed for a range of tissues including the lung^{27,28}, kidney²⁹, liver^{30–33}, heart^{34,35}, and blood-brain barrier^{36–38}. The success of these models in recapitulating tissue structure and functionality is attributable to the advantages they offer over conventional culturing techniques.

By cultivating cells at the microscale, OOACs provide cell-media ratios representative of native tissue, which facilitates paracrine signalling at *in vivo* levels due to small-volume effects.^{39–41} Integrating relevant physiological scaling also minimizes metabolite dilution, which increases the speed of cellular responses compared to conventional macroscale culture.⁴¹ Although models of other airway mucosa utilizing appropriate physiological scaling have reported improved tissue development, the effects for the VF mucosa have yet to be studied.^{42–44}

Culture dimensionality is an important consideration for *in vitro* model development because of the significant difference between cellular processes that occur in 2D vs 3D including apoptosis, migration, proliferation, and differentiation.⁴⁵ Transwell 3D culture currently offers the most effective method for cultivating VF mucosa tissue with morphological and genetic features of native tissue.^{17–19,46–48} Adapting these established culture protocols for use in an OOAC system could merge the microfluidic advantages of small volumes and minimal dilution with the *in vivo*-like behavior provided by 3D cell culture.⁴⁹

Perfusion is a prominent feature of many OOAC models via the passage of culture medium through the cell-lined microchannels of the chip using either active or passive pump systems.³⁹ In OOACs, perfusion maintains a stable concentration gradient for oxygen, carbon dioxide, nutrients, and waste convective transport.^{50,51} Perfusion of a VF fibroblast monoculture in a bioreactor setup was found to aid pH and cell viability maintenance.⁵² For other cell types such as osteoblasts^{53,54}, gut epithelial cells⁵⁵, and hepatocytes⁵⁶, perfusion had beneficial effects on cell viability^{54,56}, polarization⁵⁵, morphology⁵⁵, proliferation^{53,54}, differentiation⁵³, and ECM synthesis⁵³. Empirically evaluating the effect of perfusion in a VF-OOAC could highlight its importance for mucosal tissue development. At present, this information can only be inferred based on findings from other human tissues.

OOAC systems offer the flexibility to include mechanical stimuli that can initiate cellular mechanotransduction representative of the native tissue microenvironment.⁵⁷ A prominent force experienced by cells *in vivo* is fluidic shear, which occurs during the passage of bodily fluids or airflow parallel to the surfaces of cells. Fluidic shear's importance has been highlighted for fibroblast-myofibroblast behaviour, where its regulation of TGF- β 1 expression helps control the transition.⁵⁸ Shear effects have been examined in VF bioreactor setups via an airflow and media perfusion⁵², or rheometry⁵⁹. Although quantitative evidence was limited, shear stress appears to be a key factor in collagen synthesis for VF fibroblasts.⁵² However, as these culture systems did not include VF epithelial cells, the impact of fluidic shear on VF mucosa development has yet to be fully elucidated.

Airway-related OOAC models have been shown to recapitulate tissue structure and functionality surpassing that of transwell culture.^{60,61} For instance, a lung-alveolus OOAC was able to mimic lung pathogen-induced inflammation, including neutrophil migration and endothelium permeability.²⁸ Separately, a lung-airway OOAC successfully simulated cytokine hypersecretion of COPD patients in response to pathogens and cigarette smoke.^{27,62}

Despite success in modelling lower airway tissues, microfluidic technology has rarely been applied for upper airway organs, including the nasal cavity, pharynx, and larynx. The limited number of studies published have focused on simulating the nasopharyngeal response to environmental irritants^{43,63}, allergens⁴⁴, and drug therapeutics⁶⁴. However, these models had a

restricted capacity for replicating physiological responses as they were based on 2D monocultures or lacked perfusion and thus may not be translatable to VF applications.

The primary goal of this study was to microengineer a VF-OOAC platform to mimic structural and functional features of native tissue. A range of microfluidic culture setups were contrasted to investigate the effects of physiological scaling, culture dimensionality, perfusion, and fluidic shear on VF mucosal development. The finalized VF-OOAC is anticipated to produce a VF mucosa with tissue architecture exceeding that of conventional transwell culture.

Materials & Methods

Multiple culture setups were used to systematically compare the four parameters of interest, namely, physiological scaling, dimensionality, perfusion, fluidic shear (**Figure 4.1**). These comparisons were designed to isolate the individual effects of each parameter on VF mucosa tissue development. It was hypothesized each parameter would stimulate increased structural and functional development in the cultivated VF mucosa (**Table 4.1**).

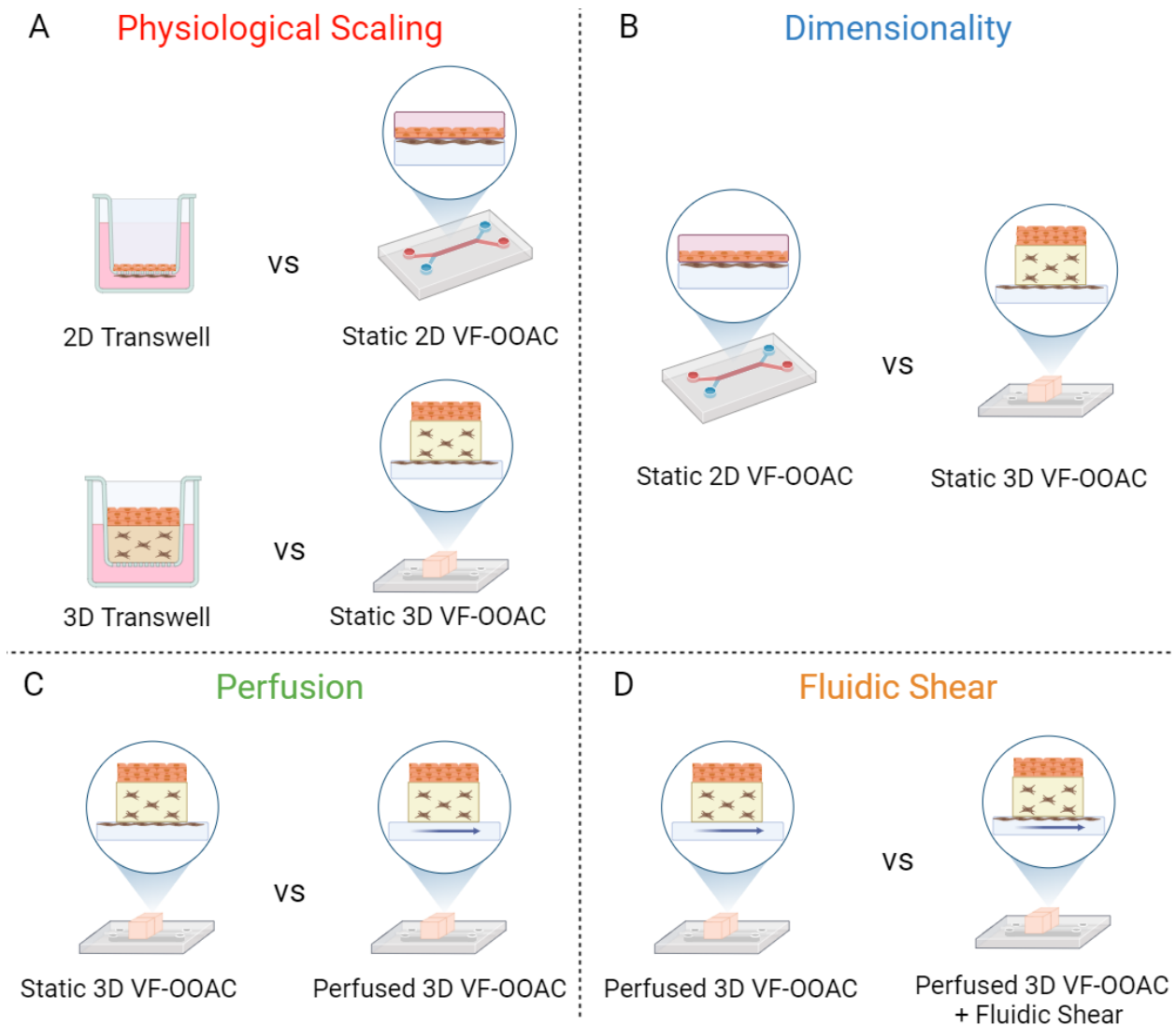


Figure 4.1. Study design overview. The influence of multiple culture parameters on structural and functional development of VF mucosae was systematically evaluated. (A) The effect on tissue development of cultivating VF mucosae in microscale systems was assessed in 2D and 3D setups. (B) Prospective static VF-OOAC culture systems were compared to determine how dimensionality influences VF mucosa growth. (C) Perfusion was integrated into the 3D VF-OOAC to determine tissue culture benefits. (D) By incorporating fluidic shear into the 3D VF-OOAC setup, the effect of mechanical stimulation on tissue development was examined.

Table 4.1. Six unique setups were applied in this study. Physiological scaling was examined in the context of 2D or 3D culture by comparing two different VF-OOAC designs with relevant transwell controls. Dimensionality was inspected by comparing both VF-OOAC designs. Perfusion was integrated into the VF-OOAC design that provided the greatest tissue development up to this point. Finally, fluidic shear was added to the perfused model.

Parameter	Model Comparison(s)	Anticipated Outcomes
Physiological Scaling	2D Transwell vs Static 2D VF-OOAC	Microscale culture will facilitate greater structural and functional tissue development ⁶⁵
	3D Transwell vs Static 3D VF-OOAC	

Dimensionality	<i>Static 2D VF-OOAC</i> vs <i>Static 3D VF-OOAC</i>	3D culture will enhance cell polarization ^{45,66-68}
Perfusion	<i>Static 3D VF-OOAC</i> vs <i>Perfused 3D VF-OOAC</i>	Perfusion will stimulate differentiation and proliferation ^{39,69}
Fluidic Shear	<i>Perfused 3D VF-OOAC</i> vs <i>Perfused 3D VF-OOAC + Fluidic Shear</i>	Fluidic shear will promote mechanosensitive gene expression ⁷⁰⁻⁷⁷

Cell Culture Maintenance

Vocal Fold Fibroblast Culture

Human primary VF fibroblast (pVFF) 21T cells⁵, donated by the Thibeault laboratory (University of Wisconsin-Madison) were maintained in Dulbecco's modified Eagle's medium (DMEM) (Sigma, #D6429) supplemented with 10% (v/v) FBS (ThermoFisher, #12484028), 1% (v/v) penicillin streptomycin (ThermoFisher, #15140122) and 1% (v/v) non-essential amino acids (ThermoFisher, #11140050). pVFF cultures were stored in a humidified incubator (37 °C, 5% CO₂). Culture media was changed every other day.

At approximately 90% confluency, media was removed, and cells were rinsed with DPBS without calcium or magnesium (Sigma, #D8537) before TrypLE Express (ThermoFisher, #12604013) was applied and incubated at 37 °C for 3-5 min. A light microscope (Laxco, LMI-3000) was used to confirm cell detachment. Cells were transferred to a centrifuge tube and counted using trypan blue (ThermoFisher, #15250061) and a haemocytometer (Fisher Scientific, #0267110). Cells were pelleted via centrifugation at 200 g for 5 min, re-suspended in 5 mL of fresh media, and split at a 1:5 ratio. pVFFs were passaged at least once prior to use in experiments, with passage number 4-6 used throughout this study.

Laryngeal Epithelial Cell Culture

The human immortalized laryngeal posterior commissure cell line (iLECs), HuLa-PC (ATCC CRL-3342), was maintained in dermal cell basal medium (ATCC, #PCS-200-030) supplemented with a keratinocyte growth kit (ATCC, #PCS-200-040) as recommended by the manufacturer. Cells from the laryngeal posterior commissure were selected due to their high exposure to environmental and systemic irritants.⁷⁸ Immortalized epithelial cells have the benefit of rapid expansion in culture, allowing multiple trials to optimize and refine experimental

parameters.^{27,78–80} In contrast, primary VF epithelial cells cannot be reliably cultured beyond a few passages.^{48,81} iLECs were seeded in 100 mm dishes at a density of 1×10^6 cells/mL and media changes were performed every 2-3 days.

At approximately 70-80% confluency, iLECs were passaged. Media was removed and cells were rinsed with DPBS before TrypLE Express was applied and incubated at 37 °C for 10 min. Cell detachment was confirmed using a light microscope. Cells were collected, counted, and pelleted via centrifugation at 300 g for 8 min. Cells were split to new vessels at a 1:5 ratio and were passaged at least once prior to use in experiments.

Prior to use in co-culture models, iLECs were primed via exposure to stratified DMEM. A stock of basal DMEM was prepared by supplementing DMEM/F12 with 2% B27 (ThermoFisher, #17504044), 1% N2 (ThermoFisher, #17502048), and 1% pen strep. To obtain stratified DMEM, 0.4 µg/mL hydrocortisone (Stemcell Technologies, #07925) 8.4 ng/mL cholera toxin (Sigma, #C9903), 5 µg/mL insulin (Sigma, #91077C), 24 µg/mL adenine (Sigma, #A8626), and 20 ng/mL EGF (Stemcell Technologies, #78006) were freshly added to basal DMEM.^{18,48} To induce iLECs, media was removed, cells washed twice with DPBS, and stratified DMEM was applied to the cells, with media refreshed after 48 hr. After 72 hr, cells were harvested and used in experimental cultures.

Transwell Experimental Set-up

2D Transwell Co-Culture

pVFFs were pelleted and re-suspended in basal DMEM at a concentration of 0.5×10^6 cells/mL. Transwell inserts from a 24-well plate (Corning, #3412) were flipped and 100 µL of cell suspension added directly to the basal membrane. Inverted plates were incubated for 1 hr to permit pVFF adherence. After incubation, plates were flipped back to normal orientation and 500 µL of basal DMEM was applied to each well before an additional 100 µL was added to the apical compartment of each insert. The transwell plate was then incubated for a further 48 hr.

To prepare co-cultures, primed iLECs were harvested, counted, pelleted, and re-suspended in stratified DMEM at 1×10^6 cells/mL. All media was removed from the transwell plate and 100 µL of iLECs added to each insert's apical membrane. 600 µL of stratified DMEM was added to

the well. The transwell plate was incubated and media changed thereafter every 48 hr. Cells were co-cultured in submerged conditions for 3 days to permit attachment and proliferation.

Three days post-iLEC cell seeding, an air-liquid interface (ALI) was established by removing media from the insert. At this point, media in the well was changed to flavonoid adenine dinucleotide (FAD) medium to initiate stratification. FAD media was prepared by first mixing DMEM medium-high glucose (Sigma, #D6429) with Ham's F12 (ThermoFisher, #11765054) in a 1:3 ratio. This mix was supplemented with FBS (2.5%), pen strep (1%), hydrocortisone (0.4 $\mu\text{g/mL}$), cholera toxin (8.4 ng/mL), insulin (5 $\mu\text{g/mL}$) (Sigma, #91077C), adenine (24 $\mu\text{g/mL}$) (Sigma, #A8626), and EGF (10 ng/mL).¹⁸ Media in the well was changed every 48 hr. Cells were cultivated at the ALI for a further 10 days.

3D Transwell Co-Culture

Collagen gels were prepared according to the manufacturer's instructions. Briefly, 6.7 mL collagen I (ThermoFisher, #A10483-01), 1 mL 10 \times MEM (ThermoFisher, #11430030), and 2.13 mL of distilled water (ThermoFisher, #15230170) were combined on ice. The pH of the collagen gel was adjusted to 7.2-7.4 using 1 N NaOH (ThermoFisher, #124260010) and verified with pH strips.

pVFFs were pelleted and re-suspended in ice-cold FBS at 5×10^6 cells/mL. 1 mL of cell suspension was added to the collagen gel on-ice to generate a final concentration of 0.5×10^6 cells/mL.⁸² 110 μL of gel-cell mix was dispensed into the insert of a 24-well transwell plate and incubated at 37 °C for 75 min to initiate gel formation. Following incubation, gels were gently detached from the membrane and 600 μL of basal DMEM added to each well alongside 100 μL to each insert. The plate was incubated a further 24 hr to allow gel contraction.

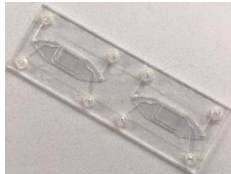

Induced iLECs were harvested, counted, pelleted, and re-suspended in stratified DMEM at 1×10^6 cells/mL. All media was removed from the transwell plate and 100 μL of iLECs added atop each collagen gel. 600 μL of stratified DMEM was also added to the well. Media thereafter was changed every 48 hr. Cells were co-cultured in submerged conditions for 3 days to allow attachment and proliferation.

Three days post-iLEC cell seeding, an ALI was established by removing media from the insert. At this point, media in the well was changed to FAD. Well media was changed every 48 hr. Cells were cultivated at the ALI for a further 10 days.

VF-OOAC Experimental Culture

Commercial microfluidic chip devices (ChipShop and BEOnChip) were used to develop VF-OOAC models by co-culturing pVFFs and iLECs. The channel configuration and architecture differed between the devices (**Table 4.2**). The ChipShop device had two overlapping microchannels separated by a porous membrane for the adjacent monolayer culture of pVFFs and iLECs, representing a 2D culture setup. The BEOnChip device had a culture well separated from a microchannel by a porous membrane. The culture well permitted culture of pVFFs embedded in a collagen gel supporting iLECs, representing a 3D culture setup. Although the membrane material of each device differed, these common tissue culture plastics have been widely applied in biological research with minimal differences in biological behaviour.⁸³ In addition, as each membrane was coated with collagen, direct contact between cells and the membrane was limited. As such, differences between cell cultures due to membrane material were assumed to be minimal.

Table 4.2. Comparison of microfluidic chip devices used for investigating the impact of different culture parameters on VF mucosae in VF-OOAC setups.

	ChipShop Device	BEOnChip Device
Cell Culture	2D	3D
Microchannels	2	1
Membrane	Polyethylene Terephthalate	Polycarbonate
Membrane Thickness	12 µm	10 µm
Pore Size	0.4 µm	0.4 µm
Pore Density	1×10 ⁵ pores cm ²	1×10 ⁵ pores cm ²
Inlets	Slip	Threaded
Device		

2D VF-OOAC

ChipShop Microfluidic Chip Design

Cross-Flow membrane microfluidic devices were manufactured by Microfluidic ChipShop GmbH (Jena, Germany, #10001555) (**Table 4.2**). The device consisted of two chambers separated

by a porous polyethylene terephthalate membrane.⁸⁴ Including the inlet/outlet channels, the respective volumes of the upper and lower chambers were 220 μL and 120 μL . The device was covered by an optically clear cyclo-olefin-copolymer bonding foil. Additionally, the device was hydrophilized to promote cell attachment within the channels. This device has previously been utilized to recreate airway tissue-tissue interfaces, with its design well suited for co-culture barrier studies.^{85,86}

Static 2D VF-OOAC Co-culture

Channels of the sterile microfluidic device were filled with DMEM and incubated overnight to equilibrate the device and minimize air bubble formation. Chip channels were then coated with collagen to facilitate improved cell adherence. Collagen I coating solution was prepared by adding 50 μL of collagen to 3 mL of DMEM and pipetting it into each channel. Coated chips were incubated for 1 hr at 37 °C before the channel was washed to remove excess coating solution. Channels were left filled with DMEM and incubated whilst cells were prepared for seeding.

The lower channel was filled with pVFFs re-suspended in basal DMEM at 0.5×10^6 cells/mL. The chip was inverted and incubated overnight to permit cell attachment. The next day, media was refreshed and the chip incubated for 48 hr, with a media change after 24 hr to ensure cells were supplied with fresh nutrients whilst minimizing waste and acidity build-up.

iLECs were seeded in the chip 48 hr after pVFF seeding. iLECs were re-suspended in stratified DMEM at 1×10^6 cells/mL and applied to the upper channel. At this point, media in the lower channel was also changed to stratified DMEM. Chips were incubated overnight and media thereafter was changed at least every 24 hr via pipetting. Static 2D VF-OOAC co-cultures were maintained in submerged culture conditions for 13 days before characterization.

3D VF-OOAC

BEOnChip Microfluidic Chip Design

BE-Transflow microfluidic devices were manufactured by BEOnChip (Zaragoza, Spain) (**Table 4.2**). The device consisted of a microchannel and culture well separated by a porous polycarbonate membrane. The respective well and channel volumes were 195 μL and 44 μL . The chip body was fabricated from cyclic-olefin-polymer. This device was selected because it enabled

the use of a modified transwell 3D culture protocol that had successfully recapitulated some structural and functional features of the VF mucosa.^{17–19,46–48} In addition, the device design enabled the effect of fluidic shear to be decoupled from perfusion by removing the fibroblast monolayer in the microchannel. As pVFFs were still present in the collagen gel supporting the epithelium, this removal had no impact on co-culture status. The 3D VF-OOAC was used for three distinct culture setups: (1) static 3D VF-OOAC, (2) perfused 3D VF-OOAC, and (3) perfused 3D VF-OOAC + fluidic shear.

Static 3D VF-OOAC Co-culture

The channel of the sterile microfluidic device was filled with DMEM and incubated overnight to equilibrate the device and minimize air bubble formation. The channel was then coated with collagen as described for 2D VF-OOAC.

pVFFs were seeded within the channel of the chip as performed for 2D VF-OOAC. 24 hr after pVFF seeding, pVFF-collagen gels were prepared as described for transwell 3D culture. 110 μ L of pVFF-collagen gel mixture was dispensed into the well of the microfluidic chip. Chips were incubated at 37 °C for 75 min to initiate gel formation. At this point, gels were gently detached from the chip membrane and fresh basal DMEM media was added to the well and channel. Chips were incubated a further 24 hr.

The following day, iLECs were seeded atop collagen gels as described for 3D transwell. Chips were cultured in submerged conditions for three days with media changed daily. After three days, an ALI was established by media removal from the well. Static 3D VF-OOAC were cultivated for a further 10 days, with FAD media changed daily in the channel via pipetting.

Perfused 3D VF-OOAC Co-culture

To investigate the impact of perfusion on VF mucosae, the pVFF monolayer was not seeded in the microchannel. Instead, after establishing an ALI in 3D VF-OOAC cultures, the chip was connected to a peristaltic pump (Ismatec, Wertheim, Germany, #ISM933) that continuously drove media through the device at 40 μ L/h via silicon tubing (A-M Systems, #807300) and connectors (BEOnChip) (**Figure 4.2**). Cells were cultivated in this perfused setup for 10 days before samples were prepared for biological characterization.

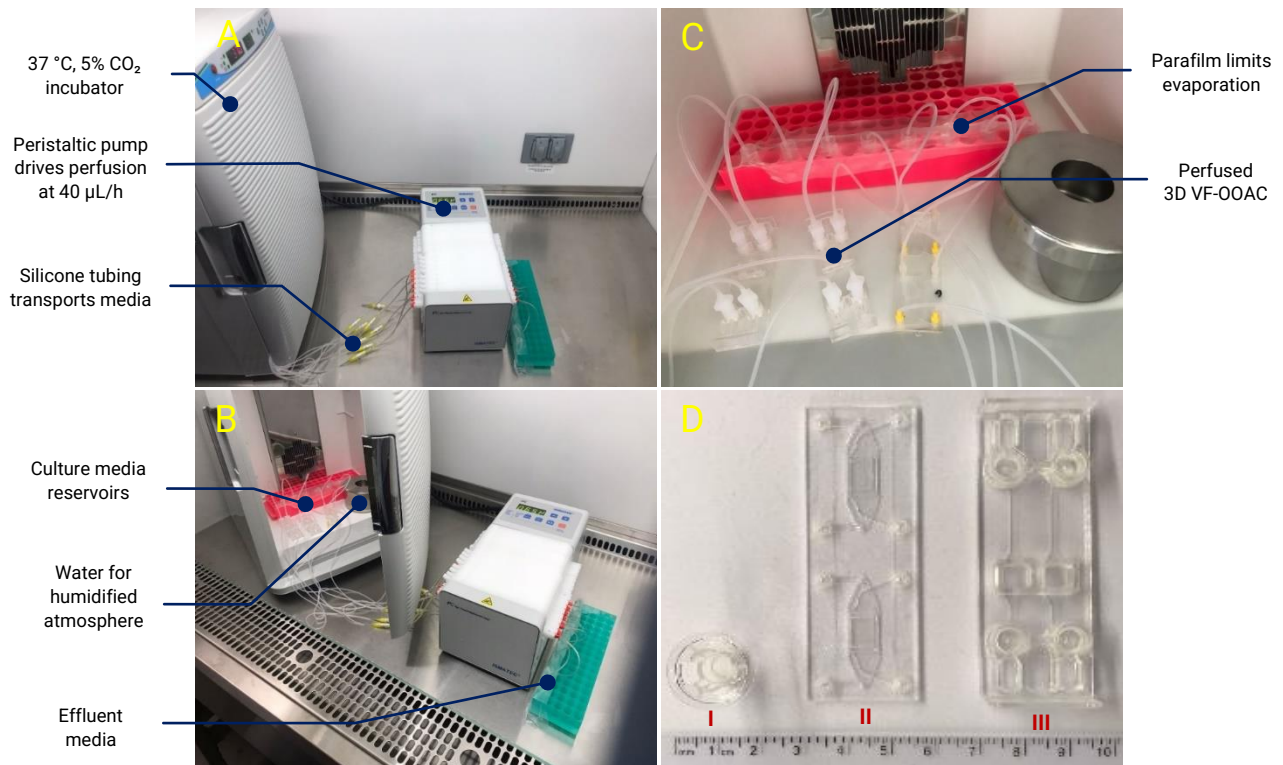


Figure 4.2. Perfusion-based culture system. (A) The setup enabled continuous perfusion of 3D VF-OOAC whilst maintaining sterility within a biological safety cabinet. (B) During operation, the peristaltic pump pulls media from media reservoirs, through the microchannel of the device before dispensing waste media into effluent collectors. (C) Cultures are stored in a humidified, 37 °C, 5% CO₂ incubator. (D) Comparison of vessels applied for (I) transwell, (II) 2D VF-OOAC, (III) 3D VF-OOAC culture. Centimetre ruler for scale.

Perfused 3D VF-OOAC + Fluidic Shear Co-culture

To study the effect of fluidic shear, the pVFF monolayer was again seeded in the device microchannel as described for static 3D VF-OOAC. After ALI establishment, the channel was perfused at 40 μL/h using the same system described for perfused 3D VF-OOAC. During perfusion, the pVFF monolayer experienced fluidic shear. This perfused setup was also maintained for 10 days before characterization.

Immunocytochemistry

Immunocytochemistry was used to evaluate protein expression related to epithelium structure and barrier integrity. Epithelial stratification was assessed via staining for cytokeratin 5 and 14 (K5, K14).^{17–19,48} The presence of adherens junctions was determined using E-Cadherin (E-Cad).^{18,27,87} Basement membrane development was examined with laminin alpha 5

(LAMA5).^{19,48,88} Vimentin was used for monitoring intermediate filament expression.⁸⁹ Primary antibodies and relevant secondary antibodies applied are indicated in **Table 4.3**. Slides stained with secondary antibody only served as negative controls.

Table 4.3. Antibodies for immunocytochemistry evaluation of VF mucosae. AF = Alexa Fluor, K5 = Cytokeratin 5, K14 = Cytokeratin 14, LAMA5 = Laminin alpha 5, E-Cad = E-Cadherin.

Target	Primary Ab	Dilution	Supplier (Cat #)	Secondary Ab	Dilution	Supplier (Cat #)
Stratified epithelium	AF 488 Rabbit to K5	1:200	Abcam (ab193894)	-	-	-
Stratified epithelium	AF 532 Mouse to K14	1:100	Novus Biologicals (NBP2-34675AF532)	-	-	-
Basement membrane	Mouse to LAMA5	1:100	Abcam (ab77175)	AF 647 Goat anti-Mouse	1:1000	ThermoFisher (A-21236)
Intercellular junction marker	AF 647 Rabbit to E-Cad	1:100	Abcam (ab194982)	-	-	-
Intermediate filaments	Chicken to Vimentin	1:200	Abcam (ab24525)	AF 633 Goat anti-chicken	1:1000	ThermoFisher (A-21103)
Nuclear DNA	DAPI	1:5000	Abcam (ab228549)	-	-	-

The immunostaining protocol used was adapted from that of the Thibeault Laboratory.^{18,19,48} Media was removed and samples washed three times with DPBS. Samples were fixed in 4% paraformaldehyde (ThermoFisher, #J19943K2) for 30 min before washing twice. At this point, samples were transferred to a cryomold (Ted Pella, #271471) filled with O.C.T. Compound (Fisher, #4585). For 2D transwell and 2D VF-OOAC, the cell-seeded membrane was harvested. For 3D transwell and 3D VF-OOAC, the collagen gel construct was extracted.

Samples were flash frozen using liquid nitrogen before being sectioned (10 μ m thickness) vertically using a cryostat (Leica CM1860). Sections were transferred to microscope slides (Fisher, #1255015). Slides were dried for 1 hr at room temperature and stored at -80 °C until immunostaining.

All staining was performed at room temperature. Slides were washed with PBS and permeabilized with 0.1% Triton X-100 (Sigma, #X100-5ML) for 15 min. After three washes, blocking buffer comprising 10% goat serum (Abcam, #ab7481), 1% Tween-20 (Abcam, #ab128987) in PBS was applied for 45 min. After blocking, samples were incubated with relevant primary antibodies in blocking buffer for 1 hr.

After washing with 0.05% Tween-20 in PBS, relevant fluorescence-conjugated secondary antibodies in blocking buffer were applied and incubated for 1 hr. Slides were washed and

counterstained with 1:5000 DAPI (Abcam, #ab228549) in PBS for 5 min to label cell nuclei.⁹⁰ Samples were rinsed with PBS and mounted in Vectashield Antifade mounting medium (Vector Labs, #H-1700) to prevent photobleaching.

Slides were imaged with an inverted LSM710 confocal fluorescence microscope (Zeiss) and 20× objective. Images collected were the vertical cross-section depicting fibroblasts embedded in the collagen gel below the epithelial layers (3D transwell and 3D VF-OOAC) or a fibroblast monolayer below the epithelial cell layers (2D transwell and 2D VF-OOAC). Image acquisition and analysis were performed using Zen System software (Zeiss) and Imaris version 7.5.6 (Bitplane) software.

Immunohistochemistry

To verify the presence and distribution of cells and collagen in developed mucosae, 10 µm-thick sections were subjected to hematoxylin-eosin (H&E) staining (Abcam, #ab245880) using the manufacturer's protocol. Slides were dipped in Hematoxylin and incubated 5 min. Sections were rinsed twice in distilled water then dipped in bluing reagent for 15 sec. Sections were rinsed twice in distilled water and dipped in absolute alcohol, with the excess blotted off. Sections were immersed in Eosin and incubated for 2 min. Slides were rinsed, dehydrated in an absolute alcohol series, and mounted with Permount media (Fisher Scientific, #SP15100). Image acquisition was performed using an Axiovert 3 Widefield Microscope with 40× objectives equipped with Zen System software. Images were analyzed with Imaris.

Transmission Electron Microscopy

A Talos F200X STEM transmission electron microscope was used to assess the subcellular structure of the VF mucosa including tight junctions, adherens junctions, desmosomes, and gap junctions in perfused 3D VF-OOAC + fluidic shear cultures.¹⁷ Mucosae were washed twice with DPBS and immersion fixed overnight at 4 °C in 2.5% glutaraldehyde, 2% paraformaldehyde in a 0.1 M sodium cacodylate buffer (pH 7.4). After washing with sodium cacodylate buffer, samples were post-fixed in 1% osmium tetroxide in buffer for 2 hr at room temperature. Sample dehydration was achieved via a graded ethanol series. Samples were washed twice in propylene oxide and embedded in an Epon 812 epoxy resin under a vacuum. Samples were thin sectioned (70 nm thickness) using a Leica Microsystems EM UC6 Ultramicrotome for transmission electron

microscopy and stained with Reynolds lead citrate and 8% uranyl acetate in 50% ethanol to increase contrast.

Gene Expression

Real-time quantitative PCR (qPCR) was applied to assess up- or downregulation of structural and functional genes relative to controls. Cultures were washed twice with DPBS without calcium and magnesium. For 3D transwell and 3D VF-OOAC, 100 U/mL of collagenase type I (Gibco, #17018029) in HBSS (ThermoFisher, #14175095) was applied to samples and incubated at 37 °C for 2-3 h or until gel dissolution. For 2D transwell and 2D VF-OOAC, cells were harvested using TrypLE as described earlier for regular cell passaging. For all cultures, cells were collected, transferred to 1.5 mL microtubes, and centrifuged for 5 min at 10,000 rpm. Samples were resuspended in DPBS and centrifuged again. Supernatants were aspirated, and cell pellets snap frozen using liquid nitrogen before storage at -80 °C until RNA extraction.

Total RNA extraction was performed using the RNeasy Micro Kit (Qiagen, #74004) in accordance with the manufacturer's instructions. RNA was incubated with DNase I (Qiagen) for 15 min at room temperature to remove residual contaminating genomic DNA. Extracted RNA was assessed using a NanoDrop (ThermoScientific, NanoDrop 2000 Spectrophotometer) to determine RNA quantity and purity prior to cDNA synthesis. RNA was evaluated for quality and degradation using an Agilent 2100 Bioanalyzer (Agilent Technologies) (**Figure S1**). 500 ng of RNA was reverse transcribed to cDNA using a SuperScript VILO cDNA Synthesis Kit (ThermoFisher, #11754050) as per the manufacturer's protocol.

TaqMan assays (ThermoFisher, #4453320) for genes corresponding to K5, K14, tumor protein 63 (p63), tight junction protein 1 (ZO-1), gap junction alpha-1 protein (GJA1), mucin 1 (MUC1), mucin 4 (MUC4), hyaluronan synthase 2 (HAS2), hyaluronan synthase 3 (HAS3), and piezo 1 (PIEZO1) were used for assessment (**Table 4.4**).^{18,48,91} To perform qPCR, 96-well fast plates (ThermoFisher, #4483485) with 1 µL of cDNA per 10 µL reaction mix were used. Plates were run in triplicates for 40 cycles using a ViiA 7 Real-Time PCR System (ThermoFisher). Relative gene expression was normalized to Glyceraldehyde-3-Phosphate Dehydrogenase (GAPDH) (ΔC_t) and results were quantified using the $2^{-\Delta\Delta C_t}$ method.⁹²

Table 4.4. TaqMan assays for qPCR evaluation.

Target	Gene	TaqMan Assay ID
Stratified epithelium	K5	Hs00361185_m1
Stratified epithelium	K14	Hs00265033_m1
Basal epithelium	p63	Hs00978340_m1
Intercellular junctions	ZO-1	Hs01551871_m1
Intercellular junctions	GJA1	Hs00748445_s1
Mucus production	MUC1	Hs00159357_m1
Mucus production	MUC4	Hs00366414_m1
ECM synthesis	HAS2	Hs00193435_m1
ECM synthesis	HAS3	Hs00193436_m1
Mechanotransduction	PIEZO1	Hs00207230_m1
Housekeeping	GAPDH	Hs02786624_g1

Statistical Analysis

Gene expression data were evaluated using one-way between-subjects ANOVAs to determine the effect of physiological scaling, culture dimensionality, perfusion, and fluidic shear on VF mucosa culture. Differences were considered significant at $p < .05$.

Results & Discussion

Microscale culture supported functional gene upregulation

The initial step of VF-OOAC development investigated whether VF mucosa development benefited from microscale culture compared to transwell culture. This effect was assessed by contrasting static VF-OOAC systems with transwell models within either 2D or 3D culture setups.

Minimal effect of microscale culture on epithelium basal structure

Our results suggest physiological scaling had little impact on basal epithelium and basement membrane development. H&E staining showed 2D transwell had a multilayered, stratified epithelium with polarized cells throughout its structure (**Figure 4.3A: a**). Conversely, static 2D VF-OOAC had a thin epithelium, 1-2 cells thick, that lacked cellular polarization (**Figure 4.3A: b**).⁹³ Although presenting a thin structure, the epithelium of 2D VF-OOAC was confirmed to achieve confluency (**Figure S4.2C**). It is speculated the ALI was the dominant factor in these differences because its absence constrains epithelial differentiation and hinders stratification, leading to monolayer-like structures seen in static 2D VF-OOAC. Similar thin, flattened epithelia were reported for nasal epithelial cells cultured in the absence of an ALI.⁹⁴

Stratified epithelium of static 3D VF-OOAC was multilayered and approximately 7-8 cells thick, matching *in vivo* descriptions (**Figure 4.3A: d**).^{95,96} This epithelium had cuboidal basal and suprabasal cell layers under a flattened, terminally differentiated top layer.¹⁸ 3D transwell culture displayed similar morphology, but with 2-3 fewer cell layers (**Figure 4.3A: c**).

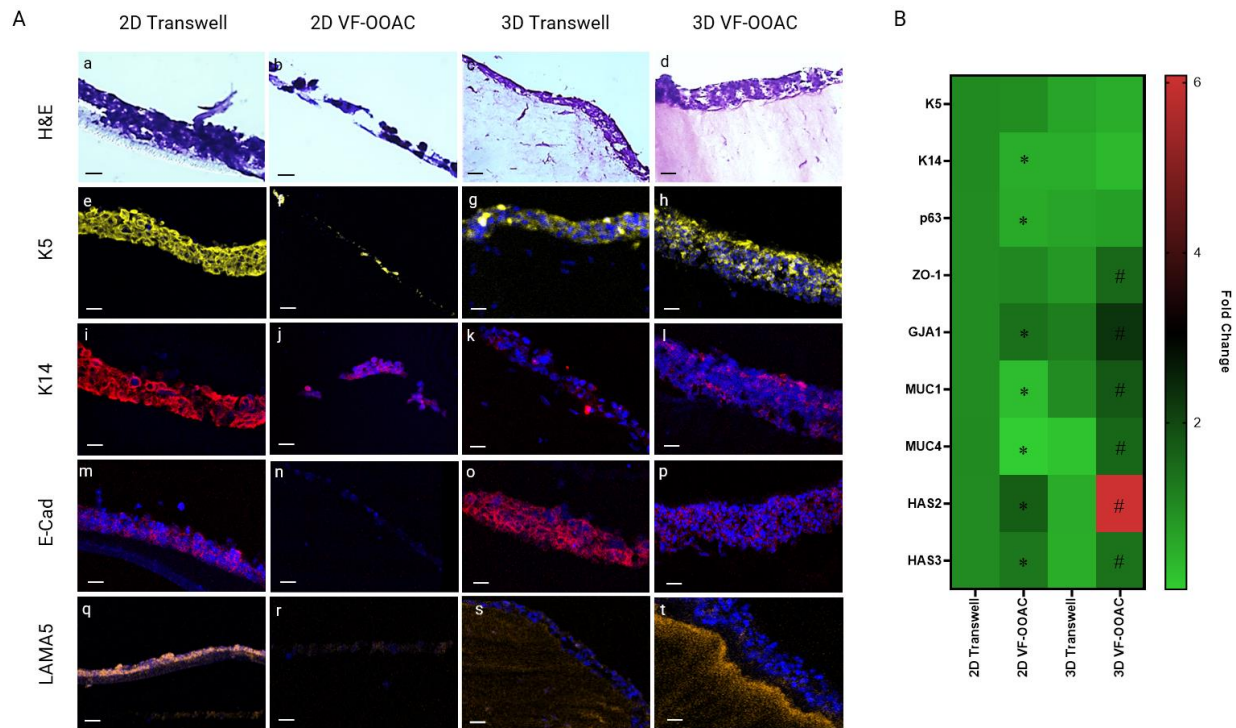


Figure 4.3. Effect of physiological scaling on VF mucosa culture in static VF-OOAC and transwell setups. (A) H&E [a-d], K5, [e-h], K14 [i-l], E-Cad [m-p], and LAMA5 [q-t] evaluated morphological features. DAPI (blue) indicates cell nuclei. H&E magnification 40 \times , scale bar = 15 μ m. Immunostaining magnification 20 \times , scale bar = 30 μ m. (B) Relative gene expression in 2D transwell, static 2D VF-OOAC, 3D transwell, static 3D VF-OOAC setups. All data presented as the fold change relative to 2D transwell. Significant differences for 2D transwell vs 2D VF-OOAC, and 3D transwell vs 3D VF-OOAC are denoted by * and # respectively.

K5 (**Figure 4.3A: e-h**) and K14 (**Figure 4.3A: i-l**) were detected in the epithelium of all cultures. Strong expression of basal cytokeratins are a feature of VF epithelium, which requires constant self-renewal to maintain tissue homeostasis.^{4,97} Our findings suggest basal epithelium in all setups displayed this self-renewal capacity. qPCR examined K5, K14, and p63 gene expression to determine epithelial stratification and differentiation.¹⁷ Static 2D VF-OOAC expressed significantly lower K14 and p63 compared to 2D transwell ($p < .05$; **Figure 4.3B**). All other K5, K14, p63 comparisons were non-significant. Decreased p63 and K14 in static 2D VF-OOAC was likely associated with ALI absence restricting epithelial development and maturation.¹⁸

The basal epithelial layer is anchored to the VF basement membrane, which is an important structure to recapitulate due to its functional role in regulating biochemical cellular signals, facilitating immune cell migration, and tissue repair.^{16,18,98,99} Each of the four culture models displayed relatively non-specific staining for LAMA5, which *in vivo* is localized below the basal epithelial layer. This may indicate anchorage of iLECs to the collagen matrix could be impaired or immature as has been reported elsewhere for immortalized VF epithelial cells (**Figure 4.3A: q-t**).⁴⁸ In particular, absence of LAMA5 staining in static 2D VF-OOAC may be a consequence of ALI absence hindering cellular ECM deposition.

Microscale culture enhanced intercellular junction capacity

E-Cad is a marker of adherens junctions, which are cell-cell anchoring junctions that help stabilise epithelial sheets during VF vibration and regulate tight junction assembly.^{100,101} For static 2D VF-OOAC and 2D transwell, E-Cad was found in the epithelium of 2D transwell only (**Figure 4.3A m, n**). The lack of E-Cad in static 2D VF-OOAC may indicate an underdeveloped epithelium with infrequent adherens junctions a consequence of limited cell polarization. For static 3D VF-OOAC and 3D transwell, E-Cad was detected throughout the epithelium of both cultures (**Figure 4.3A: o, p**). Intense E-Cad staining in static 3D VF-OOAC suggests a robust barrier capacity attributable to the strong adhesive bonds between epithelial cells.

Tight junctions maintain barrier integrity and regulate epithelial permeability to prevent the infiltration of noxious insults into VF tissue. No significant difference in ZO-1 was detected between static 2D VF-OOAC and 2D transwell. Conversely, static 3D VF-OOAC had significantly higher ZO-1 expression than 3D transwell ($p < .05$, **Figure 4.3B**), indicating increased epithelial integrity and barrier capacity. Paracrine signalling is fundamental for tight junction development in the VF epithelium.¹⁰² Upregulated ZO-1 in 3D VF-OOAC could be the small-volume effects of microfluidic culture increasing paracrine signalling efficacy compared to 3D transwell.

Gap junctions are communicating junctions responsible for cell-cell signalling and small molecule transport.^{103,104} Gap junction frequency and functionality can be regulated by adhesion proteins and the ECM.^{105,106} Both VF-OOAC models displayed significantly higher GJA1 expression than their respective transwell controls ($p < .05$; **Figure 4.3B**). Increased GJA1 expression suggests microscale culture increased intercellular communication capacity.

Greater epithelial functionality in microscale culture

The mucus barrier traps irritants for airway removal as part of VF innate immunity.^{102,107} Mucus also lubricates the VF epithelium to protect it against the damaging consequences of drying.¹⁰⁸ Static 2D VF-OOAC had significantly lower MUC1 and MUC4 expression compared to 2D transwell ($p < .05$; **Figure 4.3B**). Conversely, static 3D VF-OOAC had significantly higher MUC1 and MUC4 versus 3D transwell ($p < .05$; **Figure 4.3B**). Downregulated mucin expression in static 2D VF-OOAC was likely ALI absence constraining epithelial differentiation and synthesis of membrane-bound mucins (MUC1, MUC4) on the apical surface of epithelial cells.^{18,100} In contrast, microscale culture may have induced upregulated mucin expression in static 3D VF-OOAC by promoting greater epithelial differentiation via autocrine and paracrine effects.

Elevated tissue remodelling capacity in microscale culture

HA is synthesized by VF fibroblasts and is an important element of VF ECM for its role in regulating biomechanical properties, vibratory function, and homeostasis.^{109–111} HAS2 and HAS3 are enzymes that respectively synthesize high and low molecular weight HA. Both VF-OOAC models had significantly higher HAS2 and HAS3 expression compared to relevant transwells ($p < .05$; **Figure 4.3B**). Upregulated HAS suggests tissue modelling and ECM synthesis were increased in VF-OOAC models. This may indicate that increased paracrine signalling efficacy produced elevated fibroblast activity, including HA synthesis.^{4,40} In contrast, the larger diffusion distances in transwell culture may have inhibited cellular communication and functionality. To complement HA synthesis data, future work should measure hyaluronidase activity to gain insight into whether HA degradation is also influenced by small volume effects.

Collectively, our results highlight the importance of relevant physiological scaling for stimulating higher tissue development via small-volume effects, which increase the concentrations of autocrine and paracrine factors.^{40,65} The VF-OOAC systems provided greater volume densities than transwells, a factor notably important in static culture where small volume densities eliminate local concentration gradients and restrict tissue development.^{65,69,112,113} Both VF-OOAC models had upregulated functional genes related to the lamina propria (HAS2, HAS3) and epithelial gap junctions (GJA1) compared to transwells. Static 3D VF-OOAC further demonstrated increased structural integrity and epithelial functionality through increased tight junction (ZO-1) and mucin (MUC1, MUC4) expression. Notably, static 2D VF-OOAC had downregulation of genes

characteristic of a differentiated epithelium (p63, MUC1, MUC4), which was likely associated with ALI absence rather than physiological scaling.

Increased dimensionality improved tissue functionality

Our investigation of physiological scaling confirmed implementing a microscale culturing environment was beneficial for VF mucosal growth. The next step was to determine the impact of culture dimensionality by comparing static 2D VF-OOAC and static 3D VF-OOAC. In this specific analysis, results revealed culture dimensionality affected both epithelial polarization and fibroblast behaviour. Further, the 3D VF-OOAC controlled cellular proliferation and produced a tissue morphology more closely aligned with native VF mucosa reported in the literature.

Static 3D VF-OOAC had a densely-packed, multilayered epithelium (**Figure 4.3A: d**) considerably thicker than the 1-2 cell layers found in static 2D VF-OOAC (**Figure 4.3A: b**). Static 2D VF-OOAC displayed significantly higher K5 gene expression than static 3D VF-OOAC ($p < .05$; **Figure 4.4A**). 2D culture induces cytoskeleton reassembly, stimulating increased proliferation and migration in epithelial cells.^{114,115} K5 expression in airway epithelia has been shown to positively correlate with proliferation rate.¹¹⁶ As such, upregulated K5 in 2D VF-OOAC is likely a manifestation of the increased proliferation occurring in the basal cell layer.

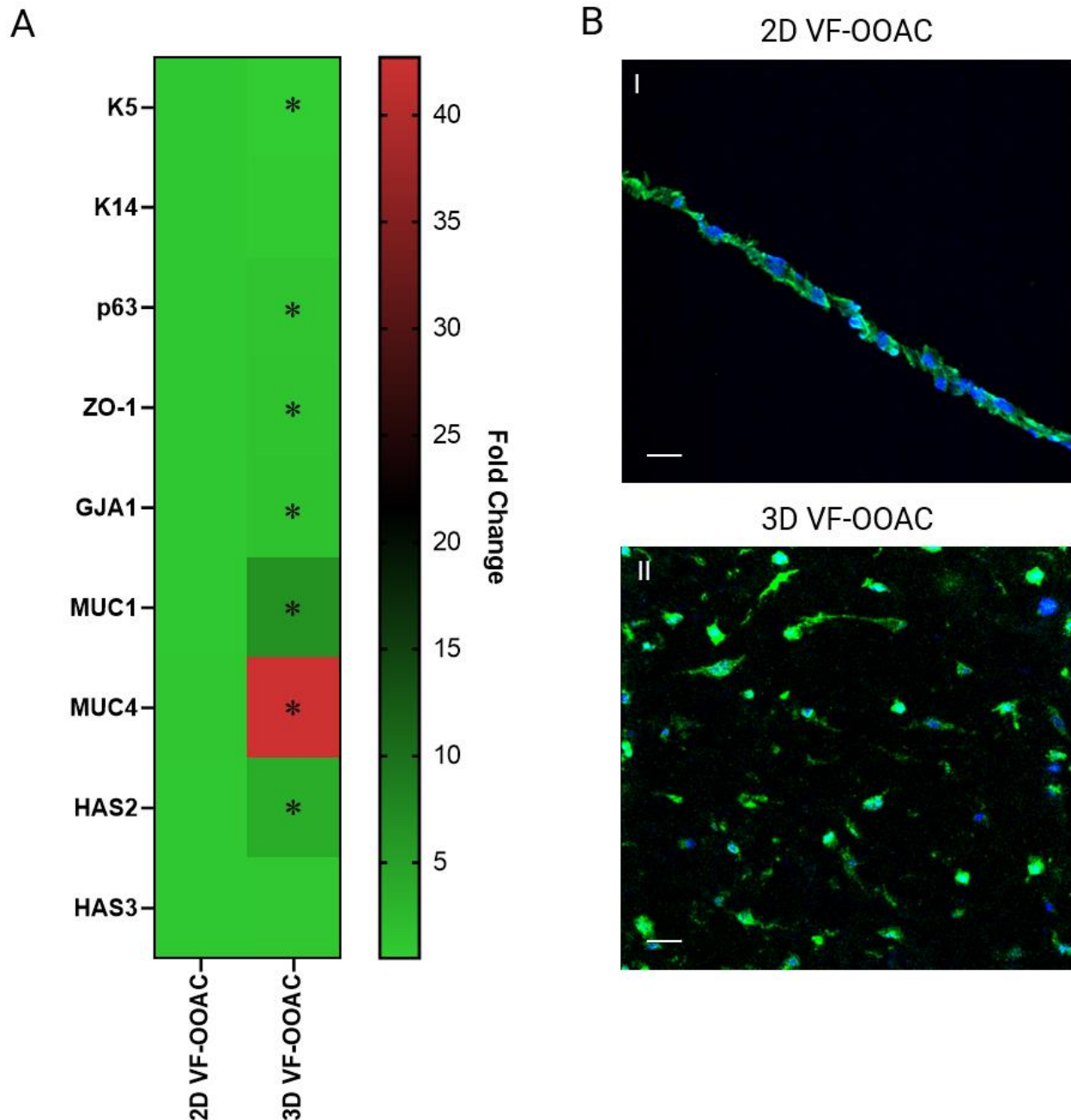


Figure 4.4. Effect of dimensionality on VF mucosae cultivated in VF-OOAC models. (A) Heatmap of relative gene expression in static 2D VF-OOAC and static 3D VF-OOAC setups. Data displayed as the fold change relative to static 2D VF-OOAC. Significant differences denoted by *. (B) Dimensionality influences mesenchymal cell morphology in each respective VF-OOAC model as seen by vimentin (green) and DAPI (blue) staining. Cells in static 2D VF-OOAC adhere to the collagen-coated membrane as a monolayer, restricting their capacity for cell-cell and cell-ECM interactions (I). Cells embedded in collagen gels in static 3D VF-OOAC spread and engage in more complex biological activity than possible in 2D culture (II). Magnification 20 \times , scale bar = 30 μ m.

Both ZO-1 and GJA1 were significantly higher in static 3D VF-OOAC implying greater epithelial barrier integrity and a denser network of communicating junctions compared to static 2D VF-OOAC ($p < .05$; **Figure 4.4A**). In 2D culture, epithelial cells lack apical-basal polarity

which causes a loss of intercellular junctions.^{114,115} Increased intercellular junction presence in 3D culture offers greater control over proliferation by providing epithelial cells with apoptosis resistance.¹¹⁷

Regarding ECM-related genes, static 3D VF-OOAC expressed significantly higher HAS2 than static 2D VF-OOAC ($p < .05$; **Figure 4.4A**).⁴ Increasing the density and spatial arrangement of ECM surrounding cells (2D \rightarrow 3D) can stimulate increased mechano-responses and cell viability.^{45,66–68}

In static 2D VF-OOAC, pVFFs are limited to a monolayer on a collagen-coated plastic substrate, inhibiting their capacity to engage in cell-cell and cell-ECM interactions (**Figure 4.4B: I**). This system restricts pVFF polarity and constrains cell adhesion distribution to 2D, creating a microenvironment unrepresentative of the native VF mucosa.⁶ The spread, spindle-shaped structure is characteristic of VF fibroblast behaviour in 2D culture that typically produces higher proliferation rates than 3D environments.¹¹⁸ As fibroblast distribution is sparse in native VF mucosa, excessive proliferation constitutes an unrepresentative depiction of the tissue.^{96,119}

Static 3D VF-OOAC provided gel-embedded pVFFs with a microenvironment containing soluble gradients, discrete matrix fibrils, sterically regulated spreading and migration, and a substrate stiffness closer to native tissue (**Figure 4.4B: II**).⁴⁵ VF fibroblast morphology in 3D gel culture has been reported to vary over 4 weeks, with cells initially presenting a rounded, cluster-like appearance before spreading and displaying spindle-like shape as ECM synthesis occurs.¹¹⁸ Fibroblast morphology in adult VF mucosa is dominated by spindle shaped cells (>80%) with the remaining population oval-shaped. The inverse pattern has been identified in newborn VF mucosa.¹²⁰ Mesenchymal cell morphology in 3D VF-OOAC cultures appears to be trending towards a population representative of that found interspersed throughout native adult VF mucosa.

Perfusion stimulated basal epithelium activity

Our investigation of dimensionality confirmed the importance of 3D culture for cultivating the VF mucosa, which is congruent with the literature.^{17,18,46} Perfusion was the next parameter integrated into the culture platform. Our results showed that by stabilizing concentration gradients, perfusion improved metabolite regulation thereby creating a microenvironment beneficial for

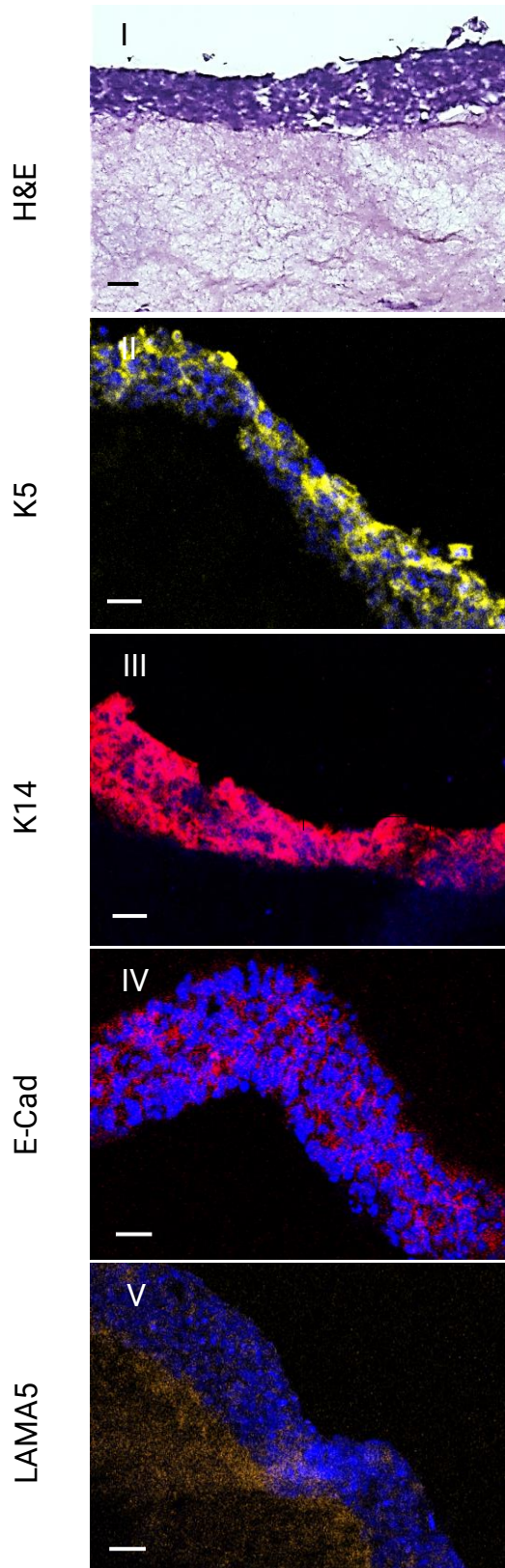
epithelial tissue development. This manifested as increased basal activity and higher mucin expression.

Perfused 3D VF-OOAC retained the densely-packed, polarized, multilayered epithelium previously observed in static culture (**Figure 4.5A: I**). Confocal microscopy showed the epithelium also retained positive staining for K5 (**Figure 4.5A: II**) and K14 (**Figure 4.5A: III**). qPCR comparisons revealed all basal genes assessed (K5, K14, p63) were significantly higher in perfused 3D VF-OOAC versus static 3D VF-OOAC ($p < .05$; **Figure 4.5B**). *In vivo*, basal epithelial cells have a high turnover and the increased basal marker expression in perfused 3D VF-OOAC could indicate a recapitulation of this proliferative capacity.^{53,100,121,122} Interstitial fluid flow can reach velocities between 0.1 and 4.0 $\mu\text{m/s}$ within the ECM of soft tissues such as the VF mucosa.^{123–125} In this study, we approximated this microenvironmental feature by perfusing cultures at the slowest available pump setting, $\sim 11 \mu\text{m/s}$. Perfusion has been suggested to stimulate proliferation by improving the supply of nutrients and dissolved oxygen, whilst simultaneously removing inhibitory metabolites such as ammonium ions, methylglyoxal, and lactate.^{53,126}

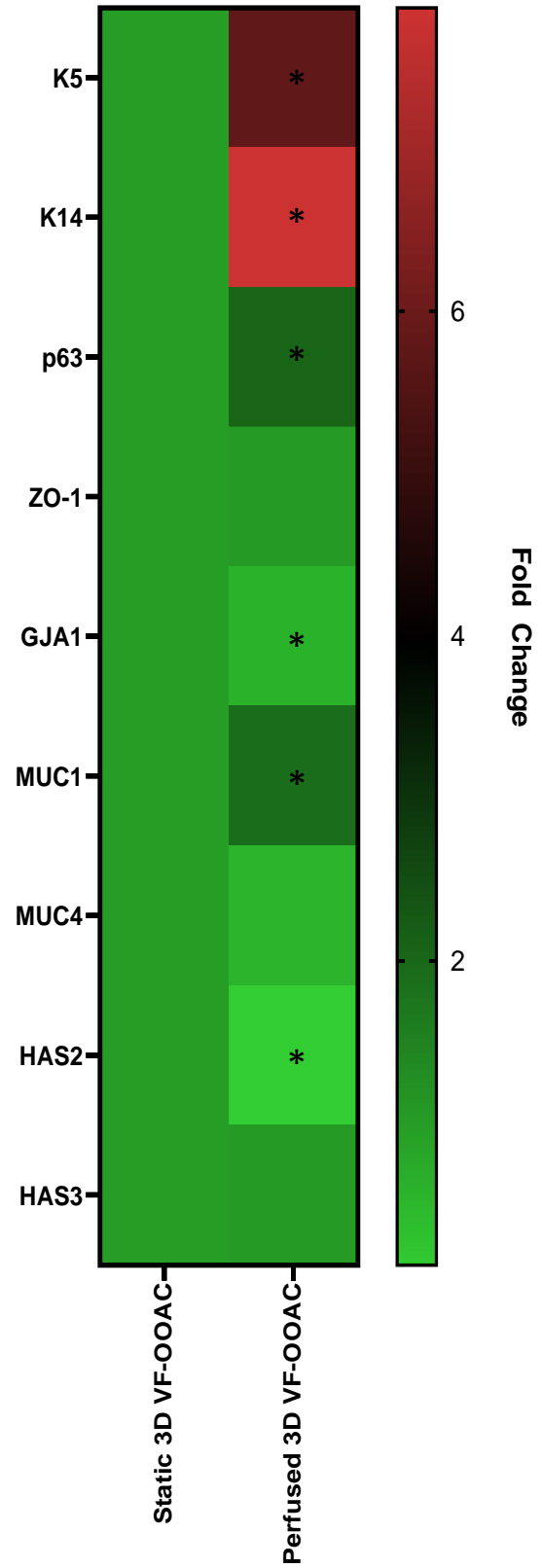
The epithelium of perfused 3D VF-OOAC had extensive positive staining for E-Cadherin, indicative of an established cell-cell adhesion network (**Figure 4.5A: IV**). Maintaining stable concentration gradients for nutrient and waste diffusion via perfusion may have controlled the development of this robust intercellular junction network.^{51,72,127,128} However, staining for LAMA5 was again non-specific, suggesting an immature basement membrane structure (**Figure 4.5A: V**).

Upregulated MUC1 suggests perfused 3D VF-OOAC had a higher capacity for mucus production in comparison to static 3D VF-OOAC ($p < .05$; **Figure 4.5B**).^{129,130} Perfusion has been reported to stimulate differentiation in primary bronchial epithelial cells leading to increased mucus production.¹³¹ Accelerated differentiation highlights the impact of perfusion on improving spatiotemporal distributions of nutrients and metabolites to create a microenvironment conducive to tissue development.¹³²

A



B



◀**Figure 4.5.** Effect of perfusion on VF mucosa culture in 3D VF-OOAC. (A) H&E [I], K5, [II], K14 [III], E-Cad [IV], and LAMA5 [V] were evaluated using confocal microscopy to assess epithelial morphological features. DAPI (blue) indicates cell nuclei. H&E magnification 40×, scale bar = 15 µm. Immunostaining magnification 20×, scale bar = 30 µm. (B) Relative gene expression in perfused 3D VF-OOAC versus static 3D VF-OOAC. Data displayed as the fold change relative to static 3D VF-OOAC. Significant differences denoted by *.

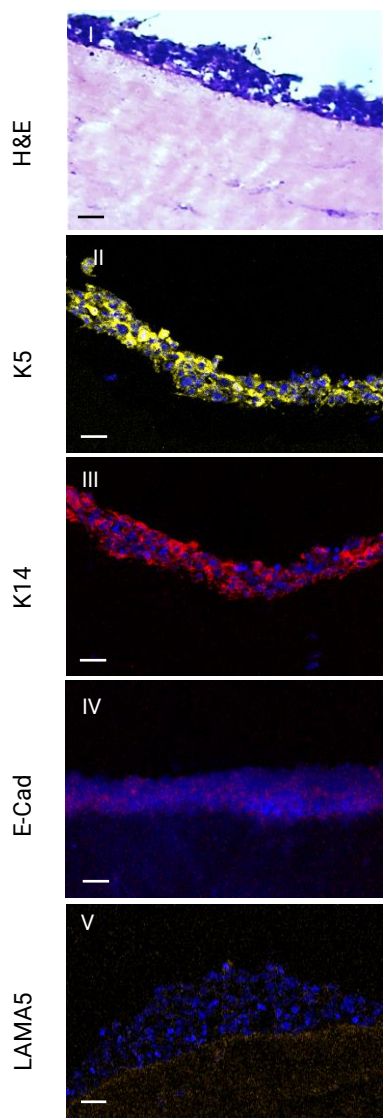
Fluidic shear induced mechanosensitive gene upregulation

Having demonstrated the benefits of perfusion for VF mucosa culture in 3D VF-OOAC, our final step was to evaluate the impact of fluidic shear on culture. To achieve this, a pVFF monolayer was included in the microchannel of 3D VF-OOAC and experienced fluidic shear during perfusion.

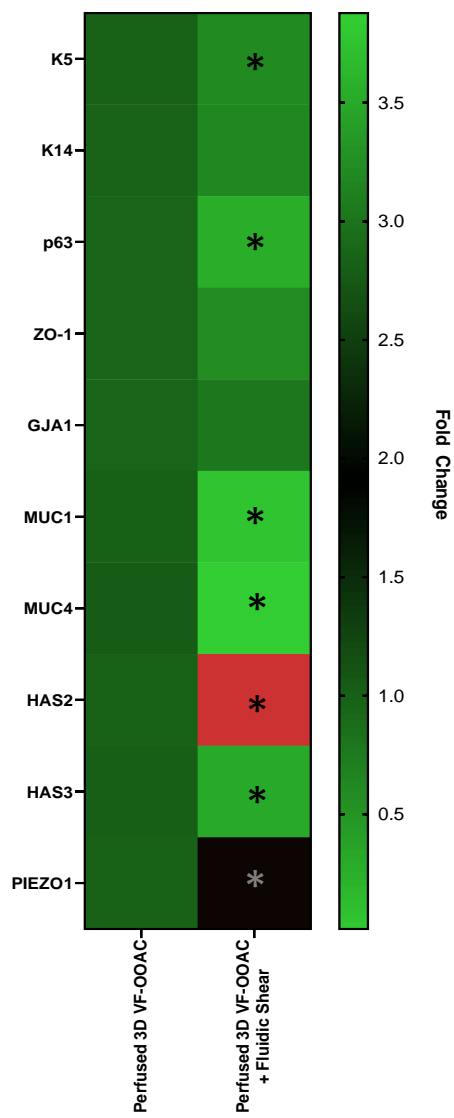
3D VF-OOAC with fluidic shear present had a stratified, multilayered (5-10 cells thick) epithelia that contained basal cuboidal cells, cellular polarization, and a terminally differentiated flattened suprabasal layer (**Figure 4.6A: I**).^{18,95,96} Confocal microscopy showed VF mucosae in 3D VF-OOAC with fluidic shear present retained basal cytokeratin (K5, K14) (**Figure 4.6A: II, III**) and E-Cadherin (**Figure 4.6A: IV**) in the epithelium. Consistent with earlier models, LAMA5 staining remained broad and relatively non-specific suggesting basement membrane immaturity (**Figure 4.6A: V**).

PIEZO1 is a mechanically activated ion channel involved in epithelium remodelling, differentiation, and cell cycle regulation.^{91,133–135} PIEZO1 has also been found to modulate the mechanical properties of atrial fibroblasts enabling them to adapt to the stiffness of their surrounding matrix.¹³⁶ Both HAS2 and PIEZO1 expression have been reported as shear-sensitive in VF epithelial cells and fibroblasts, and this was confirmed by the significantly higher gene expression for each in 3D VF-OOAC with fluidic shear ($p < .05$; **Figure 4.6B**).^{23,137,138} pVFFs are highly mechanosensitive and experience high levels of shear in the biomechanically active laryngeal microenvironment during phonation.^{6,139–141} Elevated HAS2 expression could be related to shear-mediated activation of the NF-κB pathway in pVFFs, which can induce HA synthesis.⁷³ Bioreactor studies of VF fibroblasts have previously reported HAS2 upregulation in response to mechanical stimulation.^{138,142,143} Similarly, fluidic shear likely induced PIEZO1 upregulation via activation of PIEZO1 channel receptors on the surface of pVFFs.^{144–146} The mechanosensitive response of pVFFs to fluidic shear was further demonstrated via observations of cell orientation in the flow direction of perfusion in 3D VF-OOAC, a behaviour consistent with the literature (**Figure 4.6C**).^{74–77}

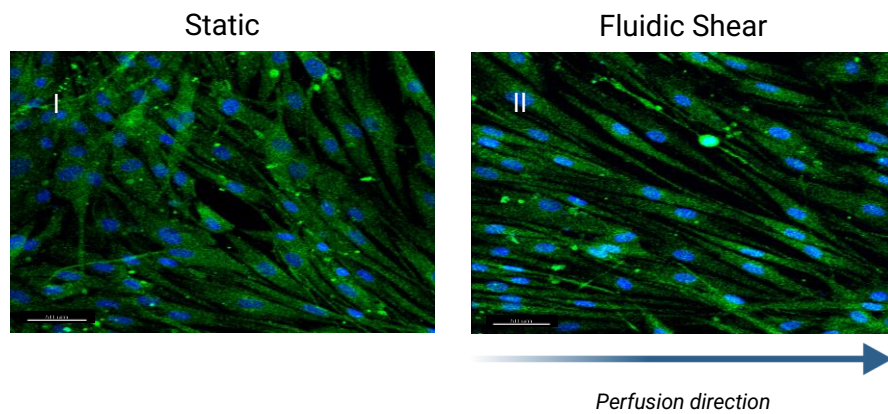
A



B



C



◀**Figure 4.6.** Effect of fluidic shear on VF mucosae cultivated in perfused 3D VF-OOAC. (A) H&E [I], K5, [II], K14 [III], E-Cad [IV], and LAMA5 [V] evaluated morphological features. DAPI (blue) indicates cell nuclei. H&E magnification 40×, scale bar = 15 μ m. Immunostaining magnification 20×, scale bar = 30 μ m. (B) Relative gene expression in perfused 3D VF-OOAC cultures with or without fluidic shear. Data displayed as the fold change relative to perfused 3D VF-OOAC without fluidic shear. (C) Vimentin staining showed fluidic shear induced mesenchymal cell alignment in the direction of fluid flow (40 μ L/h) under perfused conditions versus static controls. Magnification 20×, scale bar = 50 μ m.

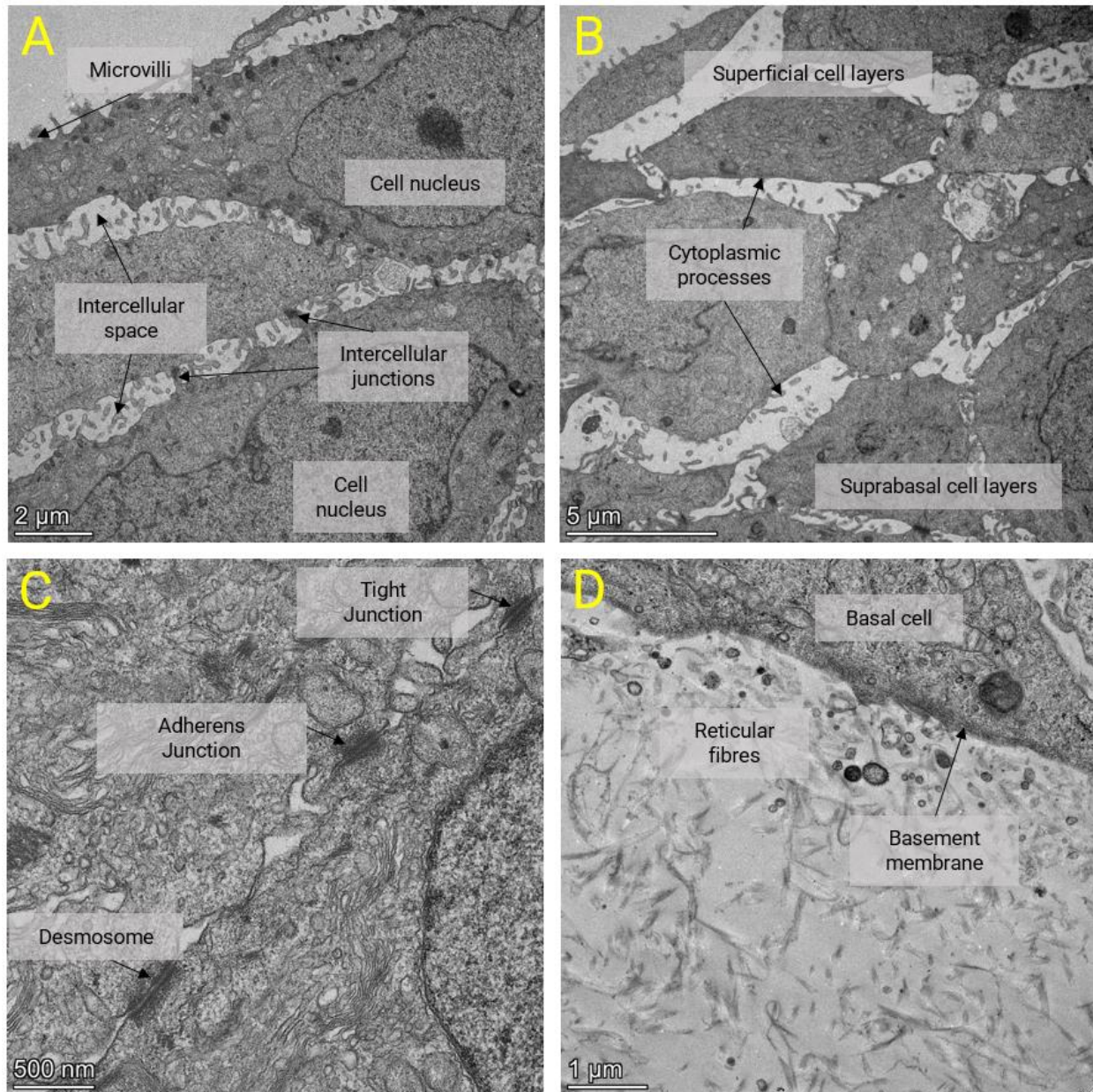


Figure 4.7. Transmission electron micrograph of engineered epithelium in 3D VF-OOAC with fluidic shear. (A) The cells of the epithelium near the superficial layer have a flattened morphology. (B) Cells in the deeper suprabasal layers display more square-like morphology. (C) Intercellular junctions present between neighbouring cells of the epithelium. (D) The basal cell layer is anchored to the basement membrane.

Transmission electron microscopy was used to validate subcellular features of VF mucosae in 3D VF-OOAC with fluidic shear. The apical cell membrane at the epithelium surface had microvilli, as found *in vivo*, that participate in mucus distribution and retention (**Figure 4.7A**).¹⁴⁷ The appearance and distribution of intercellular spaces aligned with adult human VF tissue reported in the literature (**Figure 4.7B**).⁹⁶ Tight junctions were observed in the superficial layers of the epithelium at the apical aspects of adjacent cells, with adherens junctions and desmosomes in close proximity (**Figure 4.7C**). The basement membrane was located under the basal cell layer (**Figure 4.7D**).

Limitations & Future Prospects

OOAC research has historically been challenged by a lack of standardization across the many different models proposed by individual laboratories, which can create replicability and scale-up difficulties.¹⁴⁸ By using commercial devices in this study, we created an OOAC model that provides an increasingly standardized procedure by removing in-house microfabrication variability of the device used. A drawback to this approach is that the design configuration is restricted to the manufacturer's template, and changes are not easily implemented.¹⁴⁹

For instance, although the BEOnChip microfluidic device used for 3D VF-OOAC produced the greatest tissue development, its current design is incompatible with exposing epithelial cells to a dynamic airflow parallel to the luminal epithelial surface. The static ALI provided is unrepresentative of *in vivo* breathing conditions. Conversely, ALI culture was not used for the ChipShop microfluidic device used for 2D VF-OOAC in this study, which provides a compounding factor in mucosal differences observed. Although this device is theoretically compatible with providing a dynamic airflow, it presents a trade-off between technical difficulty and physiological relevance given that 2D culture was shown to severely impact stromal cell behaviour in VF mucosa culture.

Future design modifications of the VF-OOAC should focus on incorporating an airflow channel to expose epithelial cells to physiologically relevant conditions whilst retaining a 3D tissue environment. Additionally, the fluid channel could be utilized for endothelial cells, given their important role in controlling vascular permeability and therapeutic efficacy of drugs.^{150,151}

Conclusion

The presented VF-OOAC represents the first application of microfluidic technology for engineering the VF mucosa. By incorporating relevant physiological scaling, increased dimensionality, perfusion, and fluidic shear, microfluidic devices supported improved tissue development compared to transwell culture. In particular, epithelium functionality and fibroblast ECM synthesis benefited from our perfused microscale culture system, displaying elevated expression related to intercellular junctions, mucin synthesis, and mechanosensitive activity. This versatile *in vitro* platform will aid basic research discoveries of the biological mechanisms underlying VF health and disease.

Author Contributions

PTC: Conceptualization, data collection and analysis, writing-original draft, reviewing and editing. NLJ: Conceptualization, writing-original draft, reviewing and editing, supervision, funding acquisition. VL, XL, ST: Conceptualization, reviewing and editing.

Conflicts of interest

The authors have no conflicts of interest to declare.

Acknowledgements

Microscopy images were collected, processed, and analyzed in the McGill University Advanced BioImaging Facility (ABIF). The authors thank Johanne Ouellette for assistance with TEM sample processing and ultramicrotomy at the Facility for Electron Microscopy Research of McGill University. Molecular biology experiments (qPCR, Bioanalyzer, PCR thermocycler, nanodrop quantification) were performed with the guidance of Dr. Nicolas Audet using McGill University Imaging and Molecular Biology Platform (IMBP) equipment. The authors acknowledge research grants from the National Sciences and Engineering Research Council of Canada (RGPIN-2018-03843 and ALLRP 548623-19), Canada Research Chair research stipend (NLJ), and by the National Institutes of Health (grant R01 DC-018577-01A1). The presented content is solely the responsibility of the authors and does not necessarily represent the official views of the above funding agencies.

References

1. Hirano, M. Structure and Vibratory Behavior of the Vocal Folds. Dynamic Aspects of Speech Production. in *Dynamic aspects of speech production: Current Results, Emerging Problems, and New Instrumentation* 13–27 (University of Tokyo Press, 1977).
2. Arens, C., Glanz, H., Wönckhaus, J., Hersemeyer, K. & Kraft, M. Histologic assessment of epithelial thickness in early laryngeal cancer or precursor lesions and its impact on endoscopic imaging. *Eur. Arch. Otorhinolaryngol.* **264**, 645–649 (2007).
3. Hirano, M. Morphological Structure of the Vocal Cord as a Vibrator and its Variations. *Folia Phoniatr. Logop.* **26**, 89–94 (1974).
4. Gray, S. D. Cellular physiology of the vocal folds. *Otolaryngol. Clin. North Am.* **33**, 679–

- 697 (2000).
5. Chen, X. & Thibeault, S. L. Characteristics of Age-Related Changes in Cultured Human Vocal Fold Fibroblasts. *Laryngoscope* **118**, 1700–1704 (2008).
 6. Catten, M., Gray, S. D., Hammond, T. H., Zhou, R. & Hammond, E. Analysis of cellular location and concentration in vocal fold lamina propria. *Otolaryngol. - Head Neck Surg.* **118**, 663–667 (1998).
 7. King, S. N., Chen, F., Jetté, M. E. & Thibeault, S. L. Vocal fold fibroblasts immunoregulate activated macrophage phenotype. *Cytokine* **61**, 228–236 (2013).
 8. Hahn, M. S., Kobler, J. B., Starcher, B. C., Zeitels, S. M. & Langer, R. Quantitative and Comparative Studies of the Vocal Fold Extracellular Matrix I: Elastic Fibers and Hyaluronic Acid. *Ann. Otol. Rhinol. Laryngol.* **115**, 156–164 (2006).
 9. Zeitels, S. M. *et al.* Vocal Fold Injection of Absorbable Materials: A Histologic Analysis With Clinical Ramifications. *Ann. Otol. Rhinol. Laryngol.* **128**, 71S–81S (2019).
 10. Coburn, P. T., Li, X., Li, J., Kishimoto, Y. & Li-Jessen, N. Y. K. Progress in Vocal Fold Regenerative Biomaterials: An Immunological Perspective. *Adv. NanoBiomed Res.* **2100119**, (2021).
 11. Alipour, F. & Jaiswal, S. Phonatory characteristics of excised pig, sheep, and cow larynges. *J. Acoust. Soc. Am.* **123**, 4572–4581 (2008).
 12. Balls, M. Replacement of animal procedures: Alternatives in research, education and testing. *Lab. Anim.* **28**, 193–211 (1994).
 13. Russel, W. M. S. & Burch, R. L. The Principles of Humane Experimental Technique. *Med. J. Aust.* **1**, 500–500 (1960).
 14. Robinson, N. B. *et al.* The current state of animal models in research: A review. *Int. J. Surg.* **72**, 9–13 (2019).
 15. NIH. *NIDCD Strategic Plan 2023-2027*. (2023).
 16. Sato, K. Cells and Extracellular Matrices in the Human Adult Vocal Fold Mucosa. in *Functional Histoanatomy of the Human Larynx* 125–146 (Springer Singapore, 2018).
 17. Leydon, C., Selekman, J. A., Palecek, S. & Thibeault, S. L. Human Embryonic Stem Cell-Derived Epithelial Cells in a Novel In Vitro Model of Vocal Mucosa. *Tissue Eng. Part A* **19**, 2233–2241 (2013).
 18. Lungova, V., Chen, X., Wang, Z., Kendzioriski, C. & Thibeault, S. L. Human induced pluripotent stem cell-derived vocal fold mucosa mimics development and responses to smoke exposure. *Nat. Commun.* **10**, 4161 (2019).
 19. Lungova, V., Wendt, K. & Thibeault, S. L. Exposure to e-cigarette vapor extract induces vocal fold epithelial injury and triggers intense mucosal remodeling. *Dis. Model. Mech.* **15**, (2022).
 20. Cooper, M., Charest, J. L. & Coppeta, J. Design principles for dynamic microphysiological systems. in *Microfluidic Cell Culture Systems* 1–29 (Elsevier, 2019).
 21. Wikswo, J. P. *et al.* Scaling and systems biology for integrating multiple organs-on-a-chip. *Lab Chip* **13**, 3496–3511 (2013).
 22. Kieninger, J., Weltin, A., Flamm, H. & Urban, G. A. Microsensor systems for cell metabolism-from 2D culture to organ-on-chip. *Lab Chip* **18**, 1274–1291 (2018).
 23. Gracioso Martins, A. M., Biehl, A., Sze, D. & Freytes, D. O. Bioreactors for Vocal Fold Tissue Engineering. *Tissue Eng. Part B Rev.* **28**, 182–205 (2022).
 24. Pöttler, M. *et al.* Magnetic Tissue Engineering of the Vocal Fold Using Superparamagnetic Iron Oxide Nanoparticles. *Tissue Eng. Part A* **00**, 1–8 (2019).

25. Ingber, D. E. Human organs-on-chips for disease modelling, drug development and personalized medicine. *Nat. Rev. Genet.* **23**, 467–491 (2022).
26. Huh, D. *et al.* A Human Disease Model of Drug Toxicity–Induced Pulmonary Edema in a Lung-on-a-Chip Microdevice. *Sci. Transl. Med.* **4**, (2012).
27. Benam, K. H. *et al.* Small airway-on-a-chip enables analysis of human lung inflammation and drug responses in vitro. *Nat. Methods* **13**, 151–157 (2016).
28. Huh, D. *et al.* Reconstituting Organ-Level Lung Functions on a Chip. *Science* (80-.). **328**, 1662–1669 (2010).
29. Wilmer, M. J. *et al.* Kidney-on-a-Chip Technology for Drug-Induced Nephrotoxicity Screening. *Trends Biotechnol.* **34**, 156–170 (2016).
30. Gori, M. *et al.* Investigating nonalcoholic fatty liver disease in a liver-on-a-chip microfluidic device. *PLoS One* **11**, 1–15 (2016).
31. Zhang, J., Wu, J., Li, H., Chen, Q. & Lin, J. M. An in vitro liver model on microfluidic device for analysis of capecitabine metabolite using mass spectrometer as detector. *Biosens. Bioelectron.* **68**, 322–328 (2015).
32. Rennert, K. *et al.* A microfluidically perfused three dimensional human liver model. *Biomaterials* **71**, 119–131 (2015).
33. Bhise, N. S. *et al.* A liver-on-a-chip platform with bioprinted hepatic spheroids. *Biofabrication* **8**, 014101 (2016).
34. Zhang, Y. S. *et al.* From cardiac tissue engineering to heart-on-a-chip: Beating challenges. *Biomed. Mater.* **10**, (2015).
35. Marsano, A. *et al.* Beating heart on a chip: A novel microfluidic platform to generate functional 3D cardiac microtissues. *Lab Chip* **16**, 599–610 (2016).
36. Booth, R. & Kim, H. Characterization of a microfluidic in vitro model of the blood-brain barrier (μ BBB). *Lab Chip* **12**, 1784–1792 (2012).
37. Griep, L. M. *et al.* BBB on CHIP: Microfluidic platform to mechanically and biochemically modulate blood-brain barrier function. *Biomed. Microdevices* **15**, 145–150 (2013).
38. Park, T.-E. *et al.* Hypoxia-enhanced Blood-Brain Barrier Chip recapitulates human barrier function and shuttling of drugs and antibodies. *Nat. Commun.* **10**, 2621 (2019).
39. Bhatia, S. N. & Ingber, D. E. Microfluidic organs-on-chips. *Nat. Biotechnol.* **32**, 760–772 (2014).
40. Mehling, M. & Tay, S. Microfluidic cell culture. *Curr. Opin. Biotechnol.* **25**, 95–102 (2014).
41. Young, E. W. K. K. & Beebe, D. J. Fundamentals of microfluidic cell culture in controlled microenvironments. *Chem. Soc. Rev.* **39**, 1036 (2010).
42. Lim, M. H. *et al.* Development of a Human Respiratory Mucosa-on-a-chip using Decellularized Extracellular Matrix. *Biochip J.* **14**, 279–289 (2020).
43. Byun, J. *et al.* Identification of urban particulate matter-induced disruption of human respiratory mucosa integrity using whole transcriptome analysis and organ-on-a chip. *J. Biol. Eng.* **13**, 88 (2019).
44. Na, K., Lee, M., Shin, H.-W. & Chung, S. In vitro nasal mucosa gland-like structure formation on a chip. *Lab Chip* **17**, 1578–1584 (2017).
45. Baker, B. M. & Chen, C. S. Deconstructing the third dimension-how 3D culture microenvironments alter cellular cues. *J. Cell Sci.* **125**, 3015–3024 (2012).
46. Ling, C. *et al.* Bioengineered vocal fold mucosa for voice restoration. *Sci. Transl. Med.* **7**, (2015).
47. Walimbe, T., Panitch, A. & Sivasankar, M. P. An in vitro scaffold-free epithelial-fibroblast

- coculture model for the larynx. *Laryngoscope* **127**, (2017).
48. Chen, X. *et al.* Novel immortalized human vocal fold epithelial cell line: In vitro tool for mucosal biology. *FASEB J.* **35**, 1–16 (2021).
 49. Castiaux, A. D., Spence, D. M. & Martin, R. S. Review of 3D cell culture with analysis in microfluidic systems. *Anal. Methods* **11**, 4220–4232 (2019).
 50. Cukierman, E., Pankov, R., Stevens, D. R. & Yamada, K. M. Taking Cell-Matrix Adhesions to the Third Dimension. *Science (80-.)*. **294**, 1708–1712 (2001).
 51. Leung, C. M. *et al.* A guide to the organ-on-a-chip. *Nat. Rev. Methods Prim.* **2**, (2022).
 52. Latifi, N. *et al.* A Flow Perfusion Bioreactor System for Vocal Fold Tissue Engineering Applications. *Tissue Eng. Part C Methods* **22**, 823–838 (2016).
 53. Van Den Dolder, J. *et al.* Flow perfusion culture of marrow stromal osteoblasts in titanium fiber mesh. *J. Biomed. Mater. Res. - Part A* **64**, 235–241 (2003).
 54. Cartmell, S. H., Porter, B. D., García, A. J. & Guldberg, R. E. Effects of Medium Perfusion Rate on Cell-Seeded Three-Dimensional Bone Constructs in Vitro. *Tissue Eng.* **9**, 1197–1203 (2003).
 55. Pusch, J. *et al.* The physiological performance of a three-dimensional model that mimics the microenvironment of the small intestine. *Biomaterials* **32**, 7469–7478 (2011).
 56. Domansky, K. *et al.* Perfused multiwell plate for 3D liver tissue engineering. *Lab Chip* **10**, 51–58 (2010).
 57. Kaarj, K. & Yoon, J. Y. Methods of delivering mechanical stimuli to Organ-on-a-Chip. *Micromachines* **10**, (2019).
 58. Ng, C. P., Hinz, B. & Swartz, M. A. Interstitial fluid flow induces myofibroblast differentiation and collagen alignment in vitro. *J. Cell Sci.* **118**, 4731–4739 (2005).
 59. Titze, I. R., Klemuk, S. A. & Lu, X. Adhesion of a Monolayer of Fibroblast Cells to Fibronectin Under Sonic Vibrations in a Bioreactor. *Ann. Otol. Rhinol. Laryngol.* **121**, 364–374 (2012).
 60. Sontheimer-Phelps, A., Hassell, B. A. & Ingber, D. E. Modelling cancer in microfluidic human organs-on-chips. *Nat. Rev. Cancer* **19**, 65–81 (2019).
 61. Nawroth, J. C. *et al.* Stem cell-based Lung-on-Chips: The best of both worlds? *Adv. Drug Deliv. Rev.* **140**, 12–32 (2018).
 62. Benam, K. H. *et al.* Matched-Comparative Modeling of Normal and Diseased Human Airway Responses Using a Microengineered Breathing Lung Chip. *Cell Syst.* **3**, 456–466 (2016).
 63. Wang, W. *et al.* Live human nasal epithelial cells (hNECs) on chip for in vitro testing of gaseous formaldehyde toxicity via airway delivery. *Lab Chip* **14**, 677–680 (2014).
 64. Gholizadeh, H. *et al.* Real-time quantitative monitoring of in vitro nasal drug delivery by a nasal epithelial mucosa-on-a-chip model. *Expert Opin. Drug Deliv.* **18**, 803–818 (2021).
 65. Raty, S. *et al.* Embryonic development in the mouse is enhanced via microchannel culture. *Lab Chip* **4**, 186–190 (2004).
 66. Duval, K. *et al.* Modeling Physiological Events in 2D vs. 3D Cell Culture. *Physiology* **32**, 266–277 (2017).
 67. Gauvin, R. *et al.* Microfabrication of complex porous tissue engineering scaffolds using 3D projection stereolithography. *Biomaterials* **33**, 3824–3834 (2012).
 68. Bonnier, F. *et al.* Cell viability assessment using the Alamar blue assay: A comparison of 2D and 3D cell culture models. *Toxicol. Vitro.* **29**, 124–131 (2015).
 69. Paguirigan, A. L. & Beebe, D. J. Microfluidics meet cell biology: Bridging the gap by

- validation and application of microscale techniques for cell biological assays. *BioEssays* **30**, 811–821 (2008).
70. Jetta, D., Gottlieb, P. A., Verma, D., Sachs, F. & Hua, S. Z. Shear stress-induced nuclear shrinkage through activation of Piezo1 channels in epithelial cells. *J. Cell Sci.* **132**, (2019).
 71. Lei, X. *et al.* The effect of fluid shear stress on fibroblasts and stem cells on plane and groove topographies. *Cell Adhes. Migr.* **14**, 12–23 (2020).
 72. Shi, Z. D. & Tarbell, J. M. Fluid flow mechanotransduction in vascular smooth muscle cells and fibroblasts. *Ann. Biomed. Eng.* **39**, 1608–1619 (2011).
 73. Vigetti, D. *et al.* Proinflammatory cytokines induce hyaluronan synthesis and monocyte adhesion in human endothelial cells through hyaluronan synthase 2 (HAS2) and the nuclear factor- κ B (NF- κ B) pathway. *J. Biol. Chem.* **285**, 24639–24645 (2010).
 74. Dan, L., Chua, C.-K. & Leong, K.-F. Fibroblast response to interstitial flow: A state-of-the-art review. *Biotechnol. Bioeng.* **107**, 1–10 (2010).
 75. Steward, R. L., Cheng, C. M., Ye, J. D., Bellin, R. M. & Leduc, P. R. Mechanical stretch and shear flow induced reorganization and recruitment of fibronectin in fibroblasts. *Sci. Rep.* **1**, 1–12 (2011).
 76. Gupta, R. *et al.* The effect of shear stress on fibroblasts derived from Dupuytren's tissue and normal palmar fascia. *J. Hand Surg. Am.* **23**, 945–950 (1998).
 77. Zabinyakov, N. Shear Stress Modulates Gene Expression in Normal Human Dermal Fibroblasts. *Masters Thesis* (University of Calgary, 2017). doi:10.11575/PRISM/27775.
 78. Lee, S. H., Samuels, T., Bock, J. M., Blumin, J. H. & Johnston, N. Establishment of an immortalized laryngeal posterior commissure cell line as a tool for reflux research. *Laryngoscope* **125**, E73–E77 (2015).
 79. Ahadian, S. *et al.* Organ-On-A-Chip Platforms: A Convergence of Advanced Materials, Cells, and Microscale Technologies. *Adv. Healthc. Mater.* **7**, 1700506 (2018).
 80. Huh, D. *et al.* Microfabrication of human organs-on-chips. *Nat. Protoc.* **8**, 2135–2157 (2013).
 81. Beigel, J., Fella, K., Kramer, P. J., Kroeger, M. & Hewitt, P. Genomics and proteomics analysis of cultured primary rat hepatocytes. *Toxicol. Vitro.* **22**, 171–181 (2008).
 82. Lungova, V. & Thibeault, S. Protocol: Developmental derivation of vocal fold mucosa from human induced pluripotent stem cells. 1–14.
 83. Chung, H. H., Mireles, M., Kwart, B. J. & Gaborski, T. R. Use of porous membranes in tissue barrier and co-culture models. *Lab Chip* **18**, 1671–1689 (2018).
 84. Raasch, M. *et al.* Microfluidically supported biochip design for culture of endothelial cell layers with improved perfusion conditions. *Biofabrication* **7**, 015013 (2015).
 85. Deinhardt-Emmer, S. *et al.* Co-infection with *Staphylococcus aureus* after primary influenza virus infection leads to damage of the endothelium in a human alveolus-on-a-chip model. *Biofabrication* **12**, 025012 (2020).
 86. Deinhardt-Emmer, S. *et al.* SARS-CoV-2 Causes Severe Epithelial Inflammation and Barrier Dysfunction. *J. Virol.* **95**, (2021).
 87. Benam, K. H. *et al.* Human Lung Small Airway-on-a-Chip Protocol. in *3D Cell Culture* vol. 1612 345–365 (2017).
 88. Lungova, V. Supplementary Information Human induced pluripotent stem cell-derived vocal fold mucosa mimics development and responds to smoke exposure. (2019).
 89. Tateya, I., Tateya, T., Lim, X., Sohn, J. H. & Bless, D. M. Cell production in injured vocal folds: A rat study. *Ann. Otol. Rhinol. Laryngol.* **115**, 135–143 (2006).

90. Li-Jessen, N. Y. K., Powell, M., Choi, A.-J., Lee, B.-J. & Thibeault, S. L. Cellular source and proinflammatory roles of high-mobility group box 1 in surgically injured rat vocal folds. *Laryngoscope* **127**, E193–E200 (2017).
91. Foote, A. G., Lungova, V. & Thibeault, S. L. Piezo1-expressing vocal fold epithelia modulate remodeling via effects on self-renewal and cytokeratin differentiation. *Cell. Mol. Life Sci.* **79**, 591 (2022).
92. Livak, K. J. & Schmittgen, T. D. Analysis of relative gene expression data using real-time quantitative PCR and the 2- $\Delta\Delta$ CT method. *Methods* **25**, 402–408 (2001).
93. Yamaguchi, T., Shin, T. & Sugihara, H. Reconstruction of the laryngeal mucosa. *Otolaryngol. - Head Neck Surg.* **122**, (1996).
94. Lee, M. K. *et al.* Air-liquid interface culture of serially passaged human nasal epithelial cell monolayer for in vitro drug transport studies. *Drug Deliv. J. Deliv. Target. Ther. Agents* **12**, 305–311 (2005).
95. Štiblar-MartinČič, D. Histology of Laryngeal Mucosa. *Acta Otolaryngol.* **117**, 138–141 (1997).
96. Sato, K. *Functional Histoanatomy of the Human Larynx. Functional Histoanatomy of the Human Larynx* (Springer Singapore, 2018).
97. Leydon, C., Bartlett, R. S., Roenneburg, D. A. & Thibeault, S. L. Localization of label-retaining cells in murine vocal fold epithelium. *J. Speech, Lang. Hear. Res.* **54**, 1060–1066 (2011).
98. Jain, P., Rauer, S. B., Möller, M. & Singh, S. Mimicking the Natural Basement Membrane for Advanced Tissue Engineering. *Biomacromolecules* **23**, 3081–3103 (2022).
99. Kelley, L. C., Lohmer, L. L., Hagedorn, E. J. & Sherwood, D. R. Traversing the basement membrane in vivo: A diversity of strategies. *J. Cell Biol.* **204**, 291–302 (2014).
100. Levendoski, E. E., Leydon, C. & Thibeault, S. L. Vocal Fold Epithelial Barrier in Health and Injury: A Research Review. *J. Speech, Lang. Hear. Res.* **57**, 1679–1691 (2014).
101. Troxell, M. L. *et al.* Inhibiting cadherin function by dominant mutant E-cadherin expression increases the extent of tight junction assembly. *J. Cell Sci.* **113**, 985–996 (2000).
102. Ravikrishnan, A., Fowler, E. W., Stuffer, A. J. & Jia, X. Hydrogel-Supported, Engineered Model of Vocal Fold Epithelium. *ACS Biomater. Sci. Eng.* **7**, 4305–4317 (2021).
103. Schneider, B., Teschner, M., Sudermann, T., Pikula, B. & Lautermann, J. Expression of Gap Junction Proteins (Connexin 26, 30, 32, 43) in Normal Mucosa, Hyperkeratosis and Carcinoma of the Human Larynx. *ORL* **64**, 324–329 (2002).
104. Van Deusen, M. B. & Lyon, M. J. Connexins within the rat larynx. *Otolaryngol. Neck Surg.* **139**, 823–828 (2008).
105. Hervé, J. C., Bourmeyster, N. & Sarrouilhe, D. Diversity in protein-protein interactions of connexins: Emerging roles. *Biochim. Biophys. Acta - Biomembr.* **1662**, 22–41 (2004).
106. Bruzzone, R., White, T. W. & Paul, D. L. Connections with connexins: The molecular basis of direct intercellular signaling. *Eur. J. Biochem.* **238**, 1–27 (1996).
107. Samuels, T. L. *et al.* Mucin Gene Expression in Human Laryngeal Epithelia: Effect of Laryngopharyngeal Reflux. *Ann. Otol. Rhinol. Laryngol.* **117**, 688–695 (2008).
108. Roy, N., Tanner, K., Gray, S. D., Blomgren, M. & Fisher, K. V. An evaluation of the effects of three laryngeal lubricants on phonation threshold pressure (PTP). *J. Voice* **17**, 331–342 (2003).
109. Hirano, M. & Kakita, Y. Cover-body theory of vocal cord vibration. in *Speech Science* 1–46 (College Hill Press, 1985).

110. Chan, R. W., Gray, S. D. & Titze, I. R. The importance of hyaluronic acid in vocal fold biomechanics. *Otolaryngol. - Head Neck Surg.* **124**, 607–614 (2001).
111. Butler, J. E., Hammond, T. H. & Gray, S. D. Gender-Related Differences of Hyaluronic Acid Distribution in the Human Vocal Fold. *Laryngoscope* **111**, 907–911 (2001).
112. Meyvantsson, I., Warrick, J. W., Hayes, S. & Beebe, D. J. Automated cell culture in high density tubeless microfluidic device arrays. *Lab Chip* **8**, 717–724 (2008).
113. Yu, H., Meyvantsson, I., Shkel, A. & Beebe, D. J. Diffusion dependent cell behavior in microenvironments. *Lab Chip* **5**, 1089–1095 (2005).
114. McCaffrey, L. M. & Macara, I. G. Epithelial organization, cell polarity and tumorigenesis. *Trends Cell Biol.* **21**, 727–735 (2011).
115. Page, H., Flood, P. & Reynaud, E. G. Three-dimensional tissue cultures: Current trends and beyond. *Cell Tissue Res.* **352**, 123–131 (2013).
116. Voynow, J. A., Fischer, B. M., Roberts, B. C. & Proia, A. D. Basal-like cells constitute the proliferating cell population in cystic fibrosis airways. *Am. J. Respir. Crit. Care Med.* **172**, 1013–1018 (2005).
117. Stockinger, A., Eger, A., Wolf, J., Beug, H. & Foisner, R. E-cadherin regulates cell growth by modulating proliferation-dependent β -catenin transcriptional activity. *J. Cell Biol.* **154**, 1185–1196 (2001).
118. Chen, X. & Thibeault, S. L. Biocompatibility of a synthetic extracellular matrix on immortalized vocal fold fibroblasts in 3D culture. *Acta Biomater.* **6**, 2940–2948 (2010).
119. Kuhn, M. A. Histological changes in vocal fold growth and aging. *Curr. Opin. Otolaryngol. Head Neck Surg.* **22**, 460–465 (2014).
120. Hirano, M., Sato, K. & Nakashima, T. Fibroblasts in human vocal fold mucosa. *Acta Otolaryngol.* **119**, 271–276 (1999).
121. Datta, N. *et al.* In vitro generated extracellular matrix and fluid shear stress synergistically enhance 3D osteoblastic differentiation. *Proc. Natl. Acad. Sci. U. S. A.* **103**, 2488–2493 (2006).
122. Dowdall, J. R. *et al.* Identification of distinct layers within the stratified squamous epithelium of the adult human true vocal fold. *Laryngoscope* **125**, E313–E319 (2015).
123. Wei, F. *et al.* Changes in interstitial fluid flow, mass transport and the bone cell response in microgravity and normogravity. *Bone Res.* **10**, (2022).
124. Chary, S. R. & Jain, R. K. Direct measurement of interstitial convection and diffusion of albumin in normal and neoplastic tissues by fluorescence photobleaching. *Proc. Natl. Acad. Sci. U. S. A.* **86**, 5385–5389 (1989).
125. Polacheck, W. J., Charest, J. L. & Kamm, R. D. Interstitial flow influences direction of tumor cell migration through competing mechanisms. *Proc. Natl. Acad. Sci.* **108**, 11115–11120 (2011).
126. Sato, S. Mammalian Cell Culture System. in *Fermentation and Biochemical Engineering Handbook* 17–24 (Elsevier, 2014).
127. Zhou, J., Li, Y.-S. S. & Chien, S. Shear stress-initiated signaling and its regulation of endothelial function. *Arterioscler. Thromb. Vasc. Biol.* **34**, 2191–2198 (2014).
128. Joshi, H. & Morley, S. C. Cells under stress: The mechanical environment shapes inflammasome responses to danger signals. *J. Leukoc. Biol.* **106**, 119–125 (2019).
129. Lillehoj, E. P. & Kim, K. C. Airway mucus: Its components and function. *Arch. Pharm. Res.* **25**, 770–780 (2002).
130. Levendoski, E. Investigating the Acute Effects of Acrolein on Ion Transport and Mucin

- Gene Expression in Excised Porcine Vocal Folds. *PhD Thesis, Purdue University* (2012).
131. Chandorkar, P. *et al.* Fast-track development of an in vitro 3D lung/immune cell model to study Aspergillus infections. *Sci. Rep.* **7**, 11644 (2017).
 132. Huh, D., Hamilton, G. A. & Ingber, D. E. From 3D cell culture to organs-on-chips. *Trends Cell Biol.* **21**, 745–754 (2011).
 133. Gudipaty, S. A. *et al.* Mechanical stretch triggers rapid epithelial cell division through Piezo1. *Nature* **543**, 118–121 (2017).
 134. Eisenhoffer, G. T. *et al.* Crowding induces live cell extrusion to maintain homeostatic cell numbers in epithelia. *Nature* **484**, 546–549 (2012).
 135. Jiang, Y., Yang, X., Jiang, J. & Xiao, B. Structural Designs and Mechanogating Mechanisms of the Mechanosensitive Piezo Channels. *Trends Biochem. Sci.* **46**, 472–488 (2021).
 136. Emig, R. *et al.* Piezo1 channels contribute to the regulation of human atrial fibroblast mechanical properties and matrix stiffness sensing. *Cells* **10**, 1–21 (2021).
 137. Foote, A. G., Wang, Z., Kendzierski, C. & Thibeault, S. L. Tissue specific human fibroblast differential expression based on RNA sequencing analysis. *BMC Genomics* **20**, 308 (2019).
 138. Kirsch, A. *et al.* Development and validation of a novel phonomimetic bioreactor. *PLoS One* 1–15 (2019).
 139. Bartlett, R. S., Gaston, J. D., Ye, S., Kendzierski, C. & Thibeault, S. L. Mechanotransduction of vocal fold fibroblasts and mesenchymal stromal cells in the context of the vocal fold mechanome. *J. Biomech.* **23**, 227–234 (2019).
 140. Bailly, L. *et al.* 3D multiscale imaging of human vocal folds using synchrotron X-ray microtomography in phase retrieval mode. *Sci. Rep.* **8**, 1–20 (2018).
 141. Li, N. Y. K., Heris, H. K. & Mongeau, L. Current Understanding and Future Directions for Vocal Fold Mechanobiology. *J. Cytol. Mol. Biol.* **23**, 1–7 (2013).
 142. Titze, I. R. *et al.* Design and validation of a bioreactor for engineering vocal fold tissues under combined tensile and vibrational stresses. *J. Biomech.* **37**, 1521–1529 (2004).
 143. Kutty, J. K. & Webb, K. Vibration stimulates vocal mucosa-like matrix expression by hydrogel-encapsulated fibroblasts. *J. Tissue Eng. Regen. Med.* **4**, 62–72 (2010).
 144. Ranade, S. S. *et al.* Piezo1, a mechanically activated ion channel, is required for vascular development in mice. *Proc. Natl. Acad. Sci. U. S. A.* **111**, 10347–10352 (2014).
 145. Liu, H. *et al.* Piezo1 Channels as Force Sensors in Mechanical Force-Related Chronic Inflammation. *Front. Immunol.* **13**, 1–20 (2022).
 146. Coste, B. *et al.* Piezo1 and Piezo2 Are Essential Components of Distinct Mechanically Activated Cation Channels. *Science* (80-.). **330**, 55–60 (2010).
 147. Tillmann, B., Pietzsch-Rohrschneider, I. & Huenges, H. L. The Human Vocal Cord Surface. *Cell Tissue Res.* **283**, 279–283 (1977).
 148. Probst, C., Schneider, S. & Loskill, P. High-throughput organ-on-a-chip systems: Current status and remaining challenges. *Curr. Opin. Biomed. Eng.* **6**, 33–41 (2018).
 149. Zhang, B., Korolj, A., Lai, B. F. L. & Radisic, M. Advances in organ-on-a-chip engineering. *Nat. Rev. Mater.* **3**, 257–278 (2018).
 150. Sato, K. Blood Vessels of the Larynx and Vocal Fold. in *Functional Histoanatomy of the Human Larynx* 287–303 (Springer Singapore, 2018).
 151. Azzi, S., Hebda, J. K. & Gavard, J. Vascular Permeability and Drug Delivery in Cancers. *Front. Oncol.* **3**, 1–14 (2013).

Supporting Information

RNA Quantity & Quality

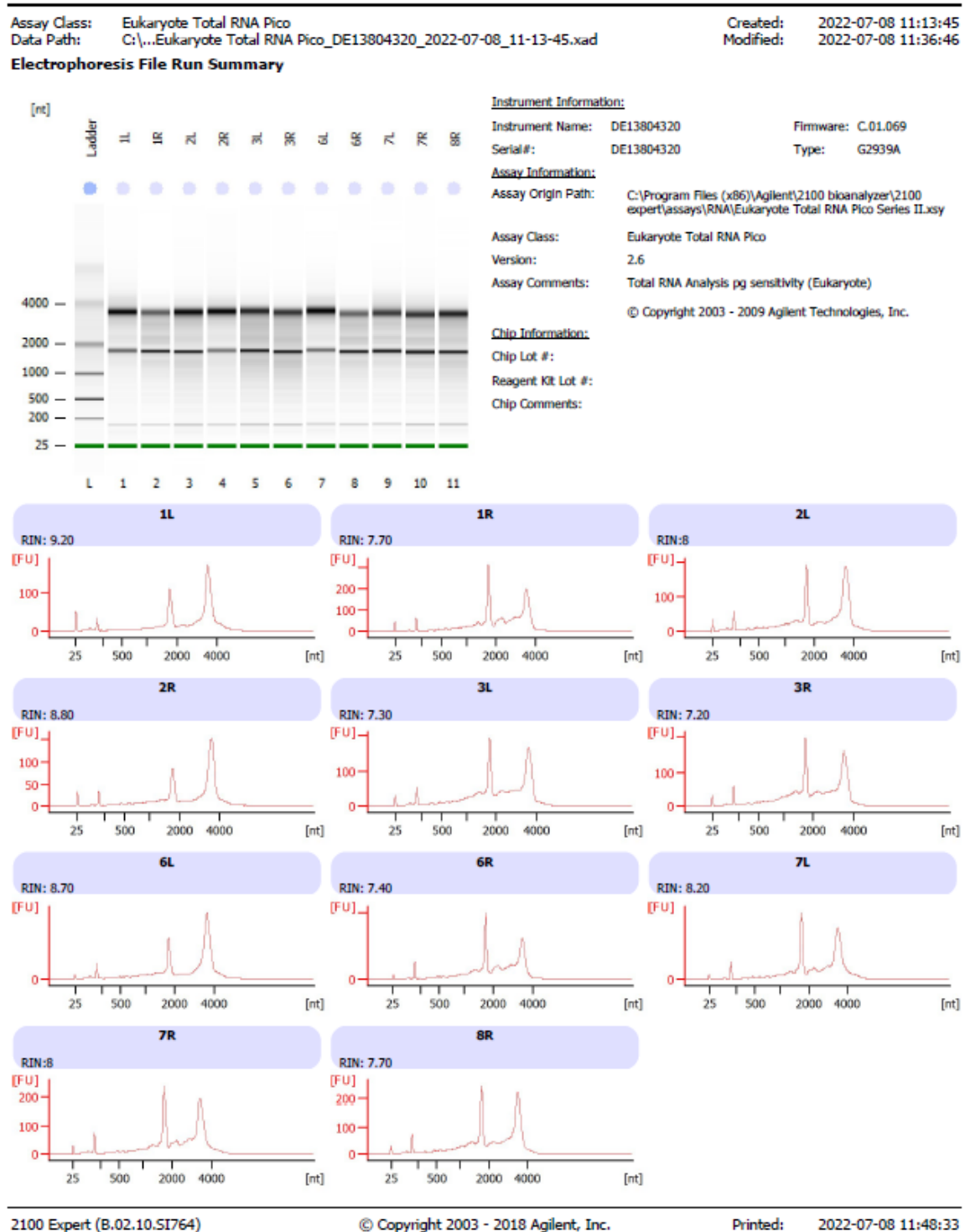


Figure S4.1. Bioanalyzer results for perfused 3D VF-OOAC samples with fluidic shear. All samples tested had a RIN >7, indicating no significant RNA degradation occurred during sample storage or processing.

Impact of Fluidic Shear in Perfused 2D VF-OOAC Culture

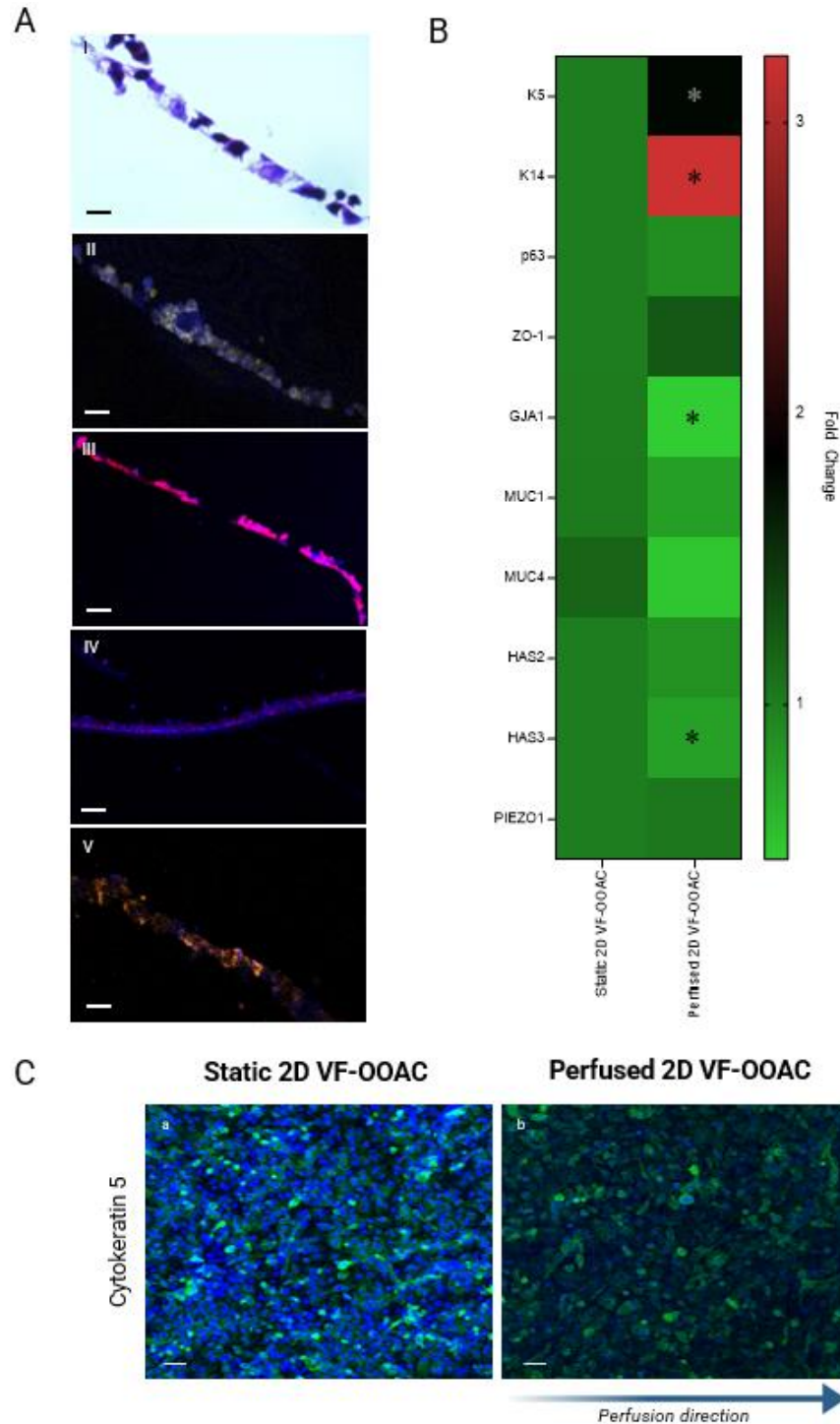


Figure S4.2. Effect of perfusion and fluidic shear on VF mucosae cultivated in 2D VF-OOAC. In perfused cultures, both the upper and lower channel are perfused for 10 days after connecting to a peristaltic pump. During perfusion of the lower channel, the pVFF monolayer experiences fluidic shear. (A) H&E [I], K5, [II], K14 [III], E-Cad [IV], and LAMA5 [V] were evaluated using confocal microscopy to assess epithelial morphological features. DAPI (blue) indicates cell nuclei. Magnification 20 \times , scale bar = 30 μ m. (B) Heatmap of relative gene expression in perfused 2D

VF-OOAC with fluidic shear compared to static 2D VF-OOAC. Data displayed as the fold change relative to static 2D VF-OOAC. Significant differences ($p < .05$) denoted by *. (C) Overhead imaging of the epithelial layer using K5 staining demonstrated that despite the absence of an ALI, the epithelial cells still formed a fully confluent layer with strong basal cytokeratin expression in both static 2D VF-OOAC and perfused 2D VF-OOAC with fluidic shear. Perfusion Magnification 10 \times , scale bar = 50 μ m.

Preface to Chapter 4: Air Pollution Threat to the Vocal Fold Mucosa

Air Pollution

Ambient air pollutants constitute a number of inhalable toxins originating from a range of anthropogenic and natural activities including vehicular and industrial combustion, road wear, forest fires, dust storms, and pollen.⁵⁶ The World Health Organization estimated in 2022 that 99% of the global population live in regions where air quality exceeds safety limits.⁵⁷ In Canada, Montréal has been established as a principal contributor to air pollution, exceeding Toronto and Vancouver levels by 50% and 300% respectively.^{58,59}

Health consequences of air pollution have been studied across a broad range of human tissues, with the respiratory, cardiovascular, and nervous systems garnering notable attention.^{60–65} However, the effect of air pollutants on the VF mucosa has seldom been explored despite the potential contribution to voice disorders such as laryngitis, laryngeal cancer, and vocal cord dysfunction.^{5,6,8,66,67}

Air pollutants can damage the VF mucosa by inducing inflammatory activity that disrupts the layered structure of the mucosa, inhibiting vibratory function.²⁰ Irritant-induced VF damage can be a combination of biophysical and biochemical effects including epithelial drying, DNA damage, and alterations in junction protein expression.^{8,68}

Systematic investigations of specific air pollutants will help define the concentration and exposure limit associated with deleterious effects on voice production. In turn, this will enhance the understanding of the contribution of air pollutants to the pathology of voice disorders.

Particulate Matter

Environmental agencies have designated certain air pollutants as ‘criteria pollutants’ based on their prevalence and threat to human health or the environment. Criteria pollutants are subject to strict monitoring and include particulate matter (PM), sulphur dioxide, nitrogen oxides, ozone, carbon monoxide, and lead.^{69,70}

In particular, PM presents a serious threat to human health and has been associated with 9 million deaths per annum.^{71,72} Both acute and chronic exposure to PM have demonstrated a dose-response relationship for inducing adverse health effects.⁵⁶ Unlike other air pollutants, PM is a heterogeneous mix of suspended micro- or nano-sized particles and droplets that includes heavy metal ions, dust, polycyclic aromatic hydrocarbons, pollen, and bacteria. Each component can generate inflammatory activity in human tissues. For instance, transition metals have been associated with increased oxidative stress and polyaromatic hydrocarbons may induce mutagenic activity, cell toxicity, and inflammatory cytokine release.⁷³ The composition of PM will vary significantly depending on factors such as temperature, weather conditions, particle origins, and particle interactions.

PM is regulated by mass concentration and particle number with several major categories specified. Coarse (PM₁₀), fine (PM_{2.5}), and ultrafine (PM_{0.1}) fractions are defined as particles with an average aerodynamic equivalent diameter of $\leq 10 \mu\text{m}$, $\leq 2.5 \mu\text{m}$, and $\leq 0.1 \mu\text{m}$ respectively.⁷⁴ These categories are of clinical importance as particle penetration depth into the respiratory system is size-dependent.

Association between Voice Disorders & Coarse Particulate Matter

In the upper airway, turbulent, high velocity airflow coupled with the aerodynamic properties of large particles results in significant PM₁₀ deposition in the upper airway.^{75–78} As the narrowest point in the airway, the larynx may have a particular vulnerability to PM₁₀ deposition due to its turbulent airflow, filter function restricting particulate movement to the lower airway, and the regions of non-ciliated squamous epithelia it contains.^{21,67,79}

PM₁₀ presents a notable environmental challenge to the VF mucosa due to the hazardous particles it comprises. Exposure to PM has been associated with multiple voice disorders including vocal cord dysfunction and fibrosis, chronic laryngitis, and laryngeal cancer.^{4–6} However, further experimental studies and long-term epidemiological data are required to fully elucidate the mechanisms by which PM₁₀ contributes to the pathophysiology of these conditions.

With around 8 billion people exposed to air that exceeds World Health Organization guidelines, it is increasingly necessary to characterize the effect of specific air pollutants on human tissues and organs.⁸⁰ For the field of laryngology, revealing the molecular mechanisms underlying

the interaction of PM₁₀ with the VF mucosa is important given its global prevalence, threat to human health, and high deposition in the upper airway. Understanding how air pollutants influence signalling pathways and cellular processes in the VF mucosa will provide therapeutic treatment targets for resolving voice disorders related to, or exacerbated by, pollution exposure.

Chapter 4. Evaluating the Resilience of the Vocal Fold Mucosa to Acute Exposure to Coarse Particulate Matter Pollutants – An Organ-on-a-Chip Analysis

Patrick T. Coburn^a, Vlasta Lungova^b, Carol X. Chen^c, Thomas M. Durcan^c, Xinyu Liu^d, Susan L. Thibeault^b, Nicole Y. K. Li-Jessen^{a,e,f,g,†}

a. School of Communication Sciences and Disorders, McGill University, Canada

b. Department of Surgery, Division of Otolaryngology – Head and Neck Surgery, University of Wisconsin, Madison, WI, USA

c. Montreal Neurological Institute, McGill University, Canada

d. Department of Mechanical Engineering, University of Toronto, Canada

e. Department of Biomedical Engineering, McGill University, Canada

f. Department of Otolaryngology – Head & Neck Surgery, McGill University, Canada

g. Research Institute of McGill University Health Centre, Canada

† Corresponding author

Abstract

The primary goal of this study was to quantify the biological effect of particulate matter on the vocal fold mucosa. Particulate matter is a significant component of environmental air pollution with serious public health consequences. Notably, coarse particulate matter (PM₁₀) tends to deposit on the surface of the vocal folds in the upper airway. Vocal fold epithelium has an intrinsic capacity to endure and adapt to irritant challenges, but the threshold limit is unknown for PM₁₀ exposure. Identifying the potential dose-response relationship between PM₁₀ and the vocal fold mucosa will contribute to a better understanding of PM-related upper airway conditions such as chronic cough and laryngitis.

Our team previously developed a vocal fold mucosa organ-on-a-chip (VF-OOAC) for toxicity assessment. Here, a dose response study (0, 50, 100, 400 µg/mL) was performed on VF-OOAC_{ILEC}, which comprises primary vocal fold fibroblasts and immortalized laryngeal epithelial cells, for an acute exposure of 24 hr. In addition, a separate version of VF-OOAC using the same fibroblast source but with an iPSC-derived vocal fold epithelium, namely VF-OOAC_{iPSC}, was included to assess if different epithelial cell sources produce divergent responses to pollutant challenges. Tissue morphology, gene expression of epithelial and inflammatory markers, and secreted cytokines were assessed via confocal microscopy, qPCR, and immunoassays respectively.

Both VF-OOAC_{iLEC} and VF-OOAC_{iPSC} models demonstrated high resistance to acute PM₁₀ exposure for all concentrations tested. For VF-OOAC_{iLEC}, no dose response was detected in any outcome measurement. VF-OOAC_{iPSC} displayed a significant increase in cytokeratin 13 gene expression when challenged with 100 µg/mL PM₁₀. Our results demonstrate the resilience of stratified squamous epithelium of the vocal folds, highlighting its robust defences against environmental irritants. Future investigations should focus on investigating how chronic, repeated exposure to PM₁₀ may lead to pathological changes in VF mucosa.

Introduction

In 2022, the World Health Organization estimated that 99% of the global population live in areas where air quality exceeds safety limits.¹ Air pollution presents a serious public health risk as it reportedly impacts every human organ and contributes to 9 million premature deaths per annum.^{2,3} Specifically for respiratory health, particulate matter (PM) has been associated with exacerbations of asthma and chronic obstructive pulmonary disease, idiopathic pulmonary fibrosis, and lung cancer.⁴⁻⁷

PM also presents a significant health-related economic impact due to healthcare costs and lost labour productivity.⁸ In 2013, the World Bank estimated a global economic impact of US\$ 143 billion in lost labour income and US\$ 3.55 trillion in welfare losses from PM exposure.⁹

The considerable health and economic impact of PM have led to its strict monitoring by environmental agencies.^{3,10-12} PM exists as a heterogeneous mix of micro- and nano-sized particles and droplets originating from anthropogenic or natural activities including automobile exhausts, industrial operations, and forest fires.^{13,14} The prevalence of PM attributed to forest fires in particular continues to intensify, with Canada subject to record wildfires in 2023, the European Union reporting peak landmass burned in 2022, Australia experiencing catastrophic bushfires in 2020, and California State suffering historic wildfires in 2020.¹⁵⁻¹⁸

PM is categorized based on its physical properties, with coarse (PM₁₀), fine (PM_{2.5}), and ultrafine (PM_{0.1}) fractions describing particles of ≤10 µm, ≤2.5 µm, and ≤0.1 µm respectively.¹⁹ The depth a particle penetrates the respiratory airway is size-dependent, with PM₁₀ deposition dominant in the upper airway and PM_{0.1-2.5} travelling deeper into the lungs.^{7,20,21}

The World Health Organization recently updated its guidelines for short- and long-term exposure to PM₁₀, suggesting an association with increased mortality at lower concentrations than previously reported.⁸ In the larynx, high airflow velocity coupled with the airway narrowing creates turbulence that promotes PM₁₀ deposition.^{22–24} In this manner, the larynx acts as a filter to limit particles reaching the lower airway, although this function may be inhibited by irritant-induced inflammatory activity.^{25,26} However, laryngeal retention of PM poses a potential inflammatory challenge to local mucosal tissues, notably for the vocal folds (VFs).

VF mucosa comprises squamous epithelium and lamina propria tissues separated by a basement membrane.²⁷ This tissue faces a daily barrage of challenges from inhaled irritants, including PM, that can damage the mucosa and inhibit vocal function. Based on epidemiological data and clinical findings, PM exposure has been associated with multiple voice disorders including vocal cord dysfunction and fibrosis, chronic laryngitis, and laryngeal cancer.^{28–30} Despite the potential serious consequences for vocal health, biological mechanisms underlying the interaction between PM₁₀ and VF mucosae are yet to be fully elucidated partly due to the lack of reliable and predictive experimental models.

In vivo animal models have been used to investigate the VF mucosa's response to several environmental irritants and allergens. For instance, rodent VF mucosae have displayed hyperplasia³¹, oedema³², cell death³², immune cell infiltration^{33,34}, and mucin upregulation³³ in response to cigarette smoke^{31,33}, acrolein³², dust mites³³, and chalk dust³⁴. However, anatomical^{35–37}, economic³⁸, and ethical^{39,40} obstacles persist regarding animal model use and efficacy in VF research.

Ex vivo studies using porcine larynges have collectively indicated the VF mucosa has a robust resilience to acute exposure to cigarette smoke condensate⁴¹, hydrogen peroxide⁴², and nanoparticles⁴³. However, these models also highlight the importance of irritant exposure time. For instance, one study indicated 1 hr exposure to 400 µm acrolein caused no change in cell viability or metabolism, which differed from findings elsewhere reporting altered barrier function at only 100 µm when exposure time was increased to 3 hr.^{44,45}

Acute exposure to environmental irritants has also been studied using *in vitro* modelling systems, specifically VF fibroblast monocultures. In response to 24 hr exposure to PM^{7,46}, cigarette

smoke^{41,47–51}, or e-cigarette smoke⁵¹, researchers reported elevated inflammatory marker expression^{7,41,46,47,49}, oxidative stress^{7,46,48,50}, DNA damage⁵¹, and cell death⁵¹.

Although these *in vitro* studies have provided some insight into irritant-induced VF cellular responses, they cannot replicate the VF's robust defences against environmental irritants. In particular, stratified squamous VF epithelium provides the first line of defence against irritant challenges. Stratified squamous epithelium has defensive structures and mechanisms specifically adapted for protecting stromal cells, mainly fibroblasts, of the lamina propria.²³ For instance, the multilayered structure of VF epithelium provides a robust obstacle to external irritants compared to the thinner, more delicate respiratory epithelia found elsewhere in the laryngeal cavity.⁵² As such, it is important to incorporate epithelial cells into *in vitro* VF models to replicate the *in vivo* defences against irritants. However, culture conditions used are key to replicating native epithelial structures *in vitro*, with cultivation at an air-liquid interface (ALI) necessary to achieve a multilayered, stratified epithelium.^{53,54}

Previously, our group proposed a vocal fold organ-on-a-chip (VF-OOAC) based on a co-culture of primary VF fibroblasts and immortalized laryngeal epithelial cells. This VF-OOAC_{iLEC} displayed structural and functional architecture exceeding that of comparable transwell controls.⁵⁵ However, immortalized airway epithelial cells may have restricted differentiation and inhibited barrier capacities compared to native tissue cells.⁵⁶ Induced pluripotent stem cells (iPSCs) offer an attractive alternative for deriving VF epithelial cells that better represent the morphology and functionality of native tissue.⁵⁴ Thus, we cultivated an iPSC-derived epithelium in a VF-OOAC_{iPSC} to evaluate potential differences between each epithelial cell source in response to environmental challenges.

The primary goal of this study was to evaluate the resilience of the VF mucosa to an acute PM₁₀ exposure series (0, 50, 100, 400 µg/mL) using VF-OOAC_{iLEC}. We hypothesized VF-OOAC_{iLEC} would demonstrate resistance to PM₁₀ due to the inherent protective mechanisms of stratified squamous epithelium. The secondary goal was to compare the response to PM₁₀ exposure of VF-OOAC_{iLEC} and VF-OOAC_{iPSC} for result validation. We first benchmarked VF-OOAC_{iPSC} against transwell controls to verify its mucosal structure prior to challenging it with PM₁₀. It was

anticipated VF-OOAC_{iPSC} would display higher resilience than VF-OOAC_{iLEC} due to the improved tissue functionality provided by iPSC-derived VF epithelial cells.⁵⁴

Materials & Methods

Cell Culture Maintenance

Vocal Fold Fibroblast Culture

Human primary vocal fold fibroblast (pVFF) 21T cells, donated by the Thibeault laboratory (University of Wisconsin-Madison) were maintained in Dulbecco's modified Eagle's medium (DMEM) (Sigma, #D6429) supplemented with 10% (v/v) FBS (ThermoFisher, #12484028), 1% (v/v) pen strep (ThermoFisher, #15140122) and 1% (v/v) non-essential amino acids (ThermoFisher, #11140050). pVFF cultures were stored in a humidified incubator (37 °C, 5% CO₂). Culture media was changed every other day and cells passaged at least once prior to use in experiments. pVFFs with passage number 4-6 used throughout this study.

Laryngeal Epithelial Cell Culture

Human immortalized laryngeal epithelial cells (iLECs) (ATCC CRL-3342, HuLa-PC) were maintained in dermal cell basal medium (ATCC, #PCS-200-030) supplemented with a keratinocyte growth kit (ATCC, #PCS-200-040) as per manufacturer recommendations. iLECs were stored in a humidified incubator (37 °C, 5% CO₂) and media changes performed every 2-3 days. iLECs were passaged at least once before priming them for stratification.

Prior to experimental use, iLECs were cultured in stratified DMEM for 72 hr. To obtain stratified DMEM, a basal DMEM solution was first prepared by supplementing DMEM/F12 (ThermoFisher, #10565018) with 2% B27 (ThermoFisher, #17504044), 1% N2 (ThermoFisher, #17502048), and 1% pen strep. Stratified DMEM was formed by adding 0.4 µg/mL hydrocortisone (Stemcell Technologies, #07925) 8.4 ng/mL cholera toxin (Sigma, #C9903), 5 µg/mL insulin (Sigma, #91077C), 24 µg/mL adenine (Sigma, #A8626), and 20 ng/mL EGF (Stemcell Technologies, #78006).

Induced Pluripotent Stem Cell Culture

Protocols from the Montreal Neurological Institute were followed for maintaining iPSCs in an undifferentiated state.⁵⁷ Matrigel coating was prepared on-ice by adding 100 μ L of Matrigel (100 \times) (Corning, #354277) to 10 mL of DMEM/F12 supplemented with Antibiotic-Antimycotic (1 \times) (ThermoFisher, #15240096). Coating was added to a 60 mm petri dish (Eppendorf, #0030701119) and incubated 1 hr at 37 °C.

iPSCs (GM25256, Coriell Institute) in complete mTeSR Plus (Stemcell Technologies, #100-0276) supplemented with 10 μ M ROCK inhibitor (Stemcell Technologies, #72302) were seeded in a prepared Matrigel-coated dish and incubated 20 h. ROCK inhibitor media was then removed and cells were washed before complete mTeSR Plus was added.

Media was changed daily and iPSCs were routinely passaged using ReLeSR (Stemcell Technologies, #05872) when confluency was ~60-70%, in accordance with the manufacturer's instructions. iPSCs were passaged at least once prior to initiating differentiation.

VF Basal Progenitor Cell Differentiation

At 80% confluency, iPSCs were subjected to a differentiation protocol developed by the Thibeault laboratory to generate VF basal progenitor cells.⁵⁴ On day 1, definitive endoderm differentiation was initiated by adding RPMI media with Glutamax (ThermoFisher, # 61870-036) supplemented with 100 ng/mL Activin A (Stemcell Technologies, #78001), 25 ng/mL Wnt 3a (R&D Systems, #5036-WN-010), and 10 μ M ROCK inhibitor to iPSCs for 24 hr. On day 2, media was changed to RPMI with Glutamax supplemented with 100 ng/mL Activin A and 0.2% FBS. Cells were incubated 48 hr with a media replenishment after 24 hr.

On day 4, anterior foregut endoderm induction commenced using Basal DMEM supplemented with 200 ng/mL noggin (Stemcell Technologies, #78060), 10 μ M SB431542 (Stemcell Technologies, #72232), 50 μ g/mL ascorbic acid (Stemcell Technologies, #72132), and 0.4 mM 1-Thioglycerol (Sigma, #M6165). Cells were incubated 96 hr with media refreshed daily.

On day 8, VF basal progenitor differentiation was induced by adding basal DMEM supplemented with 50 μ g/mL ascorbic acid, 250 ng/mL FGF-2 (Stemcell Technologies, #78003),

100 ng/mL FGF-7 (Stemcell Technologies, #78046), and 100 ng/mL FGF-10 (Stemcell Technologies, #78037) to cells for 48 hr.

At day 10, VF basal progenitor culture quality was assessed under a light microscope. If strong growth, high confluency, and limited cell stacking were observed, progenitors were used in experiments.

Particulate Matter Preparation

Cultures were exposed to the environmental irritant PM₁₀ (ERM CZ100, European Commission; **Table S1, Figure S3: PM₁₀ Composition**) for 24 hr. 10 mg/mL stock concentration of PM₁₀ was prepared by adding 100 mg of PM₁₀ to 10 mL of FAD media and vortexing for 5 min. The working concentrations prepared for individual experiments represented the potential dose of this study.⁵⁸

VF-OOAC Culture

VF-OOAC_{ILEC} Culture

BE-Transflow microfluidic chips (BEOnChip) were applied for VF-OOAC_{ILEC} culture using a previously developed protocol.⁵⁵ The chip design was compatible with 3D culture whilst enabling perfusion through its microchannel (**Table S2: Culture vessel physical parameters**).

The microchannel was coated with collagen (50 µg/mL) prior to seeding pVFFs as a monolayer and incubating for 24 hr. Collagen gels (2.5 mg/mL) (ThermoFisher, #A10483-01) were fabricated on-ice in accordance with the manufacturer's instructions and adjusted to pH 7.2-7.4 using 1 N NaOH (ThermoFisher, #124260010). pVFFs in FBS were added to produce a final concentration of 0.5×10^6 cells/mL. 110 µL of pVFF-collagen gel mix was added to the well of the microfluidic chip and incubated 75 min to initiate gel formation. Gels were detached from the membrane and basal DMEM was added to the well and channel. Chips were incubated 24 hr to facilitate gel contraction. This pVFF-gel was used to represent the lamina propria region of the VF mucosa.

The next day, iLECs were seeded atop gels at a concentration of 1×10^6 cells/mL. Plates were incubated to allow cell attachment. Cells were co-cultured under submerged conditions for three days before an ALI was established by removing media from the well.

At this point, the microfluidic chip was connected to a peristaltic pump and FAD media was perfused through the microchannel at 40 μ L/h for 10 days. FAD media was prepared from DMEM medium-high glucose (Sigma, #D6429) and Ham's F12 (ThermoFisher, #11765054) mixed in a 1:3 ratio, supplemented with FBS (2.5%), pen strep (1%), hydrocortisone (0.4 μ g/mL), cholera toxin (8.4 ng/mL), insulin (5 μ g/mL) (Sigma, #91077C), adenine (24 μ g/mL) (Sigma, #A8626), and EGF (10 ng/mL).⁵⁴

Transwell_{iLEC} co-culture controls were prepared via a protocol previously reported.⁵⁵ Preparation was similar to VF-OOAC_{iLEC} with the exception of microchannel and perfusion steps.

VF-OOAC_{iPSC} Culture

VF-OOAC_{iPSC} required the same initial collagen-pVFF gel preparation used for VF-OOAC_{iLEC}. VF basal progenitors were harvested using TrypLE Express, re-suspended in 200 μ L of stratified DMEM supplemented with FGFs, and seeded atop gels as a 10 μ L drop as detailed elsewhere.⁵⁴ After progenitor seeding, microfluidic chips were incubated 2 hr to allow attachment. At this point, stratified DMEM with FGFs was added to the well and microchannel. Media was changed daily to prevent acidity and waste build-up in the microfluidic system.

Two days after VF basal progenitor seeding, all media was changed to conditional FAD media supplemented with FGFs. To prepare conditional FAD, FAD media was applied to a stock pVFF culture at 60-70% confluency and incubated overnight.⁵⁴ Media was collected, sterile-filtered, and frozen at -20 °C until required. These stored aliquots were mixed with FAD media in a 30:70 ratio to generate conditional FAD media. Submerged culture was maintained for 2-4 days to allow cells to proliferate to cover the gel.

After epithelial confluency was reached, an ALI was established by removing media from the well containing the gel. The microfluidic chip was then connected to a peristaltic pump and FAD media was perfused through the channel at 40 μ L/h. Cells were cultivated in this perfused, ALI setup for a further 10 days to facilitate epithelial stratification.

Transwell co-culture has been reported to facilitate the successful development of an iPSC-derived VF epithelium.⁵⁴ As such, transwell_{iPSC} co-culture was used for experimental controls. Preparation VF mucosa constructs was similar to VF-OOAC_{iPSC} with the exception of microchannel and perfusion steps.

PM₁₀ Exposure Experiments

PM₁₀ Toxicity Screening

A screen test of PM₁₀ toxicity to laryngeal cells was performed for subsequent dose-response experiments. Monocultures of pVFFs and iLECs were seeded in a 24-well plate (Eppendorf, #0030741021) at a concentration of 0.5×10^5 cells/mL and cultured to confluency with media changes every 2-3 days. Upon confluency, PM₁₀ in media (0, 25, 50, 100, 200, 400, 800, 1600 $\mu\text{g/mL}$) was applied to cells and incubated for 24 hr. PM₁₀ exposure length (i.e., 24 hr) and concentration range (0-1,600 $\mu\text{g/mL}$) were selected to align with literature standards used for acute pollutant response studies in the literature.^{7,20,59,60}

After 24 hr, cells were prepared for cytotoxicity analysis using live/dead assays (**Figure 6.1A**). 24-well plate cultures were washed with DPBS and stained using a LIVE/DEAD cytotoxicity assay (Invitrogen, #1932445) in accordance with the manufacturer's instructions. The plate was incubated for 30 min in darkness at room temperature before being washed with DPBS. Samples were imaged using an inverted LSM710 confocal fluorescence microscope with a 20 \times objective. Image analysis and viability counts were performed using Imaris.

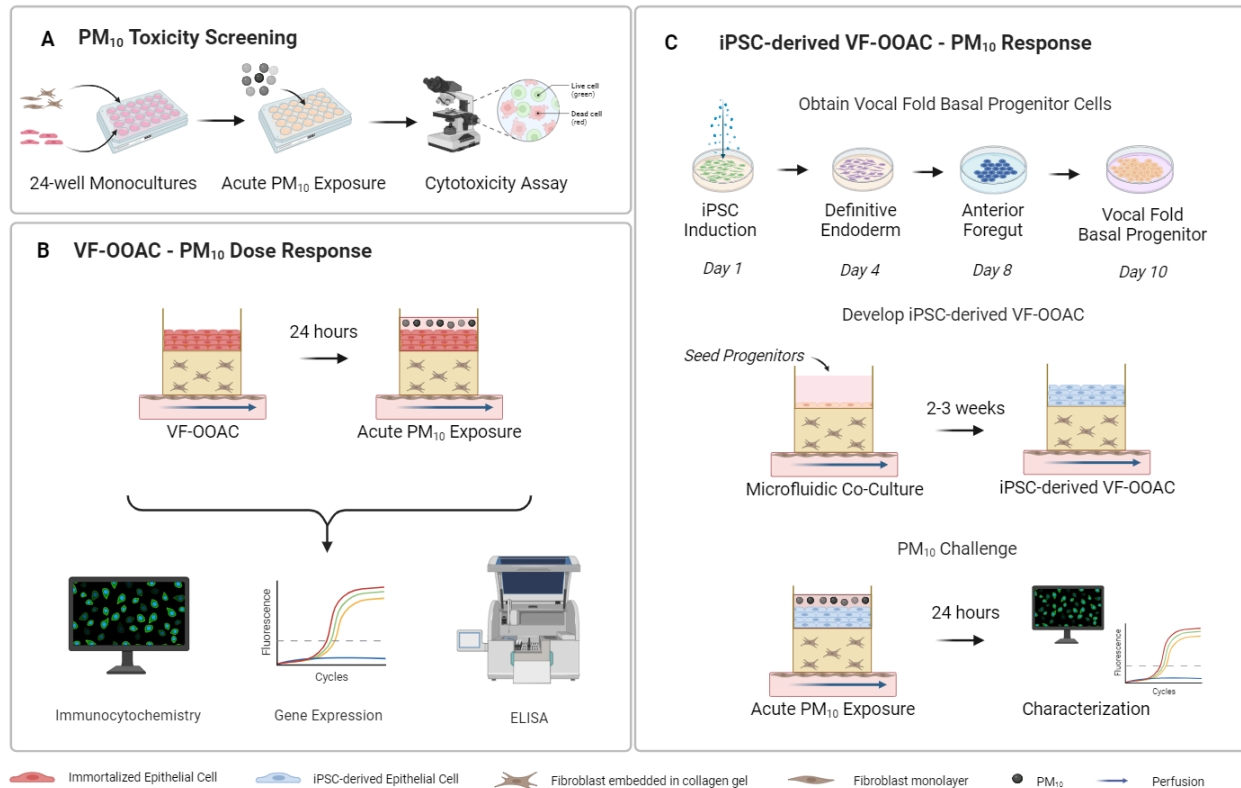


Figure 6.1. Evaluating the VF mucosa response to PM₁₀. (A) PM₁₀ toxicity screening was performed for pVFF and iLEC monocultures by applying a range of PM₁₀ concentrations (0-1600 µg/mL) to cells for 24 hr. (B) VF-OOAC_{iLEC} were challenged with a PM₁₀ dose-response series (0, 50, 100, 400 µg/mL) for 24 hr, with structural, functional, and inflammatory changes evaluated. (C) A VF-OOAC_{iPSC} was developed using iPSC-derived VF epithelial cells before challenging it with 100 µg/mL PM₁₀ for 24 hr.⁵⁴

VF-OOAC PM₁₀ Exposure

PM₁₀ was applied to the chip well of VF-OOAC cultures and incubated for 24 hr. PM₁₀ exposure length and concentration range were based on toxicological screening tests. For VF-OOAC_{iLEC} experiments, a PM₁₀ dose response series was performed using 0, 50, 100, 400 µg/mL (**Figure 6.1B**). Toxicological screening had identified 400 µg/mL as the cytotoxic dose for iLECs. For VF-OOAC_{iPSC} validation experiments, 100 µg/mL PM₁₀ was used as the test dose. This concentration enabled an investigation of epithelium's capacity to protect the lamina propria as toxicological screening identified this as the cytotoxic dose for pVFFs (**Figure 6.1C**).

During incubation, FAD media continued to be perfused through the channel. After 24 hr, samples were prepared for biological characterization. For all experiments, 0 µg/mL was utilized as a negative control and transwell culture served as experimental controls. All samples were performed in at least biological triplicate.

Immunocytochemistry Characterization

Immunocytochemistry was used to evaluate the expression of proteins related to epithelial barrier integrity and fibroblast activity in response to PM₁₀ exposure. Epithelial stratification was assessed via staining for cytokeratins 5, 13, 14 (K5, K13, K14). Adherens junctions and basement membrane presence were evaluated via E-Cadherin and laminin alpha 5 (LAMA5). Vimentin was used to monitor changes in expression of intermediate filaments. Alpha smooth muscle actin (α SMA) staining assessed myofibroblast activation and actin filament over-expression. Primary monoclonal antibodies and relevant secondary antibodies are indicated in **Table 6.1**. Slides stained with secondary antibody only served as negative controls.

Table 6.1. Summary of antibodies applied for immunocytochemistry.

Target	Primary Ab	Dilution	Supplier (Cat #)	Secondary Ab	Dilution	Supplier (Cat #)
Stratified epithelium	AF 488 Rabbit to K5	1:200	Abcam (ab193894)	-	-	-
Stratified epithelium	Rabbit to K13	1:200	Abcam (ab154346) ab133340	AF 594 Goat anti-rabbit	1:500	ThermoFisher (A-11037)
Stratified epithelium	AF 532 Mouse to K14	1:100	Novus Biologicals (NBP2-34675AF532)	-	-	-
Basement membrane	Mouse to LAMA5	1:100	Abcam (ab77175)	AF 647 Goat anti-mouse	1:1000	ThermoFisher (A-21236)
Intercellular junction marker	AF 647 Rabbit to E-Cad	1:100	Abcam (ab194982)	-	-	-
Myofibroblasts, actin filaments	AF 555 Rabbit to α SMA	1:200	Abcam (ab202509)	-	-	-
Intermediate filaments	Chicken to Vimentin	1:300	Abcam (ab24525)	AF 633 Goat anti-chicken	1:1000	ThermoFisher (A-21103)
Nuclear DNA	DAPI	1:5000	Abcam (ab228549)	-	-	-

Immunostaining followed a previously reported protocol.⁵⁵ Samples were washed three times in DPBS and fixed in 4% paraformaldehyde (ThermoFisher, #J19943K2) for 30 min. After washing twice in DPBS, collagen constructs were harvested from VF-OOAC cultures or transwell controls and transferred to cryomolds (Ted Pella, #271471) filled with O.C.T. Compound (Fisher, #4585).

Samples were flash frozen using liquid nitrogen and sectioned vertically with a cryostat (Leica CM1860). Sections were transferred to microscope slides (Fisher, #1255015), dried for 1 hr at room temperature, and stored at -80 °C until immunostaining. All staining was performed at room temperature. Slides were washed in PBS and permeabilized using 0.1% Triton X-100 (Sigma, #X100-5ML) for 15 min. After three washes, blocking buffer (10% goat serum (Abcam,

#ab7481), 1% Tween-20 (Abcam, #ab128987), in PBS) was applied for 45 min. Samples were then incubated with relevant primary antibodies in blocking buffer for 1 hr.

After washing with .05% Tween-20, relevant fluorescence-conjugated secondary antibodies in blocking buffer were applied and incubated for 1 hr. Slides were washed and counterstained with 1:5000 DAPI (Abcam, #ab228549) for 5 min to label cell nuclei. Samples were rinsed and mounted with Vectashield Antifade mounting medium (Vector Labs, #H-1700). Slides were imaged with an inverted LSM710 confocal fluorescence microscope (Zeiss) using a 10× or 20× objective. Image acquisition and analysis were performed using Zen System (Zeiss) and Imaris version 7.5.6 (Bitplane) software.

Immunohistochemistry

To verify tissue morphology of iPSC-derived VF mucosae, 10 µm-thick sections were subjected to hematoxylin-eosin (H&E) staining (Abcam, #ab245880) using the manufacturer's protocol. Slides were dipped in Hematoxylin and incubated 5 min. Sections were rinsed twice in distilled water then dipped in bluing reagent for 15 sec. Sections were rinsed twice in distilled water and dipped in absolute alcohol, with the excess blotted off. Sections were immersed in Eosin and incubated for 2 min. Slides were rinsed, dehydrated in an absolute alcohol series, and mounted with Permount media (Fisher Scientific, #SP15100). Image acquisition was performed using an Axiovert 3 Widefield Microscope with 40× objectives equipped with Zen System software. Images were analyzed with Imaris.

Gene Expression Characterization

Real-time quantitative PCR (qPCR) assessed up- or downregulation of structural, functional, and inflammatory genes in VF-OOAC cultures relevant to transwell controls. Cultures were washed twice with DPBS before collagen constructs were submerged in 100 U/mL of collagenase type I (Gibco, #17018029) in HBSS (ThermoFisher, #14175095). Samples were incubated at 37 °C for 2-3 hr or until gel dissolution. Cells were collected and washed via centrifugation. The supernatant was aspirated, and pellets were snap frozen using liquid nitrogen and stored at -80 °C until RNA extraction.

Total RNA extraction was performed using the RNeasy Micro Kit (Qiagen, #74004) in accordance with the manufacturer's instructions. Extracted RNA was assessed using a NanoDrop

(ThermoScientific, NanoDrop 2000 Spectrophotometer) to determine quantity and purity prior to cDNA synthesis. 500 ng of RNA was reverse transcribed to cDNA using a SuperScript VILO cDNA Synthesis Kit (ThermoFisher, #11754050) as per the manufacturer's protocol.

TaqMan assays (ThermoFisher, #4453320) for genes corresponding to K5, K13, K14, tumor protein 63 (p63), tight junction protein 1 (ZO-1), gap junction alpha-1 protein (GJA1), mucin 1 (MUC1), mucin 4 (MUC4), hyaluronan synthase 2 (HAS2), hyaluronan synthase 3 (HAS3), piezo 1 (PIEZO1), tumor necrosis factor alpha (TNF α), interleukin 6 (IL6), interleukin 8 (IL8), interleukin 1 alpha (IL1 α), and interleukin 1 beta (IL1 β) were used for assessment (**Table 6.2**).

To perform RT-qPCR, 96-well fast plates (ThermoFisher, #4483485) with 1 μ L of cDNA per 10 μ L reaction mix were used. Plates were run for 40 cycles using a ViiA 7 Real-Time PCR System (ThermoFisher). Relative gene expression was normalized to Glyceraldehyde-3-Phosphate Dehydrogenase (GAPDH) (Δ Ct) and results were quantified using the $2^{-\Delta\Delta C_t}$ method.⁶¹

Table 6.2. TaqMan assays for qPCR evaluation.

Gene	Association	TaqMan Assay ID
K5	Stratified epithelium	Hs00361185_m1
K13	Stratified epithelium	Hs02558881_s1
K14	Stratified epithelium	Hs00265033_m1
p63	Stratified epithelium	Hs00978340_m1
ZO-1	Tight junctions	Hs01551871_m1
GJA1	Gap junctions	Hs00748445_s1
MUC1	Mucus production	Hs00159357_m1
MUC4	Mucus production	Hs00366414_m1
HAS2	Extracellular matrix synthesis	Hs00193435_m1
HAS3	Extracellular matrix synthesis	Hs00193436_m1
PIEZO1	Mechanotransduction	Hs00207230_m1
TNF α	Inflammatory response	Hs00174128_m1
IL6	Inflammatory response	Hs00174131_m1
IL8	Inflammatory response	Hs00174103_m1
IL1 α	Inflammatory response	Hs00174092_m1
IL1 β	Inflammatory response	Hs01555410_m1
GAPDH	Housekeeping	Hs02786624_g1

Enzyme-linked Immunosorbent Assays

Enzyme-linked immunosorbent assays (ELISA) were used to quantify the concentration of the inflammatory cytokines TNF α (Abcam, #ab181421) and IL1 β (Abcam, #ab214025) in VF-OOAC_{ILEC} following PM₁₀ exposure.

Total supernatant (chip well and perfused effluent) was collected and stored at -80 °C. After thawing samples on ice, vials were briefly centrifuged to remove debris prior to loading into ELISA plates. Standard curves were applied to measure the quantity of analyte present in each sample. ELISA data was normalized to total protein content obtained via the Bradford Protein Assay (Bio-Rad Labs, #5000002). All assays were performed according to the manufacturer's requirements.

Statistical Analysis

Cytotoxicity, gene expression, and ELISA data were evaluated using one-way or two-way between subjects ANOVAs depending on the study design. Simple effects for two-way ANOVAs were assessed using Bonferroni tests. Differences were considered significant at $p < .05$.

Results & Discussion

PM₁₀ Induces Cytotoxicity in VF Cell Monocultures

Cytotoxicity screening indicated both pVFFs and iLECs resisted PM₁₀ effects at ≤ 50 $\mu\text{g/mL}$, with no significant loss of cell viability compared to negative controls (0 $\mu\text{g/mL}$) (**Figure 6.2A**). Both cell types demonstrated an overall dose response, with cell viability decreasing as PM₁₀ concentration increased ($p < .05$; **Figure 6.2A**). iLECs first displayed a significant cell viability decrease at 400 $\mu\text{g/mL}$ ($p < .05$; $90.79 \pm 0.67\%$, **Figure 6.2B**). Conversely, pVFFs displayed a significant decrease in cell viability at 100 $\mu\text{g/mL}$ ($p < .05$; $90.94 \pm 0.81\%$, **Figure 6.2C**). iLECs had significantly higher viability than pVFFs at 200 $\mu\text{g/mL}$ and 400 $\mu\text{g/mL}$ PM₁₀ ($p < .05$; **Figure 6.2A**).

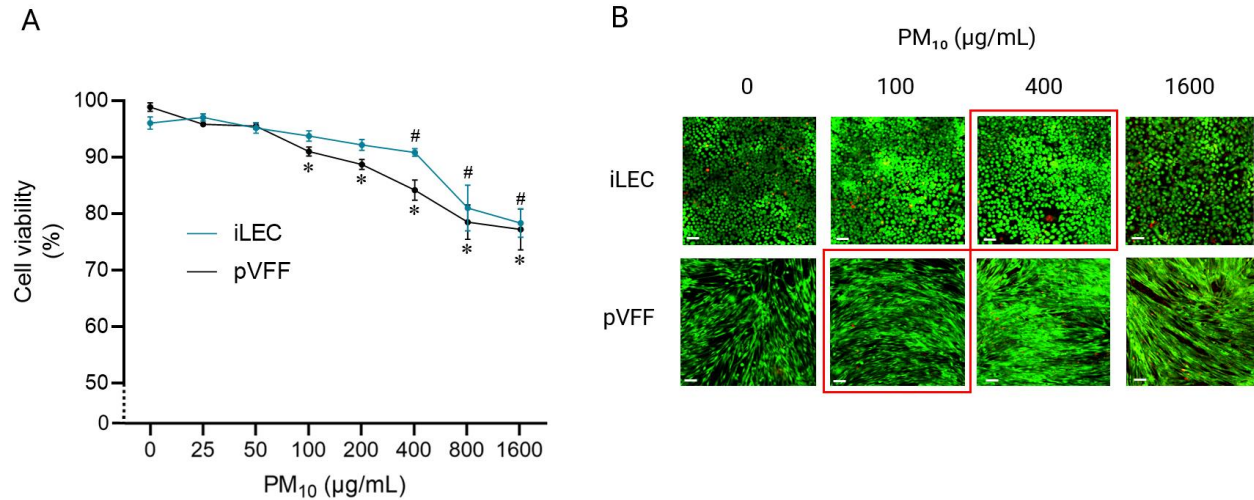


Figure 6.2. Effect of 24 hr exposure to PM₁₀ on the viability of iLEC and pVFF monocultures. (A) Cell viability of pVFF and iLEC cultures. Significant difference in cell viability versus respective 0 μg/mL controls indicated by # (iLEC) or * (pVFF). (B) LIVE/DEAD assays indicated live (green) and dead (red) cells. Red-bordered images represent the lowest PM₁₀ dose that induced significant cell death in each respective cell type. Scale bar = 50 μm.

This screen test demonstrated iLECs resisted cytotoxic effects of PM₁₀ at higher concentrations than pVFFs. Laryngeal epithelial cells have a primary role in protecting the lamina propria against environmental irritants.^{23,62} Stromal cells of the lamina propria such as pVFFs are not directly exposed to external irritants and hence do not possess the structural, defensive mechanisms of epithelial cells. Our findings highlight the defensive characteristics of iLECs and confirm they are better adapted for enduring environmental challenges compared to stromal cells of the lamina propria such as pVFFs.⁶³

VF-OOAC_{iLEC} Demonstrates High Resilience to PM₁₀

Our toxicity screen tests confirmed VF fibroblasts are more vulnerable than epithelial cells to the damaging effects of environmental irritants. Given its critical defensive role *in vivo*, it has been posited VF epithelium may be sufficiently robust to withstand acute exposures to environmental irritants.^{23,41} To determine whether the resilience iLEC displayed in toxicity screening translated to effective protection of pVFFs, we investigated a PM₁₀ dose-response in a VF mucosa 3D co-culture using VF-OOAC_{iLEC}.

No PM₁₀ was observed in the lamina propria of VF mucosae at all concentrations tested. Accumulated particles were localized to the suprabasal layers of the epithelium (**Figure 6.3A**). This phenomenon is similar to observations in a rat model, which retained particles in the VFs after chronic exposure to chalk dust.³⁴ For VF-OOAC_{iLEC}, PM₁₀ absence beyond the basement

membrane suggests epithelial barrier integrity withstood the acute exposure challenge and protected the lamina propria from damage. This resilience may be attributable to the protective mechanisms of stratified squamous epithelium and basement membrane zone. For instance, VF epithelium experiences complete turnover approximately every 96 hr, with the outermost layers sloughed off and replaced by cells of the basal layer.²³ This constant renewal aids irritant removal from the luminal surface of the epithelium.³²

The resilience to acute exposure of PM₁₀ displayed by VF mucosae was further confirmed by the absence of significant changes in tissue morphology, gene expression, and inflammatory cytokine levels. K5, K14, and p63 are stratified VF epithelium markers typically localized to the proliferative basal and parabasal layers.^{54,64,65} Confocal microscopy detected similar epithelial K5 and K14 expression at all PM₁₀ concentrations (**Figure 6.3B**). Correspondingly, no dose response for K5, K14, and p63 gene expression was found, indicating stable epithelial turnover and suggesting high VF mucosa resilience to PM₁₀ (**Figure 6.3C**).⁶⁶ The epithelial cell source used in VF-OOAC_{iLEC} may have contributed to this observed resistance. iLECs originate from the laryngeal posterior commissure, which is a laryngeal mucosa region highly adapted to enduring irritant challenges.⁶⁷ Elevated carbonic anhydrase isoenzyme III expression in the posterior commissure may provide an additional defence as this enzyme converts carbon dioxide and water into carbonic acid, protons, and bicarbonate ions to regulate pH and fluid balance.⁶³

K13 is a marker of terminally differentiated, stratified VF epithelium but displayed minimal expression in iLECs. VF mucosa exhibits some differences in cytokeratin composition compared to other regions of the larynx covered by intermediate epithelia.⁶⁵ An alternative explanation for K13 absence may be the inability of iLECs to reach terminal differentiation. This has been noted as a general constraint of airway epithelial cell lines and highlights a limitation of using iLECs to model the VF mucosa.⁵⁶

The VF basement membrane presents an additional protective barrier for the lamina propria against environmental irritants and can be identified via LAMA5 staining.⁶⁴ Increasing PM₁₀ concentration did not induce any changes in LAMA5 staining (**Figure 6.3B**), which aligns with findings elsewhere for transwell VF mucosae challenged with cigarette smoke extract for 7 days.⁵⁴ Of note, LAMA5 staining was relatively broad and non-specific for all samples, possibly indicating immaturity of the basement membrane structure.

Cell junctions are integral to epithelial barrier integrity and functionality. Chronic exposure to PM has been suggested as necessary to induce major changes in adherens junctions of E-Cad expression.⁶⁸ In this study, acute PM₁₀ exposure seemed to slightly increase E-Cad staining intensity at 100 µg/mL and 400 µg/mL (**Figure 6.3B**). No dose-response was detected for tight junction (ZO-1) and gap junction (GJA1) gene expression (**Figure 6.3C**). Overall, acute PM₁₀ exposure had a minimal impact on intercellular junction expression.

Membrane-bound mucins enable stratified squamous epithelium to generate a mucus layer which functions as a viscoelastic physical barrier to protect underlying tissue from exposure to environmental irritants. The mucus layer can also initiate defence mechanisms when challenged with microorganisms, a component of real-world PM₁₀, such as increasing epithelial turnover and mucin densities.⁶⁹ No dose response was detected for MUC1 or MUC4 expression, which aligns with literature findings demonstrating the VF mucosa is generally resistant to irritant-induced mucin changes when challenged with acute irritant exposure.^{70–72}

Changes in intermediate and actin filament expression related to fibroblast activation and myofibroblast transition were monitored via vimentin and αSMA staining.^{73–75} Vimentin indicated pVFFs displayed a spread, spindle-like morphology and expression did not vary with PM₁₀ dose (**Figure 6.3B**). The weak staining of αSMA indicated pVFFs were not activated to undergo myofibroblast transition (**Figure 6.3B**). These findings support the assumption that epithelial barrier integrity was maintained and protected pVFFs from PM₁₀ exposure.

Human VF *in vitro* investigations of acute exposure to environmental irritants have generally reported significant increases in inflammatory activity.^{7,41,46–51} However, these findings have relied on 2D fibroblast monocultures that likely overestimate the magnitude of the *in vivo* response as they do not include epithelial defences or epithelial-fibroblast crosstalk. Our VF-OOAC_{ILEC} demonstrated no dose-response for inflammatory gene expression (TNFα, IL6, IL8, IL1α, IL1β; **Figure 6.3D**). In addition, culture supernatants were also assayed via ELISA methods to quantify secreted inflammatory cytokines as both airway epithelial cells and fibroblasts have the capacity to secrete TNFα and IL1β.^{76–78} No dose response was detected for either TNFα or IL1β (**Figure 6.3E**). ELISA results supported gene expression data demonstrating the absence of an inflammatory response, highlighting the epithelium's capacity to protect pVFFs from PM₁₀ exposure.

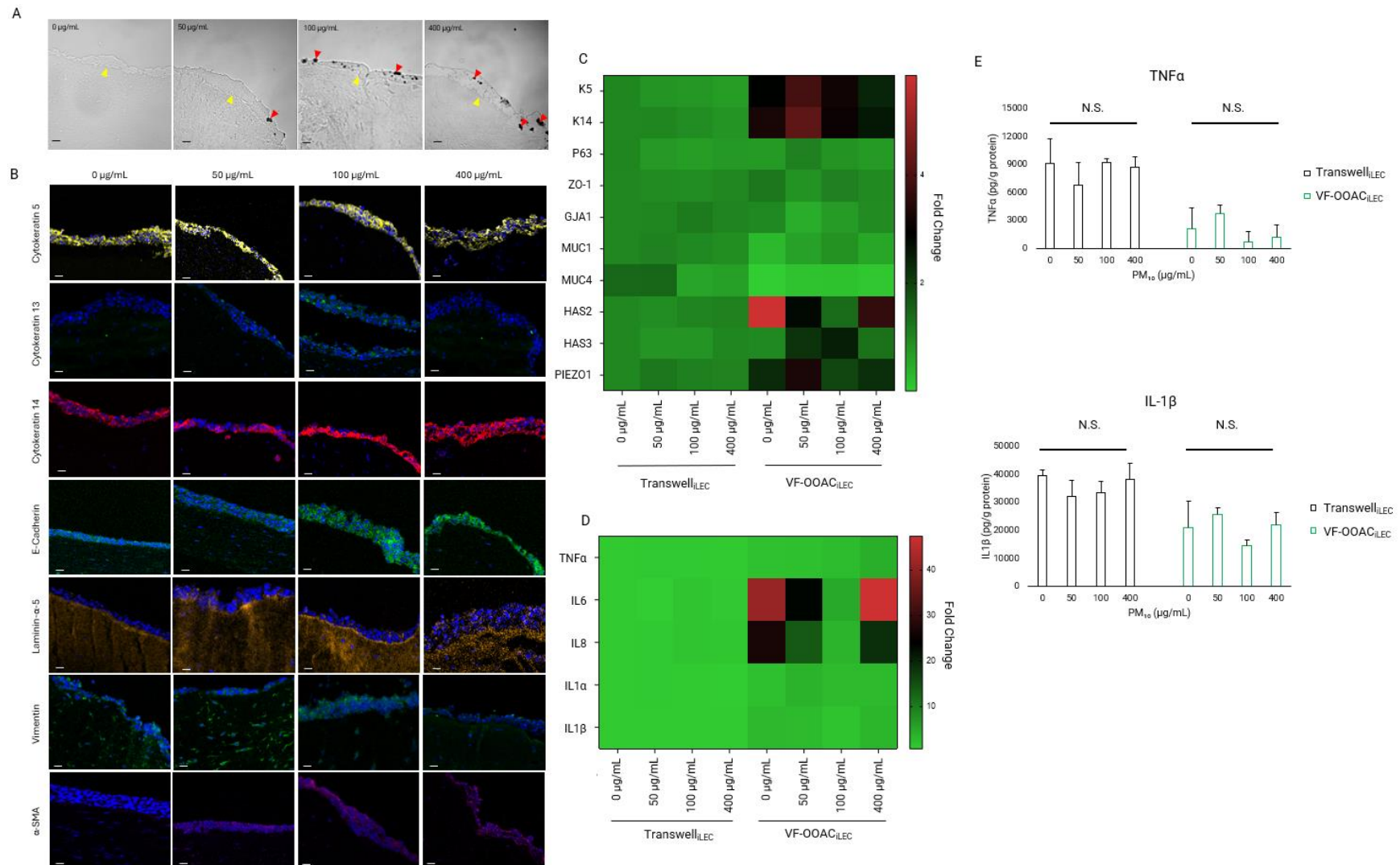


Figure 6.3. Dose response study of 24 hr PM₁₀ exposure. (A) Transmitted light visualized PM₁₀ distribution at the epithelium surface (black particles). Yellow arrows indicate the basement membrane. Red arrows indicate PM₁₀ particles. (B) Morphological features of VF-OOAC_{iLEC} cultures. K5, K13, K14, and E-Cad evaluated epithelium structure. LAMA5 assessed basement membrane. Vimentin and αSMA evaluated epithelial-to-mesenchymal transition presence. Samples counterstained with DAPI (blue). Magnification 20x, scale bar = 30 µm. (C) Functional and structural gene expression. (D) Inflammatory gene expression. All gene expression data displayed relative to transwell_{iLEC} (0 µg/mL) controls. (E) Average inflammatory cytokine secretion and standard deviation in response to PM₁₀. Data normalized to total protein content.

VF-OOAC_{iPSC} Increased Tissue Functionality versus Transwell Controls

To potentially improve the predictive efficacy of our VF-OOAC platform, we developed a further model with an iPSC-derived VF epithelium. The structure and functionality of the VF-OOAC_{iPSC} was benchmarked against transwell controls, which have been applied in the literature for cultivating iPSC-derived VF mucosae.⁵⁴

Morphological evaluation of VF-OOAC_{iPSC} epithelium detected 5-10 cell layers, which approximates the thickness of native VF epithelium.^{79,80} The iPSC-derived epithelium contained mostly cuboidal-shaped cells and a flattened, terminally differentiated top cell layer (**Figure 6.4A: I**). Transwell controls were also observed to have a multilayered epithelium (**Figure 6.4B: I**).

In human VF epithelium, K13 is typically localized to suprabasal cell layers.^{64,81} K13 was observed in the stratified epithelium of VF-OOAC_{iPSC} (**Figure 6.4A: II**) whilst LAMA5 staining confirmed basement membrane presence (**Figure 6.4A: III**). The thinner epithelium of transwell controls also displayed K13 (**Figure 6.4B: II**) and a basement membrane (**Figure 6.4B: III**).

For gene expression comparisons VF-OOAC_{iPSC} displayed significantly higher ZO-1, GJA1, MUC1, PIEZO1, and significantly lower HAS2 compared to transwell controls ($p < .05^{\#}$; **Figure 6.4C**). No significant difference was detected in K5, K13, p63, HAS3 expression.

Upregulated ZO-1 and GJA1 in VF-OOAC_{iPSC} suggests an increased barrier integrity and functionality.⁸²⁻⁸⁴ By limiting metabolite dilution and diffusion distances in VF-OOAC_{iPSC}, small volume effects enhance paracrine signalling efficacy, which underpins intercellular junction development in VF epithelium.^{55,85} Also, MUC1 upregulation in VF-OOAC_{iPSC} implies greater epithelial differentiation and the establishment of a mucus barrier, which is an important defence mechanism for trapping and removing irritants.^{85,86} Increased mucin synthesis may be related to small-volume effects and perfusion, both of which stimulated MUC1 expression in our previous work developing VF-OOAC_{iLEC}.⁵⁵

Moreover, PIEZO1 is a shear-sensitive, mechanically activated ion channel that helps regulate epithelial remodelling and fibroblast mechanosensitivity.⁸⁷⁻⁹¹ Its upregulation in VF-OOAC_{iPSC} may be a response to increased fluidic shear compared to transwell_{iPSC}.⁵⁵ On the other hand, decreased HAS2 expression in VF-OOAC_{iPSC} could indicate low mesenchymal presence in the epithelium, which suggests increased iPSC differentiation efficiency compared to

transwell_{iPSC}.^{92,93} As fibroblast-epithelial crosstalk is critical to VF mucosa development *in vivo*, this result may indicate fibroblasts in VF-OOAC_{iPSC} better supported epithelial development due to improved paracrine signalling.⁶⁴

For a functionality check, we compared the morphological and genetic response between mucosae cultivated in VF-OOAC_{iPSC} and transwell controls following 24 hr exposure to 100 µg/mL PM₁₀. Interestingly, for VF-OOAC_{iPSC} epithelium, thickness appeared to increase whilst compactness decreased after PM₁₀ exposure (**Figure 6.4A: IV**). This observation was further supported by a significant increase in K13 gene expression in response to PM₁₀ exposure ($p < .05^*$; **Figure 6.4C**). Increased K13 may be an early indicator of laryngeal hyperplasia, a clinical condition related to excessive proliferation associated with exposure to environmental irritants.^{94–96} A divergent response to PM₁₀ exposure occurred between VF-OOAC_{iPSC} and transwell setups as no significant changes in morphology or gene expression were detected in transwell controls (**Figure 6.4B**).

Observable changes in VF-OOAC_{iPSC} appeared to be confined to the suprabasal epithelium, with no changes detected in basement membrane morphology (**Figure 6.4A VI**) or stromal-related HAS gene expression (**Figure 6.4B**) following PM₁₀ exposure. Indeed, other than K13, no significant differences were detected for all other structural and functional genes (**Figure 6.4B**) or inflammatory genes (**Figure 6.4C**) in response to PM₁₀. These results indicate VF-OOAC_{iPSC} demonstrated comparable resilience to PM₁₀ as reported for VF-OOAC_{iLEC} culture, although some differences were noted.

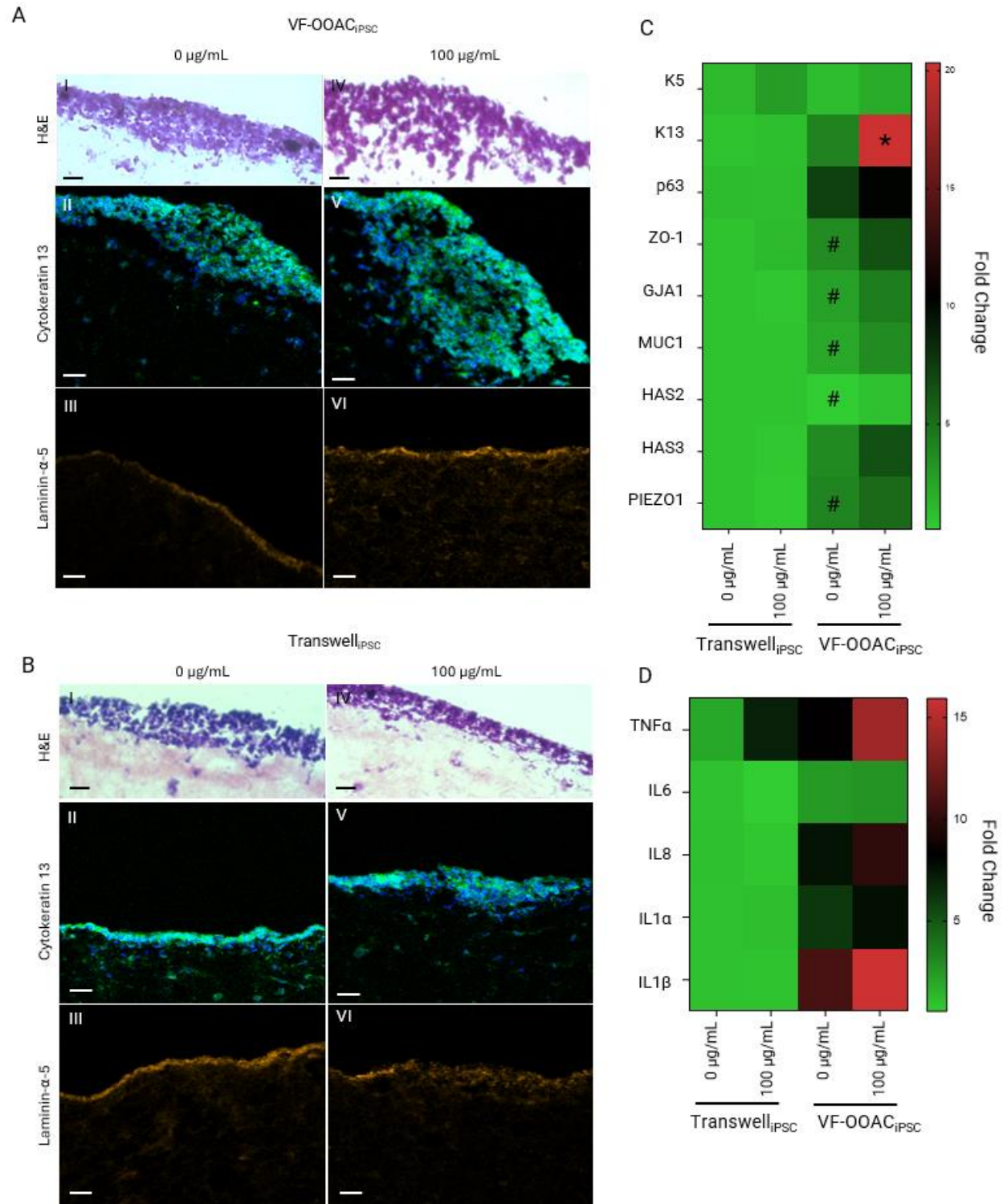


Figure 6.4. VF-OOAC_{iPSC} model development and response to 24 hr exposure to 100 µg/mL PM₁₀. (A) Morphological features of VF-OOAC_{iPSC}. H&E, K13 (green) and DAPI (blue) assessed epithelial stratification and cell distribution, whilst LAMA5 (orange) evaluated the basement membrane. (B) Corresponding transwell controls. Scale bars: H&E = 15 µm, Immunostaining = 30 µm. (C) Structural and functional gene expression. (D) Inflammatory gene expression. All gene expression data presented as fold-

change relative to transwell_{iPSC} (0 µg/mL). Significant differences ($p < .05$) between VF-OOAC_{iPSC} and transwell_{iPSC} (0 µg/mL) indicated by #. Significant differences ($p < .05$) induced by 100 µg/mL PM₁₀ within VF-OOAC group indicated by *.

Minimal impact of epithelial cell source on high resilience displayed by VF-OOAC to PM₁₀ challenge

No literature exists comparing genetic and morphological differences between iLECs and iPSC-derived VF epithelial cells. However, the comparison here is important in evaluating their capacity to recapitulate the resilience native VF epithelium displays to environmental irritants. A deeper analysis was therefore performed to directly compare the responses observed in each VF-OOAC model when challenged by PM₁₀.

In general, both VF-OOAC_{iLEC} and VF-OOAC_{iPSC} had little change in basement membrane staining in response to PM₁₀ (**Figure 6.3B**, **Figure 6.4A VI**). Functional and inflammatory gene expression changes were also insignificant for each model's respective PM₁₀ challenge.

One observable difference between VF-OOAC_{iLEC} and VF-OOAC_{iPSC} was K13 staining. The stain was only intense for VF-OOAC_{iPSC}, potentially indicating the model's higher capacity for epithelial differentiation. K13 absence in VF-OOAC_{iLEC} may be related to the limited terminal differentiation of immortalized epithelial cells noted in the general airway literature.⁵⁶

In addition, some differences in the genetic response were noted when comparing the response of VF-OOAC_{iLEC} and VF-OOAC_{iPSC} to 100 µg/mL PM₁₀ (**Table 6.3**). VF-OOAC_{iLEC} had a significant increase in MUC1 expression and a significant decrease in HAS2, IL6, and IL8 expression ($p < .05$). VF-OOAC_{iPSC} experienced no significant changes in expression.

Table 6.3. Comparison of functional and inflammatory gene expression in VF-OOAC_{iLEC} and VF-OOAC_{iPSC} challenged with 100 µg/mL PM₁₀ for 24 hr. Significant differences (* $p < .05$) and effect size are displayed compared to negative controls (0 µg/mL) within each model group. ↑ = upregulated. ↓ = downregulated. N.S. = Non-significant.

Gene	VF-OOAC _{iLEC}		VF-OOAC _{iPSC}	
	Significance	Effect size	Significance	Effect size
ZO-1	N.S.	.033	N.S.	.438
GJA1	N.S.	.284	N.S.	.360
MUC1	.006* ↑	.873	N.S.	.219
PIEZO1	N.S.	.040	N.S.	.051
HAS2	.005* ↓	.887	N.S.	.343
HAS3	N.S.	.351	N.S.	.236
TNFα	N.S.	.398	N.S.	.192
IL6	<.001* ↓	.985	N.S.	.010
IL8	<.001* ↓	.996	N.S.	.048

IL1 α	N.S.	.339	N.S.	.027
IL1 β	N.S.	.404	N.S.	.044

We further performed two-way between subject ANOVAs for gene expression data to determine whether the PM₁₀ response differed in magnitude between VF-OOAC_{iLEC} and VF-OOAC_{iPSC}. A significant interaction effect was found between epithelial cell type and PM₁₀ exposure for MUC1, HAS2, and IL6 ($p < .05$). Further analyses indicated significant main effects of cell type and PM₁₀ exposure for MUC1, a significant main effect of cell type for HAS2, and a significant main effect of PM₁₀ exposure for IL6 (**Figure 6.5**). Bonferroni tests indicated a significant difference in the magnitude of changes detected for MUC1, IL6, and HAS2 expression in each model. VF-OOAC_{iLEC} had larger changes in MUC1 and IL6 expression ($p < .05$) whereas VF-OOAC_{iPSC} experienced greater changes in HAS2 expression ($p < .05$).

The exact mechanisms underlying the differences between each cell type are unknown and will require further investigation. That said, it is likely the VF-OOAC_{iPSC} provides the most reliable depiction of the *in vivo* VF mucosal response to PM₁₀ given the phenotypical and morphological limitations of iLECs. Further development of VF-OOAC_{iPSC} will target increasing the maturity of the epithelium derived. This could potentially be achieved by increasing the length of culture at an air-liquid interface to more closely align with transwell models in the literature that reach maturity only after a 32-day protocol.^{54,71}

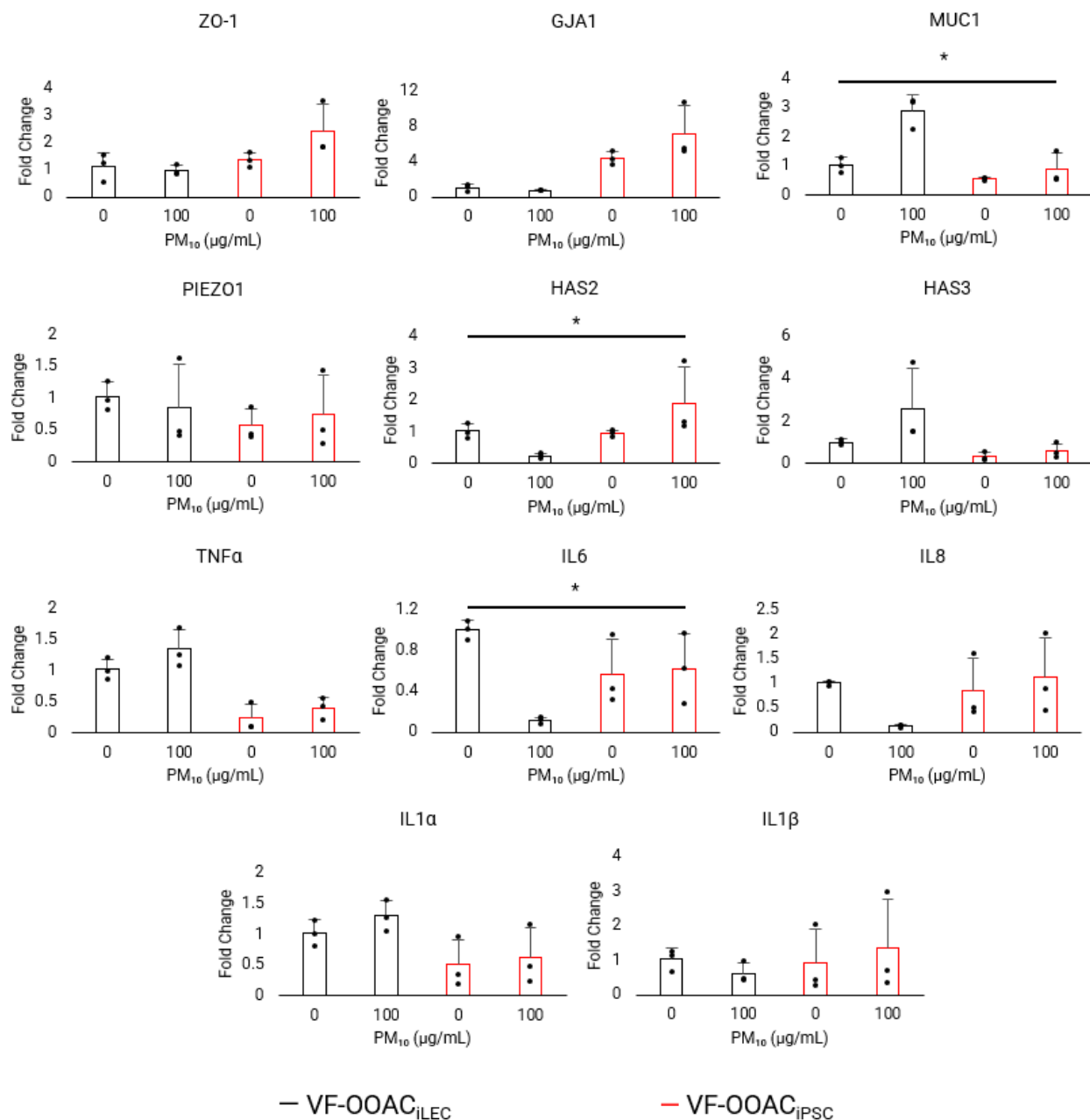


Figure 6.5. Average gene expression and standard deviation for VF-OOAC_{iLEC} and VF-OOAC_{iPSC} cultures challenged with 100 μg/mL PM₁₀ for 24 hr. Significant interaction effects indicated by * (p < .05).

Limitations, Future Prospects, & Conclusion

The VF-OOAC displayed a high resilience to PM₁₀ acute exposure when using either immortalized or iPSC-derived epithelia. Our findings highlight the robustness of stratified squamous VF epithelium in dealing with the short-term environmental irritant challenges. From clinical observations and animal model findings, chronic exposure to PM₁₀ may induce more

severe and damaging effects in VF mucosal tissue.^{28,70,97} Longer-term studies are therefore necessary to validate our findings.

This study used a standardized material of selected polycyclic aromatic hydrocarbons (PAHs) found in PM₁₀ to challenge cells. PAH cytotoxicity in other human tissues led us to isolate this PM₁₀ fraction and monitor its impact on VF mucosal biology. However, other components of real-world PM₁₀ may induce chemical-dependent (or specific) toxicity in the VF mucosa. For instance, heavy metals have been linked to oxidative stress, whilst microorganisms have been associated with elevated inflammation. Additional studies are therefore necessary to explore how these fractions may impact the VF mucosa.

To further enhance VF-OOAC's physiological relevance, endothelial cells and neutrophils can be included in future model expansion. Seeding endothelial cells in the microchannel of the VF-OOAC would simulate the VF vascular network and permit exploration of the impact of PM₁₀ on endothelial barrier permeability.^{98,99} Subsequent recirculation of neutrophils through the endothelial-lined channel could be used to simulate diapedesis and leukocyte-driven inflammatory activity of the VF mucosa.^{100–103}

Our future focus will also seek to integrate complementary *in silico* models to mimic PM deposition and adsorption profiles in the upper airway as well as subsequent VF biological effects.^{104–108} This approach will provide valuable insight into potential changes to the VF-OOAC device configuration that could improve PM₁₀ exposure and dose accuracy.

In this investigation, our VF-OOAC presented a reliable platform for studying the genetic and molecular behaviour of the VF mucosa's interaction with PM₁₀. *In vitro* models with improved predictive efficacy are a crucial tool for revealing the mechanisms by which environmental and systemic irritants contribute to the pathophysiology of voice disorders.

Author Contributions

PTC: Conceptualization, data collection and analysis, writing-original draft, reviewing and editing. NLJ: Conceptualization, writing-original draft, reviewing and editing, supervision, funding acquisition. VL, CC, TD, XL, ST: Conceptualization, reviewing and editing.

Conflicts of interest

The authors have no conflicts of interest to declare.

Acknowledgements

Microscopy images were collected, processed, and analyzed in the McGill University Advanced BioImaging Facility (ABIF). Molecular biology experiments (qPCR, PCR thermocycler, nanodrop quantification) were performed with the guidance of Dr. Nicolas Audet using McGill University Imaging and Molecular Biology Platform (IMBP) equipment. The authors acknowledge research grants from the National Sciences and Engineering Research Council of Canada (RGPIN-2018-03843 and ALLRP 548623-19), Canada Research Chair research stipend (NLJ), and by the National Institutes of Health (grant R01 DC-018577-01A1). The presented content is solely the responsibility of the authors and does not necessarily represent the official views of the above funding agencies.

References

1. World Health Organization. News Release - Billions of People Still Breathe Unhealthy Air: New WHO Data. *World Health Organization* <https://www.who.int/news/item/04-04-2022-billions-of-people-still-breathe-unhealthy-air-new-who-data> (2022).
2. Schraufnagel, D. E. *et al.* Air Pollution and Noncommunicable Diseases: A Review by the Forum of International Respiratory Societies' Environmental Committee, Part 2: Air Pollution and Organ Systems. *Chest* **155**, 417–426 (2019).
3. Burnett, R. *et al.* Global estimates of mortality associated with long-term exposure to outdoor fine particulate matter. *Proc. Natl. Acad. Sci.* **115**, 9592–9597 (2018).
4. Guarnieri, M. & Balmes, J. R. Outdoor air pollution and asthma. *Lancet* **383**, 1581–1592 (2014).
5. Liu, S. *et al.* Association between exposure to ambient particulate matter and chronic obstructive pulmonary disease: results from a cross-sectional study in China. *Thorax* **72**, 788–795 (2017).
6. Cooper, D. M. & Loxham, M. Particulate matter and the airway epithelium: the special case of the underground? *Eur. Respir. Rev.* **28**, 190066 (2019).
7. Won, H. *et al.* Effect of Urban Particulate Matter on Vocal Fold Fibrosis through the MAPK/NF- κ B Signaling Pathway. *Int. J. Environ. Res. Public Health* **21**, 6643 (2020).
8. World Health Organization global air quality guidelines. *Particulate matter (PM_{2.5} and PM₁₀), ozone, nitrogen dioxide, sulfur dioxide and carbon monoxide.* (2021).
9. World Bank and Institute for Health Metrics and Evaluation. *The cost of air pollution: strengthening the economic case for action.* (2016).
10. Shusterman, D. The Effects of Air Pollutants and Irritants on the Upper Airway. *Proc. Am. Thorac. Soc.* **8**, 101–105 (2011).
11. US Environmental Protection Agency. National Ambient Air Quality Standards. <https://www.epa.gov/criteria-air-pollutants/naaqs-table> (2021).
12. Lelieveld, J. *et al.* Cardiovascular disease burden from ambient air pollution in Europe reassessed using novel hazard ratio functions. *Eur. Heart J.* **40**, 1590–1596 (2019).
13. World Health Organization. Ambient air pollution: Pollutants. <https://www.who.int/airpollution/ambient/pollutants/en/> (2019).
14. International Agency for Research on Cancer - World Health Organization: *Outdoor Air Pollution - The evaluation of carcinogenic risks to humans.* vol. 109 (2015).
15. Filkov, A. I., Ngo, T., Matthews, S., Telfer, S. & Penman, T. D. Impact of Australia's catastrophic 2019/20 bushfire season on communities and environment. Retrospective

- analysis and current trends. *J. Saf. Sci. Resil.* **1**, 44–56 (2020).
16. Tasker, J. P. Canada reports worst wildfire season on record — and there's more to come this fall. *CBC News* <https://www.cbc.ca/news/politics/canada-wildfire-season-worst-ever-more-to-come-1.6934284> (2023).
 17. San-Miguel-Ayanz, J. *et al.* *Advance report on forest fires in Europe, Middle East and North Africa 2022. Publications Office of the European Union, Luxembourg* <https://data.europa.eu/doi/10.2760/091540> (2023).
 18. Keeley, J. E. & Syphard, A. D. Large California wildfires: 2020 fires in historical context. *Fire Ecol.* **17**, 22 (2021).
 19. Schraufnagel, D. E. The health effects of ultrafine particles. *Exp. Mol. Med.* **52**, 311–317 (2020).
 20. Lee, D. C. *et al.* Urban particulate matter regulates tight junction proteins by inducing oxidative stress via the Akt signal pathway in human nasal epithelial cells. *Toxicol. Lett.* **333**, 33–41 (2020).
 21. Fujii, T., Hayashi, S., Hogg, J. C., Vincent, R. & Van Eeden, S. F. Particulate Matter Induces Cytokine Expression in Human Bronchial Epithelial Cells. *Am. J. Respir. Cell Mol. Biol.* **25**, 265–271 (2001).
 22. Martonen, T. B. & Division, P. Measurements of particle dose distribution in a model of a human larynx and tracheobronchial tree. *J. Aerosol Sci.* **14**, 11–22 (1983).
 23. Levendoski, E. E., Leydon, C. & Thibeault, S. L. Vocal Fold Epithelial Barrier in Health and Injury: A Research Review. *J. Speech, Lang. Hear. Res.* **57**, 1679–1691 (2014).
 24. Darquenne, C. Deposition Mechanisms. *J. Aerosol Med. Pulm. Drug Deliv.* **33**, 181–185 (2020).
 25. Igarashi, E. *Nanomedicines and nanoproducts: applications, disposition, and toxicology in the human body.* (CRC Press, Taylor & Francis Group, 2015).
 26. Thibeault, S. L., Rees, L., Pazmany, L. & Birchall, M. A. At the crossroads: mucosal immunology of the larynx. *Mucosal Immunol.* **2**, 122–128 (2009).
 27. Hirano, M. Structure and Vibratory Behavior of the Vocal Folds. Dynamic Aspects of Speech Production. in *Dynamic aspects of speech production: Current Results, Emerging Problems, and New Instrumentation* 13–27 (University of Tokyo Press, 1977).
 28. Wang, J., Lin, C., Chu, Y., Deng, H. & Shen, Z. Association between long-term exposure to air pollution and the risk of incident laryngeal cancer: a longitudinal UK Biobank-based study. *Environ. Sci. Pollut. Res.* **30**, 58295–58303 (2023).
 29. Perkner, J. J. *et al.* Irritant-Associated Vocal Cord Dysfunction. *J. Occup. Environ. Med.* **40**, 136–143 (1998).
 30. Joo, Y.-H., Lee, S.-S., Han, K. & Park, K.-H. Association between Chronic Laryngitis and Particulate Matter Based on the Korea National Health and Nutrition Examination Survey 2008–2012. *PLoS One* **10**, e0133180 (2015).
 31. Duarte, J. L., de Faria, F. A. C., Ceolin, D. S., Cestari, T. M. & de Assis, G. F. Effects of passive smoke inhalation on the vocal cords of rats. *Braz. J. Otorhinolaryngol.* **72**, 210–216 (2006).
 32. Liu, X., Durkes, A. C., Schrock, W., Zheng, W. & Sivasankar, M. P. Subacute acrolein exposure to rat larynx in vivo. *Laryngoscope* **129**, E313–E317 (2019).
 33. Mouadeb, D. A. *et al.* The effects of allergens and tobacco smoke on the laryngeal mucosa

- of guinea pigs. *Otolaryngol. - Head Neck Surg.* **140**, 493–497 (2009).
34. Marcelino, F. C. & Oliveira, D. T. Histopathological Changes of Vocal Folds Induced by Chronic Pollutant Exposure: An Experimental Study. *J. Voice* **19**, 529–533 (2005).
 35. Zeitels, S. M. *et al.* Vocal Fold Injection of Absorbable Materials: A Histologic Analysis With Clinical Ramifications. *Ann. Otol. Rhinol. Laryngol.* **128**, 71S–81S (2019).
 36. Coburn, P. T., Li, X., Li, J., Kishimoto, Y. & Li-Jessen, N. Y. K. Progress in Vocal Fold Regenerative Biomaterials: An Immunological Perspective. *Adv. NanoBiomed Res.* **2100119**, (2021).
 37. Alipour, F. & Jaiswal, S. Phonatory characteristics of excised pig, sheep, and cow larynges. *J. Acoust. Soc. Am.* **123**, 4572–4581 (2008).
 38. Balls, M. Replacement of animal procedures: Alternatives in research, education and testing. *Lab. Anim.* **28**, 193–211 (1994).
 39. Russel, W. M. S. & Burch, R. L. The Principles of Humane Experimental Technique. *Med. J. Aust.* **1**, 500–500 (1960).
 40. Robinson, N. B. *et al.* The current state of animal models in research: A review. *Int. J. Surg.* **72**, 9–13 (2019).
 41. Branski, R. C., Zhou, H., Kraus, D. H. & Sivasankar, M. The effects of cigarette smoke condensate on vocal fold transepithelial resistance and inflammatory signaling in vocal fold fibroblasts. *Laryngoscope* **121**, 601–605 (2011).
 42. Alper, R., Fu, X., Erickson-Levendoski, E., Zheng, W. & Sivasankar, M. Acute stress to excised vocal fold epithelium from reactive oxygen species. *Laryngoscope* **121**, 2180–2184 (2011).
 43. Liu, X., Walimbe, T., Schrock, W. P., Zheng, W. & Sivasankar, M. P. Acute Nanoparticle Exposure to Vocal Folds: A Laboratory Study. *J. Voice* **31**, 662–668 (2017).
 44. Erickson-Direnzo, E., Sivasankar, M. P., Thibeault, S. L., Preeti Sivasankar, M. & Thibeault, S. L. Utility of Cell Viability Assays for Use With Ex Vivo Vocal Fold Epithelial Tissue. *Laryngoscope* **125**, E180–E185 (2015).
 45. Liu, X., Zheng, W. & Sivasankar, M. P. Acute acrolein exposure induces impairment of vocal fold epithelial barrier function. *PLoS One* **11**, 1–15 (2016).
 46. Choi, H. & Kim, C. S. Polycyclic Aromatic Hydrocarbons from Fine Particulate Matter Induce Oxidative Stress and the Inflammatory Response in Human Vocal Fold Fibroblast Cells. *Oxid. Med. Cell. Longev.* **2021**, 1–10 (2021).
 47. Gugatschka, M. *et al.* Proteomic analysis of vocal fold fibroblasts exposed to cigarette smoke extract: Exploring the pathophysiology of Reinke’s edema. *Mol. Cell. Proteomics* **18**, 1511–1525 (2019).
 48. Wang, J., Fang, R., Peterson, A. & Jiang, J. J. The protective role of autophagy in human vocal fold fibroblasts under cigarette smoke extract exposure: A new insight into the study of reinke’s edema. *Orl* **78**, 26–35 (2016).
 49. Berchtold, C. M., Coughlin, A., Kasper, Z. & Thibeault, S. L. Paracrine potential of fibroblasts exposed to cigarette smoke extract with vascular growth factor induction. *Laryngoscope* **123**, 2228–2236 (2013).
 50. Branski, R. C. *et al.* Cigarette smoke and reactive oxygen species metabolism: Implications for the pathophysiology of reinke’s edema. *Laryngoscope* **119**, 2014–2018 (2009).
 51. Martinez, J. D., Easwaran, M., Ramirez, D. & Erickson-DiRenzo, E. Effects of Electronic

- (E)-cigarette Vapor and Cigarette Smoke in Cultured Vocal Fold Fibroblasts. *Laryngoscope* **133**, 139–146 (2023).
52. Herbert, R. A., Janardhan, K. S., Pandiri, A. R., Cesta, M. F. & Miller, R. A. Nose, Larynx, and Trachea. in *Boorman's Pathology of the Rat* 391–435 (Elsevier, 2018).
 53. Chen, X. *et al.* Novel immortalized human vocal fold epithelial cell line: In vitro tool for mucosal biology. *FASEB J.* **35**, 1–16 (2021).
 54. Lungova, V., Chen, X., Wang, Z., Kendzierski, C. & Thibeault, S. L. Human induced pluripotent stem cell-derived vocal fold mucosa mimics development and responses to smoke exposure. *Nat. Commun.* **10**, 4161 (2019).
 55. Coburn, P. T., Lungova, V., Liu, X., Thibeault, S. L. & Li-Jessen, N. Y. K. A Vocal Fold Organ-on-a-Chip Platform for Studying the Impact of Environmental Irritants on Upper Airway Health. *Prep.*
 56. Bukowy-Bieryłło, Z. Long-term differentiating primary human airway epithelial cell cultures: how far are we? *Cell Commun. Signal.* **19**, 1–18 (2021).
 57. Chen, X., Rocha, C., Rao, T. & Durcan, T. EDDU Protocols - iPSC Culture. 1–38 (2019) doi:10.5281/zenodo.3733913.
 58. EPA. Exposure Assessment Tools by Routes - Inhalation. *US Environmental Protection Agency* <https://www.epa.gov/expobox/exposure-assessment-tools-routes-inhalation> (2023).
 59. Chen, X. *et al.* Urban particulate matter (PM) suppresses airway antibacterial defence. *Respir. Res.* **19**, 1–11 (2018).
 60. Kim, J.-S. *et al.* Effect of fluticasone propionate on human nasal fibroblasts exposed to urban particulate matter. *Auris Nasus Larynx* **47**, 415–424 (2020).
 61. Livak, K. J. & Schmittgen, T. D. Analysis of relative gene expression data using real-time quantitative PCR and the 2- $\Delta\Delta$ CT method. *Methods* **25**, 402–408 (2001).
 62. Leydon, C., Imaizumi, M., Bartlett, R. S., Wang, S. F. & Thibeault, S. L. Epithelial cells are active participants in vocal fold wound healing: An in vivo animal model of injury. *PLoS One* **9**, 1–14 (2014).
 63. Gill, G. A. *et al.* Laryngeal Epithelial Defenses Against Laryngopharyngeal Reflux: Investigations of E-cadherin, Carbonic Anhydrase Isoenzyme III, and Pepsin. *Ann. Otol. Rhinol. Laryngol.* **114**, 913–921 (2005).
 64. Leydon, C., Selekman, J. A., Palecek, S. & Thibeault, S. L. Human Embryonic Stem Cell-Derived Epithelial Cells in a Novel In Vitro Model of Vocal Mucosa. *Tissue Eng. Part A* **19**, 2233–2241 (2013).
 65. Dowdall, J. R. *et al.* Identification of distinct layers within the stratified squamous epithelium of the adult human true vocal fold. *Laryngoscope* **125**, E313–E319 (2015).
 66. Voynow, J. A., Fischer, B. M., Roberts, B. C. & Proia, A. D. Basal-like cells constitute the proliferating cell population in cystic fibrosis airways. *Am. J. Respir. Crit. Care Med.* **172**, 1013–1018 (2005).
 67. Bulmer, D. M., Ali, M. S., Brownlee, I. A., Dettmar, P. W. & Pearson, J. P. Laryngeal mucosa: Its susceptibility to damage by acid and pepsin. *Laryngoscope* **120**, 777–782 (2010).
 68. Smyth, T. & Georas, S. N. Effects of ozone and particulate matter on airway epithelial barrier structure and function: a review of in vitro and in vivo studies. *Inhal. Toxicol.* **33**,

- 177–192 (2021).
69. An, R., Robbins, D., Rey, F. E. & Thibeault, S. L. Vocal fold mucus layer: Comparison of histological protocols for visualization in mice. *Laryngoscope Invest. Otolaryngol.* **7**, 444–453 (2022).
 70. Levendoski, E. E. & Sivasankar, M. P. Vocal fold ion transport and mucin expression following Acrolein exposure. *J. Membr. Biol.* **247**, 441–450 (2014).
 71. Lungova, V., Wendt, K. & Thibeault, S. L. Exposure to e-cigarette vapor extract induces vocal fold epithelial injury and triggers intense mucosal remodeling. *Dis. Model. Mech.* **15**, (2022).
 72. Easwaran, M., Martinez, J. D., Ramirez, D. J., Gall, P. A. & Erickson-DiRenzo, E. Short-term whole body cigarette smoke exposure induces regional differences in cellular response in the mouse larynx. *Toxicol. Reports* **8**, 920–937 (2021).
 73. Tateya, I., Tateya, T., Lim, X., Sohn, J. H. & Bless, D. M. Cell production in injured vocal folds: A rat study. *Ann. Otol. Rhinol. Laryngol.* **115**, 135–143 (2006).
 74. Cherng, S., Young, J. & Hongbao, M. Alpha-smooth muscle actin (α -SMA). *J. Am. Sci.* **4**, 7–9 (2008).
 75. Rockey, D. C., Weymouth, N. & Shi, Z. Smooth Muscle α Actin (Acta2) and Myofibroblast Function during Hepatic Wound Healing. *PLoS One* **8**, (2013).
 76. Kendall, R. T. & Feghali-Bostwick, C. A. Fibroblasts in fibrosis: novel roles and mediators. *Front. Pharmacol.* **5**, 1–13 (2014).
 77. Davis, J. D. & Wypych, T. P. Cellular and functional heterogeneity of the airway epithelium. *Mucosal Immunol.* **14**, 978–990 (2021).
 78. Sellati, T. J. & Sahay, B. Cells of Innate Immunity: Mechanisms of Activation. in *Pathobiology of Human Disease* 258–274 (Elsevier, 2014).
 79. Štiblar-MartinČič, D. Histology of Laryngeal Mucosa. *Acta Otolaryngol.* **117**, 138–141 (1997).
 80. Sato, K. *Functional Histoanatomy of the Human Larynx. Functional Histoanatomy of the Human Larynx* (Springer Singapore, 2018).
 81. King, R. E., Ward-Shaw, E. T., Hu, R., Lambert, P. F. & Thibeault, S. L. Expanded Basal Compartment and Disrupted Barrier in Vocal Fold Epithelium Infected with Mouse Papillomavirus MmuPV1. *Viruses* **14**, (2022).
 82. Kojima, T. *et al.* Regulation of Tight Junctions in Upper Airway Epithelium. *Biomed Res. Int.* **2013**, 1–11 (2013).
 83. Schneider, B., Teschner, M., Sudermann, T., Pikula, B. & Lautermann, J. Expression of Gap Junction Proteins (Connexin 26, 30, 32, 43) in Normal Mucosa, Hyperkeratosis and Carcinoma of the Human Larynx. *ORL* **64**, 324–329 (2002).
 84. Van Deusen, M. B. & Lyon, M. J. Connexins within the rat larynx. *Otolaryngol. Neck Surg.* **139**, 823–828 (2008).
 85. Ravikrishnan, A., Fowler, E. W., Stuffer, A. J. & Jia, X. Hydrogel-Supported, Engineered Model of Vocal Fold Epithelium. *ACS Biomater. Sci. Eng.* **7**, 4305–4317 (2021).
 86. Samuels, T. L. *et al.* Mucin Gene Expression in Human Laryngeal Epithelia: Effect of Laryngopharyngeal Reflux. *Ann. Otol. Rhinol. Laryngol.* **117**, 688–695 (2008).
 87. Gudipaty, S. A. *et al.* Mechanical stretch triggers rapid epithelial cell division through Piezo1. *Nature* **543**, 118–121 (2017).

88. Eisenhoffer, G. T. *et al.* Crowding induces live cell extrusion to maintain homeostatic cell numbers in epithelia. *Nature* **484**, 546–549 (2012).
89. Jiang, Y., Yang, X., Jiang, J. & Xiao, B. Structural Designs and Mechanogating Mechanisms of the Mechanosensitive Piezo Channels. *Trends Biochem. Sci.* **46**, 472–488 (2021).
90. Foote, A. G., Lungova, V. & Thibeault, S. L. Piezo1-expressing vocal fold epithelia modulate remodeling via effects on self-renewal and cytokeratin differentiation. *Cell. Mol. Life Sci.* **79**, 591 (2022).
91. Emig, R. *et al.* Piezo1 channels contribute to the regulation of human atrial fibroblast mechanical properties and matrix stiffness sensing. *Cells* **10**, 1–21 (2021).
92. Volpato, V. & Webber, C. Addressing variability in iPSC-derived models of human disease: Guidelines to promote reproducibility. *DMM Dis. Model. Mech.* **13**, (2020).
93. Nawroth, J. C. *et al.* Stem cell-based Lung-on-Chips: The best of both worlds? *Adv. Drug Deliv. Rev.* **140**, 12–32 (2018).
94. Hirano, M. & Sato, K. Laser surgery for epithelial hyperplasia of the vocal fold. *Ann. Otol. Rhinol. Laryngol.* **102**, 85–91 (1993).
95. Ferlito, A. *et al.* Squamous epithelial changes of the larynx: Diagnosis and therapy. *Head Neck* **34**, 1810–1816 (2012).
96. Renne, R. A. & Gideon, K. M. Types and Patterns of Response in the Larynx Following Inhalation. *Toxicol. Pathol.* **34**, 281–285 (2006).
97. Sataloff, R. T. The Impact of Pollution on the Voice. *Otolaryngol. - Head Neck Surg.* **106**, 701–705 (1992).
98. Sato, K. Blood Vessels of the Larynx and Vocal Fold. in *Functional Histoanatomy of the Human Larynx* 287–303 (Springer Singapore, 2018).
99. Wang, T. *et al.* Particulate matter air pollution disrupts endothelial cell barrier via calpain-mediated tight junction protein degradation. *Part. Fibre Toxicol.* **9**, 1–12 (2012).
100. Benam, K. H. *et al.* Small airway-on-a-chip enables analysis of human lung inflammation and drug responses in vitro. *Nat. Methods* **13**, 151–157 (2016).
101. Si, L. *et al.* A human-airway-on-a-chip for the rapid identification of candidate antiviral therapeutics and prophylactics. *Nat. Biomed. Eng.* **5**, 815–829 (2021).
102. Huh, D. *et al.* Reconstituting Organ-Level Lung Functions on a Chip. *Science* (80-.). **328**, 1662–1669 (2010).
103. Nawroth, J. C. *et al.* A Microengineered Airway Lung Chip Models Key Features of Viral-induced Exacerbation of Asthma. *Am. J. Respir. Cell Mol. Biol.* **63**, 591–600 (2020).
104. Zhang, Z. & Kleinstreuer, C. Airflow structures and nano-particle deposition in a human upper airway model. *J. Comput. Phys.* **198**, 178–210 (2004).
105. Zhang, T., Gao, B., Zhou, Z. & Chang, Y. The movement and deposition of PM2.5 in the upper respiratory tract for the patients with heart failure: an elementary CFD study. *Biomed. Eng. Online* **15**, 138 (2016).
106. Hinderliter, P. M. *et al.* ISDD: A computational model of particle sedimentation, diffusion and target cell dosimetry for in vitro toxicity studies. *Part. Fibre Toxicol.* **7**, 36 (2010).
107. Garg, A. *et al.* Towards a Physiological Scale of Vocal Fold Agent-Based Models of Surgical Injury and Repair: Sensitivity Analysis, Calibration and Verification. *Appl. Sci.* **9**, 2974 (2019).

108. Seekhao, N. *et al.* High-Performance Host-Device Scheduling and Data-Transfer Minimization Techniques for Visualization of 3D Agent-Based Wound Healing Applications. *PDPTA* **19**, 69–76 (2019).
109. M. Piaścik, Przyk, E. P. & Held, A. *The Certification of the Mass Fractions of selected Polycyclic Aromatic Hydrocarbons (PAHs) in fine dust (PM10-like matrix) Certified Reference Material ERM-CZ100.* (European Reference Materials, 2010). doi:10.2787/32299.

Supporting Information

PM₁₀ Composition

The PM₁₀ in this study was a standardized, reference material prepared from road tunnel dust by the European Institute for Reference Materials and Measurements. A certification report for the Mass Fractions of Selected Polycyclic Aromatic Hydrocarbons present in the material is available online at <https://crm.jrc.ec.europa.eu/p/40455/40459/By-material-matrix/Soils-sludges-sediment-dust/ERM-CZ100-FINE-DUST-PM10-LIKE-PAHs/ERM-CZ100>.¹⁰⁹ The tables and figure below are extracted from the report and detail the fractions and particle size present.

Table S6.1. Certified fraction values present in ERM-CZ PM₁₀-like dust from ¹⁰⁹.

PAH	Mass Fraction	
	Certified value ¹⁾ [mg/kg]	Uncertainty ²⁾ [mg/kg]
Benzo[a]anthracene	0.91	0.07
Benzo[a]pyrene	0.72	0.05
Benzo[b]fluoranthene	1.42	0.14
Benzo[j]fluoranthene	0.75	0.14
Benzo[k]fluoranthene	0.67	0.06
Dibenzo[a,h]anthracene	0.18	0.04
Indeno[1,2,3-c,d]pyrene	1.07	0.10
Sum of benzo[b]fluoranthene, benzo[k]fluoranthene and benzo[j]fluoranthene ³⁾	2.84	0.21

¹⁾ The value is the unweighted mean of accepted sets of data, each set being obtained in a different laboratory and/or with a different method. The certified values are reported on the mass of the sample after conditioning the sample using conditions as described in EN12341 and are traceable to the SI.

²⁾ Expanded uncertainty with a coverage factor $k = 2$ according to the Guide to the Expression of Uncertainty in Measurement (GUM), corresponding to a level of confidence of about 95 %.

³⁾ The sum of the compounds was calculated as the sum of the individual certified values. The uncertainty was calculated as the combined expanded uncertainty of the uncertainties of the individual compounds.

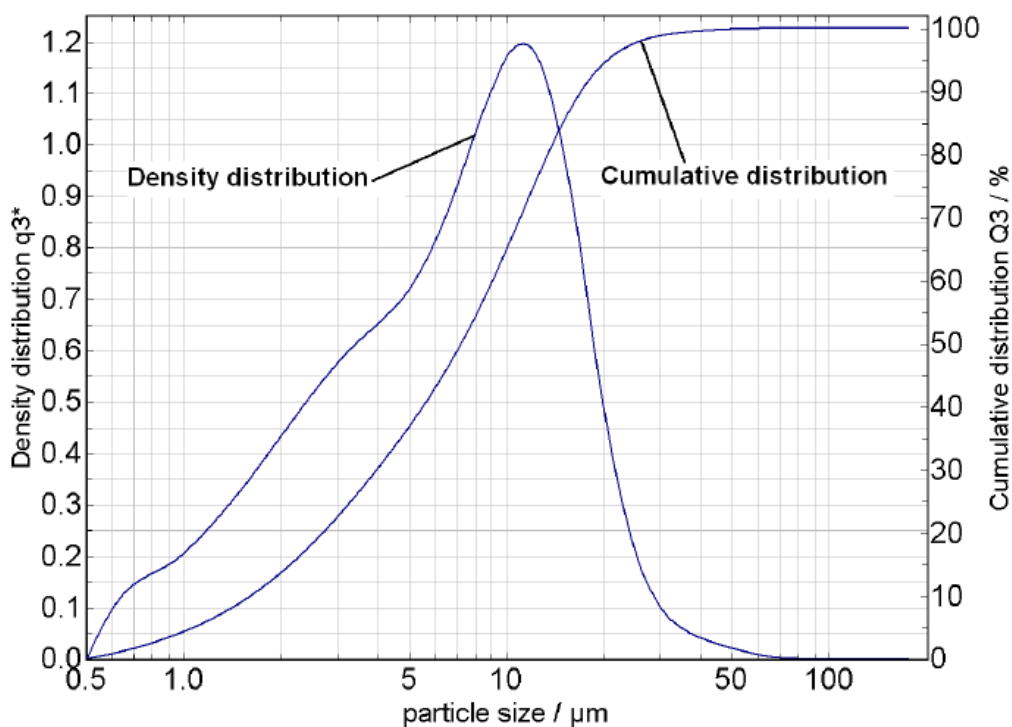




Figure S6.1. Particle size distribution (in vol. %) present in ERM-CZ PM₁₀-like dust from ¹⁰⁹.

Culture Vessel Parameters

Table S6.2. Parameters of the VF-OOAC and transwell controls used for VF mucosa culture.

	VF-OOAC	Transwell Control
Culture System	BEOnChip Microfluidic Chip	Corning Transwell Insert
Culture Dimensionality	3D	3D
Perfusion	Yes	No
Microchannels	1	0
Media Volume	44 μL	600 μL
Membrane Material	Polycarbonate	Polycarbonate
Membrane Thickness	10 μm	10 μm
Membrane Pore Size	0.4 μm	0.4 μm
Membrane Pore Density	1×10 ⁵ pores cm ²	1×10 ⁸ pores cm ²
Device		

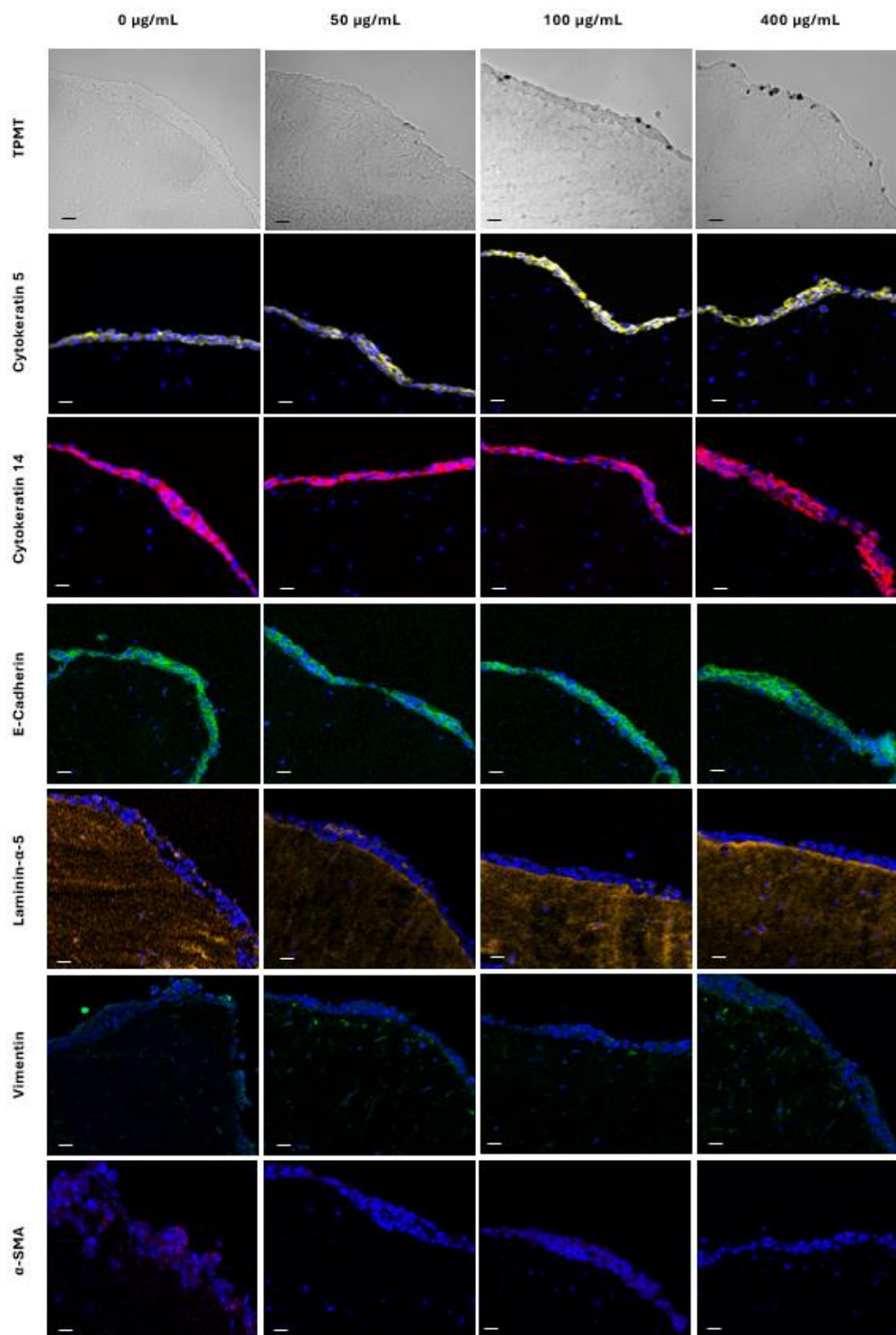


Figure S6.2. Dose response to 24 hr PM₁₀ exposure for transwell_{iLEC}. Transmitted light visualized PM₁₀ distribution at the epithelium surface (black particles). K5, K14, and E-Cad evaluated epithelium structure. LAMA5 assessed basement membrane. Vimentin and α SMA evaluated epithelial-to-mesenchymal transition presence. Samples counterstained with DAPI (blue). Magnification 20x, scale bar = 30 μ m.

Chapter 5. Discussion

This thesis aimed to evaluate the impact of PM₁₀ on structural, functional, and inflammatory characteristics of the VF mucosa. To investigate this, a microfluidic perfused culture system was proposed with the capacity to enhance VF mucosa tissue development compared to conventional techniques. This VF-OOAC model provided a reliable platform for studying the interaction of environmental irritants (i.e. PM₁₀) with the VF mucosa. Overall, the presented work has enriched the repertoire of *in vitro* systems available to the voice research field and built a foundation for further model expansion. That said, opportunities to further improve upon the proposed VF-OOAC exist and are outlined here.

Microfluidic Chip Configuration

The BEOnChip device utilized as the principal microfluidic culture vessel in this thesis was effectively demonstrated to benefit VF mucosa tissue development. However, although the benefits of perfused, microscale culture were validated, the current device configuration is incompatible with cultivating epithelial cells at a dynamic ALI to mimic physiological breathing. To retain the advantages of using commercialized devices, namely minimizing batch-to-batch variability and improving protocol standardization, alternative devices can be procured. For example, SynVivo (Alabama, U.S.) offers a device with two microchannels either side of a central compartment applicable for 3D hydrogel culture.⁸¹ This setup would therefore retain the benefits of cultivating VF fibroblasts in a 3D environment and permit media perfusion through one microchannel and airflow through the other. This configuration ensures fibroblasts and epithelial cells are cultivated in physiologically relevant conditions.

Notably, limitations are attached to this modified setup. Firstly, physically separating the VF epithelium from lamina propria tissue via a porous plastic membrane is not a representative model of native tissue and will diminish cell-basement membrane interactions. A potential method to overcome this would be using ECM hydrogels as walls to divide each device compartment. This concept has been explored in several airway OOAC models to separate epithelial monocultures from medium compartments or to partition epithelial and endothelial tissue components.⁸²⁻⁸⁴ These ECM structures could function as a scaffold to guide tissue development whilst slowly being degraded and replaced by cell-synthesized ECM. As this design would require robust barrier

integrity to maintain a functional ALI, it is better suited to iPSC-derived VF epithelial cells due to their increased functionality and barrier capacity.¹¹ However, it should be noted that the use of such a setup would necessitate in-house fabrication of the device. Whilst this would provide greater design flexibility, it will also lengthen model optimization due to fabrication failures lowering the yield of successful experiments. This can be caused by misalignment of microchannel walls or incomplete bonding between device layers.⁸⁵ Potentially, open collaborative strategies alongside commercial suppliers could overcome these limitations.

Particulate Matter Toxicity & Exposure

The VF-OOAC displayed a robust resilience to acute PM₁₀ exposure as presented in this thesis. Future investigation of the aryl hydrocarbon receptor is warranted to potentially reveal specific molecular mechanisms controlling the interaction between VF mucosa tissue and PM₁₀. For instance, this receptor has been suggested to stimulate reactive oxygen species production in VF fibroblasts *in vitro* via the CYP1A1 pathway.¹⁰⁴ Quantifying oxidative stress in cultivated VF mucosae is particularly useful for longer-term studies as a marker of wound healing or disease development. For example, controlled regulation of reactive oxygen species was found to be crucial for tissue repair and inflammatory resolution in an injured VF rat model.¹⁰⁵ Fundamentally, monitoring aryl hydrocarbon receptor activity could be used to explore how specific PM₁₀ compositions relate to pollutant-induced injuries.

In addition, the physiological relevance of the exposure method employed can be markedly improved. In the native human airways, PM₁₀ travels through the upper airway as an airborne suspension of particles. As such, replicating the true doses experienced by the VF mucosa *in vivo* requires PM₁₀ to be delivered as an aerosolized challenge.

Two different methods are possible to achieve this. The first, as described above, involves reconfiguring the microfluidic device to integrate a microchannel for airflow. In this setup, aerosolized PM₁₀ could then be driven through the OOAC using a pneumatic pump, vacuum pressure pump, or an equivalent device.⁸⁶ Overall, this setup would provide much tighter regulation of PM₁₀ doses delivered to cells and constitute a more realistic exposure.

The second method could utilize the VF-OOAC configuration presented in this thesis and combine it with existing exposure technology, such as that offered by Cultex® or Vitrocell® to

challenge the VF epithelium with realistic, aerosolized PM₁₀ doses.^{87,88} These chamber systems permit exposure of cell cultures to aerosolized material, vapours, and gases. Such instruments could provide the VF-OOAC with relevant exposure. However, this strategy would require a collaborative effort with commercial suppliers to adapt the system to suit the dimensions and needs of the VF-OOAC exposure experiment.

Overall, improving the physiological relevance of the VF-OOAC's exposure to airborne irritants and therapeutics should be a key goal for future iterations of the model. The solutions proposed here are reasonable and practical approaches that could utilize many of the experimental protocols established in this thesis. Ultimately, achieving a dynamic, airborne exposure will provide even greater physiological relevance whilst increasing the platform's versatility and reliability as a preclinical model.

iPSC Applications for Health & Disease Modelling

OOAC models integrating iPSC-derived cells remains a severely understudied area of upper airway research, especially given the significant benefits of each technology. OOAC culture offers significant benefits for tissue functionality and iPSC culture models provide increased clinical translation power.⁵⁵

Advances in iPSC technology have overcome ethical and technical challenges associated with personalized medicine approaches. For example, although embryonic stem cells offer a pluripotent cell source with the capacity to derive any human cell type, the use of these cells is strictly regulated and controversial. Alternatively, obtaining primary VF epithelial cells from a healthy larynx involves a highly invasive procedure that is challenging to perform and presents a significant risk of VF scarring.¹¹ In contrast to these methods, iPSCs obtained via reprogramming an individual's accessible somatic cells offer a pluripotent cell source without the associated ethical constraints. As such, iPSCs offer the opportunity to create patient-specific models for personal drug, treatment response and toxicology screening.⁵⁴

This thesis reports the first iPSC-derived OOAC in VF biological research. Whilst this model represents a significant advancement for upper airway research, limitations are attached to this engineered VF microtissue. As for many iPSC differentiation protocols, the differentiation efficacy and homogeneity of the progenitor population could be improved to increase the yield of

target cells. Progenitor culture in the VF-OOAC setup will require further optimization. In this thesis, the advantages of microscale culture for increasing tissue development speed were enacted by cultivating VF basal progenitor cells at the ALI for approximately 1 week less than used in the original transwell protocols.^{11,89,90} However, those transwell protocols only reported significant cytokeratin production (K5, K13, K14) after 32 days.¹¹ To improve structural composition and maturity of our VF-OOAC iPSC-derived epithelium, it is recommended to extend ALI culture time to further explore its influence on tissue development.

Future Directions

Now the initial VF-OOAC platform has been established, a number of research avenues are available to pursue. This notably includes improving the cellular architecture or studying immune responses. For example, pVFFs were cultured in the microchannel to investigate how fluidic shear imparted by interstitial fluid flow regulates fibroblast behaviour and controls VF mucosa tissue development. However, an alternative approach to advance cellular architecture complexity is to incorporate endothelial cells in the perfused microchannel. Endothelial cells have an important role in controlling vascular permeability and therapeutic drug efficacy.⁹¹ Their inclusion in the VF-OOAC would enable the platform to model the response to drug therapeutics with increased precision.⁹² In addition, including endothelial tissue in the VF-OOAC can mimic the rich, vascular network of the VFs and assess how PM₁₀ impacts endothelial barrier integrity.^{93,94} Finally, incorporating luminal vasculature is an integral feature of multiorgan OOAC systems, where endothelial cell-lined channels are used to connect individual organs.⁵⁴ As such, integrating an endothelium in the VF-OOAC increases the number of research opportunities available for future exploration.

Immune cells are a further notable absent component from the VF-OOAC. Their inclusion could significantly improve the physiological relevance of inflammatory activity observed in response to environmental irritants. For example, the VF mucosa contains a significant population of tissue-resident macrophages that regulate inflammatory activity and the response to environmental irritants.³⁶ Incorporating macrophages into the VF-OOAC would require embedding them in the collagen gel alongside the pVFFs. From this location, they would be able to migrate towards threats present at the luminal epithelial surface and respond accordingly.

An alternative use of immune cells could be to recirculate leukocytes, such as neutrophils, through endothelial-lined microchannels in a modified VF-OOAC. This would allow the study of neutrophil-driven inflammatory activity in the VF mucosa and, providing membrane pore size was increased from 0.4 μm to $\geq 3 \mu\text{m}$, permit the recapitulation of diapedesis in response to pathogens or environmental irritants.^{95–98} Recirculating neutrophils has been achieved in lower airway OOAC models using a peristaltic pump.^{96,99} The VF-OOAC is highly compatible with integrating this technique, although the addition of further cell types will require re-optimization of culture media conditions.

Finally, as a longer-term goal, the VF-OOAC could be connected with other OOAC models to study organ-level crosstalk and build an important screening tool for use in therapeutics development.⁵⁴ For instance, to investigate drug toxicity related to voice disorder treatments, the VF-OOAC could be fluidically linked to liver and kidney tissues to monitor drug metabolism and excretion.^{54,100–103}

Chapter 6. Conclusions

The overall objective of the presented research was to develop a VF-OOAC and evaluate its capacity to model the *in vivo* response of the VF mucosa to environmental irritants. By recapitulating more aspects of native tissue, the VF-OOAC was intended to reproduce higher-level functions exceeding conventional culture models such as transwell systems.

The first aim investigated the influence of various culture parameters (culture scale, dimensionality, perfusion, fluidic shear) on VF mucosa tissue development. It was hypothesized culture scale would enhance tissue functionality, 3D culture would stimulate cell polarization, perfusion would increase differentiation and proliferation, and fluidic shear would promote mechanosensitive activity. Transitioning from macroscale to microscale culture was indeed found to increase tissue functionality, which was highlighted by upregulated gene expression related to intercellular junctions, mucin synthesis, and ECM production. Increasing culture dimensionality from 2D to 3D was confirmed to enhance epithelium polarization and produce *in vivo*-like fibroblast morphology. Integrating perfusion was observed to stimulate basal epithelial proliferation. Finally, fluidic shear induced an upregulation of mechanosensitive genes and initiated fibroblast realignment. Overall, VF mucosae cultivated using VF-OOAC culture displayed higher structural and functional tissue development compared to transwell controls.

The second aim evaluated resilience of the VF-OOAC_{iLEC} to acute irritant exposure by challenging it with increasing concentrations of PM₁₀. It was hypothesized VF-OOAC_{iLEC} would display a high resilience to PM₁₀ due to the protective mechanisms provided by stratified squamous epithelium. When challenged with PM₁₀, VF-OOAC_{iLEC} exhibited a high resilience to PM₁₀, resisting any dose-response effects. This behaviour mimics *in vivo* observations in the literature suggesting VF epithelium is well-adapted to resisting acute exposure (≤ 24 hr) to environmental irritants. This had not previously been replicated using *in vitro* culture due to a reliance on simple VF fibroblast monocultures. To better imitate the VF mucosa's defensive capabilities, an iPSC-derived epithelium was successfully cultivated in the VF-OOAC setup. It was further hypothesized that this model would better recapitulate the defensive mechanisms of native epithelial tissue, including its barrier capacity and tissue functionality. As such, the VF-OOAC_{iPSC} was anticipated to demonstrate greater resilience to PM₁₀ than VF-OOAC_{iLEC}. Compared to transwell controls,

VF-OOAC_{iPSC} displayed upregulated gene expression relate to intercellular junctions, mucin synthesis, and mechanosensitivity. VF-OOAC_{iPSC} also displayed a high resilience to the challenge of PM₁₀ exposure, with only structural gene expression (K13) in the stratified suprabasal epithelial layers impacted. Furthermore, when contrasting functional and inflammatory gene expression in VF-OOAC_{iLEC} and VF-OOAC_{iPSC}, only VF-OOAC_{iPSC} resisted any significant changes following PM₁₀ exposure.

Overall, I developed and validated a novel *in vitro* microfluidic platform of the VF mucosa. The VF-OOAC model demonstrates performance surpassing that of the current ‘gold standard’ *in vitro* system in VF mucosa research, namely transwell culture. As such, the VF-OOAC could offer deeper insight into the cellular and molecular mechanisms that regulate VF mucosal health and disease. Future work with this model should build on the foundations provided by this thesis and continue to improve *in vivo* conditions by integrating further aspects of the native tissue microenvironment.

References

1. Roy, N., Merrill, R. M., Gray, S. D. & Smith, E. M. Voice disorders in the general population: Prevalence, risk factors, and occupational impact. *Laryngoscope* **115**, 1988–1995 (2005).
2. Cohen, S. M., Kim, J., Roy, N., Asche, C. & Courey, M. The impact of laryngeal disorders on work-related dysfunction. *Laryngoscope* **122**, 1589–1594 (2012).
3. Lunga, T., Thibeault, S. L. & Francis, D. O. Economic Burden Associated With Management of Paradoxical Vocal Fold Motion Disorder. *Laryngoscope* **132**, 142–147 (2022).
4. Wang, J., Lin, C., Chu, Y., Deng, H. & Shen, Z. Association between long-term exposure to air pollution and the risk of incident laryngeal cancer: a longitudinal UK Biobank-based study. *Environ. Sci. Pollut. Res.* **30**, 58295–58303 (2023).
5. Perkner, J. J. *et al.* Irritant-Associated Vocal Cord Dysfunction. *J. Occup. Environ. Med.* **40**, 136–143 (1998).
6. Joo, Y.-H., Lee, S.-S., Han, K. & Park, K.-H. Association between Chronic Laryngitis and Particulate Matter Based on the Korea National Health and Nutrition Examination Survey 2008–2012. *PLoS One* **10**, e0133180 (2015).
7. Leydon, C., Selekman, J. A., Palecek, S. & Thibeault, S. L. Human Embryonic Stem Cell-Derived Epithelial Cells in a Novel In Vitro Model of Vocal Mucosa. *Tissue Eng. Part A* **19**, 2233–2241 (2013).
8. Levendoski, E. E., Leydon, C. & Thibeault, S. L. Vocal Fold Epithelial Barrier in Health and Injury: A Research Review. *J. Speech, Lang. Hear. Res.* **57**, 1679–1691 (2014).
9. Bukowy-Bieryłło, Z. Long-term differentiating primary human airway epithelial cell cultures: how far are we? *Cell Commun. Signal.* **19**, 1–18 (2021).
10. Chen, X. *et al.* Novel immortalized human vocal fold epithelial cell line: In vitro tool for mucosal biology. *FASEB J.* **35**, 1–16 (2021).
11. Lungova, V., Chen, X., Wang, Z., Kendzierski, C. & Thibeault, S. L. Human induced pluripotent stem cell-derived vocal fold mucosa mimics development and responses to smoke exposure. *Nat. Commun.* **10**, 4161 (2019).
12. Nawroth, J. C. *et al.* Stem cell-based Lung-on-Chips: The best of both worlds? *Adv. Drug Deliv. Rev.* **140**, 12–32 (2018).
13. Boltežar, L. & Bahar, M. Š. Voice disorders in occupations with vocal load in Slovenia. *Zdr. Varst.* **53**, 304–310 (2014).
14. Roy, N., Merrill, R. M., Thibeault, S., Gray, S. D. & Smith, E. M. Voice Disorders in Teachers and the General Population. *J. Speech Lang. Hear. Res.* **47**, 542 (2004).
15. Huston, M. N., Puka, I. & Naunheim, M. R. Prevalence of Voice Disorders in the United States: A National Survey. *Laryngoscope* 1–6 (2023) doi:10.1002/lary.30929.
16. Cohen, S. M., Kim, J., Roy, N., Asche, C. & Courey, M. Prevalence and causes of dysphonia in a large treatment-seeking population. *Laryngoscope* **122**, 343–348 (2012).
17. Coyle, S. M., Weinrich, B. D. & Stemple, J. C. Shifts in relative prevalence of laryngeal pathology in a treatment-seeking population. *J. Voice* **15**, 424–440 (2001).
18. Hirano, M. Structure and Vibratory Behavior of the Vocal Folds. Dynamic Aspects of Speech Production. in *Dynamic aspects of speech production: Current Results, Emerging Problems, and New Instrumentation* 13–27 (University of Tokyo Press, 1977).
19. Coburn, P. T., Li, X., Li, J., Kishimoto, Y. & Li-Jessen, N. Y. K. Progress in Vocal Fold

- Regenerative Biomaterials: An Immunological Perspective. *Adv. NanoBiomed Res.* **2100119**, (2021).
20. Gray, S. D. Cellular physiology of the vocal folds. *Otolaryngol. Clin. North Am.* **33**, 679–697 (2000).
 21. Štiblar-MartinČič, D. Histology of Laryngeal Mucosa. *Acta Otolaryngol.* **117**, 138–141 (1997).
 22. Arens, C., Glanz, H., Wönckhaus, J., Hersemeyer, K. & Kraft, M. Histologic assessment of epithelial thickness in early laryngeal cancer or precursor lesions and its impact on endoscopic imaging. *Eur. Arch. Otorhinolaryngol.* **264**, 645–649 (2007).
 23. Kaiser, M. L. *et al.* Laryngeal epithelial thickness: a comparison between optical coherence tomography and histology. *Clin. Otolaryngol.* **34**, 460–466 (2009).
 24. Sekiguchi, R. & Yamada, K. M. Basement Membranes in Development and Disease. in *Physiology & behavior* vol. 176 143–191 (2018).
 25. Gray, S. D., Pignatari, S. S. N. & Harding, P. Morphologic ultrastructure of anchoring fibers in normal vocal fold basement membrane zone. *J. Voice* **8**, 48–52 (1994).
 26. Howat, W. J., Holmes, J. A., Holgate, S. T. & Lackie, P. M. Basement membrane pores in human bronchial epithelium: A conduit for infiltrating cells? *Am. J. Pathol.* **158**, 673–680 (2001).
 27. Knight, D. A. & Holgate, S. T. The airway epithelium: Structural and functional properties in health and disease. *Respirology* **8**, 432–446 (2003).
 28. Rousseau, B., Suehiro, A., Echemendia, N. & Sivasankar, M. Raised intensity phonation compromises vocal fold epithelial barrier integrity. *Laryngoscope* **121**, 346–351 (2011).
 29. Fisher, K. V., Telser, A., Phillips, J. E. & Yeates, D. B. Regulation of vocal fold transepithelial water fluxes. *J. Appl. Physiol.* **91**, 1401–1411 (2001).
 30. Ciara, L., Mahalakshmi, S., Danielle, L. F., Christopher, A. & Kimberly, V. F. Vocal fold surface hydration: A review. *J. Voice* **23**, 658–665 (2009).
 31. Gill, G. A. *et al.* Laryngeal Epithelial Defenses Against Laryngopharyngeal Reflux: Investigations of E-cadherin, Carbonic Anhydrase Isoenzyme III, and Pepsin. *Ann. Otol. Rhinol. Laryngol.* **114**, 913–921 (2005).
 32. Suzuki, T. Regulation of intestinal epithelial permeability by tight junctions. *Cell. Mol. Life Sci.* **70**, 631–659 (2013).
 33. Samitas, K., Carter, A., Kariyawasam, H. H. & Xanthou, G. Upper and lower airway remodelling mechanisms in asthma, allergic rhinitis and chronic rhinosinusitis: The one airway concept revisited. *Allergy* **73**, 993–1002 (2018).
 34. Gray, S. D., Alipour, F., Titze, I. R. & Hammond, T. H. Biomechanical and histologic observations of vocal fold fibrous proteins. *Ann. Otol. Rhinol. Laryngol.* **109**, 77–85 (2000).
 35. Prades, J. M. *et al.* Lamina propria of the human vocal fold: Histomorphometric study of collagen fibers. *Surg. Radiol. Anat.* **32**, 377–382 (2010).
 36. Catten, M., Gray, S. D., Hammond, T. H., Zhou, R. & Hammond, E. Analysis of cellular location and concentration in vocal fold lamina propria. *Otolaryngol. - Head Neck Surg.* **118**, 663–667 (1998).
 37. Chen, X. & Thibeault, S. L. Characteristics of Age-Related Changes in Cultured Human Vocal Fold Fibroblasts. *Laryngoscope* **118**, 1700–1704 (2008).
 38. Desmoulière, A. Factors influencing myofibroblast differentiation during wound healing and fibrosis. *Cell Biol. Int.* **19**, 471 (1995).
 39. Hahn, M. S., Kobler, J. B., Starcher, B. C., Zeitels, S. M. & Langer, R. Quantitative and

- Comparative Studies of the Vocal Fold Extracellular Matrix I: Elastic Fibers and Hyaluronic Acid. *Ann. Otol. Rhinol. Laryngol.* **115**, 156–164 (2006).
40. Chan, R. W., Gray, S. D. & Titze, I. R. The importance of hyaluronic acid in vocal fold biomechanics. *Otolaryngol. - Head Neck Surg.* **124**, 607–614 (2001).
 41. Zeitels, S. M. *et al.* Vocal Fold Injection of Absorbable Materials: A Histologic Analysis With Clinical Ramifications. *Ann. Otol. Rhinol. Laryngol.* **128**, 71S–81S (2019).
 42. Alipour, F. & Jaiswal, S. Phonatory characteristics of excised pig, sheep, and cow larynges. *J. Acoust. Soc. Am.* **123**, 4572–4581 (2008).
 43. Balls, M. Replacement of animal procedures: Alternatives in research, education and testing. *Lab. Anim.* **28**, 193–211 (1994).
 44. Russel, W. M. S. & Burch, R. L. The Principles of Humane Experimental Technique. *Med. J. Aust.* **1**, 500–500 (1960).
 45. Robinson, N. B. *et al.* The current state of animal models in research: A review. *Int. J. Surg.* **72**, 9–13 (2019).
 46. Caliari, S. R. & Burdick, J. A. A practical guide to hydrogels for cell culture. *Nat. Methods* **13**, 405–414 (2016).
 47. Greek, R. & Menache, A. Systematic Reviews of Animal Models: Methodology versus Epistemology. *Int. J. Med. Sci.* **10**, 206–221 (2013).
 48. Yamaguchi, T., Shin, T. & Sugihara, H. Reconstruction of the laryngeal mucosa. *Otolaryngol. - Head Neck Surg.* **122**, (1996).
 49. Baker, B. M. & Chen, C. S. Deconstructing the third dimension-how 3D culture microenvironments alter cellular cues. *J. Cell Sci.* **125**, 3015–3024 (2012).
 50. Cooper, M., Charest, J. L. & Coppeta, J. Design principles for dynamic microphysiological systems. in *Microfluidic Cell Culture Systems* 1–29 (Elsevier, 2019).
 51. Wikswo, J. P. *et al.* Scaling and systems biology for integrating multiple organs-on-a-chip. *Lab Chip* **13**, 3496–3511 (2013).
 52. Kieninger, J., Weltin, A., Flamm, H. & Urban, G. A. Microsensor systems for cell metabolism-from 2D culture to organ-on-chip. *Lab Chip* **18**, 1274–1291 (2018).
 53. Bhatia, S. N. & Ingber, D. E. Microfluidic organs-on-chips. *Nat. Biotechnol.* **32**, 760–772 (2014).
 54. Ingber, D. E. Human organs-on-chips for disease modelling, drug development and personalized medicine. *Nat. Rev. Genet.* **23**, 467–491 (2022).
 55. Jalili-Firoozinezhad, S., Miranda, C. C. & Cabral, J. M. S. Modeling the Human Body on Microfluidic Chips. *Trends Biotechnol.* **39**, 838–852 (2021).
 56. Anderson, J. O., Thundiyil, J. G. & Stolbach, A. Clearing the Air: A Review of the Effects of Particulate Matter Air Pollution on Human Health. *J. Med. Toxicol.* **8**, 166–175 (2012).
 57. World Health Organization. News Release - Billions of People Still Breathe Unhealthy Air: New WHO Data. *World Health Organization* (2022).
 58. World Health Organization. WHO | 2011 Database: outdoor air pollution in cities. http://www.who.int/phe/health_topics/outdoorair/databases/en/index.html (2012).
 59. WHO. Database: outdoor air pollution in cities. *World Health Organization web site* http://www.who.int/phe/health_topics/outdoorair/databases/cities-2011/en/ (2014).
 60. Pope, C. A. & Dockery, D. W. Health Effects of Fine Particulate Air Pollution: Lines that Connect. *J. Air Waste Manage. Assoc.* **56**, 709–742 (2006).
 61. Seaton, A., Godden, D., MacNee, W. & Donaldson, K. Particulate air pollution and acute health effects. *Lancet* **345**, 176–178 (1995).

62. Dockery, D. Acute Respiratory Effects of Particulate Air Pollution. *Annu. Rev. Public Health* **15**, 107–132 (1994).
63. Raaschou-Nielsen, O. *et al.* Air pollution and lung cancer incidence in 17 European cohorts: Prospective analyses from the European Study of Cohorts for Air Pollution Effects (ESCAPE). *Lancet Oncol.* **14**, 813–822 (2013).
64. Brunekreef, B. & Holgate, S. T. Air pollution and health. *Lancet* **360**, 1233–1242 (2002).
65. Suh, H. H., Bahadori, T., Vallarino, J. & Spengler, J. D. Criteria Air Pollutants and Toxic Air Pollutants. *Environ. Health Perspect.* **108**, 625–633 (2000).
66. Sataloff, R. T. The Impact of Pollution on the Voice. *Otolaryngol. - Head Neck Surg.* **106**, 701–705 (1992).
67. Igarashi, E. *Nanomedicines and nanoproducts: applications, disposition, and toxicology in the human body.* (CRC Press, Taylor & Francis Group, 2015).
68. Sivasankar, M., Erickson, E., Rosenblatt, M. & Branski, R. C. Hypertonic challenge to porcine vocal folds: Effects on epithelial barrier function. *Otolaryngol. - Head Neck Surg.* **142**, 79–84 (2010).
69. Shusterman, D. The Effects of Air Pollutants and Irritants on the Upper Airway. *Proc. Am. Thorac. Soc.* **8**, 101–105 (2011).
70. US Environmental Protection Agency. National Ambient Air Quality Standards. <https://www.epa.gov/criteria-air-pollutants/naaqs-table> (2021).
71. Burnett, R. *et al.* Global estimates of mortality associated with long-term exposure to outdoor fine particulate matter. *Proc. Natl. Acad. Sci.* **115**, 9592–9597 (2018).
72. Lelieveld, J. *et al.* Cardiovascular disease burden from ambient air pollution in Europe reassessed using novel hazard ratio functions. *Eur. Heart J.* **40**, 1590–1596 (2019).
73. Cho, C. C. *et al.* In vitro and in vivo experimental studies of PM_{2.5} on disease progression. *Int. J. Environ. Res. Public Health* **15**, 1–26 (2018).
74. Schraufnagel, D. E. The health effects of ultrafine particles. *Exp. Mol. Med.* **52**, 311–317 (2020).
75. Lee, D. C. *et al.* Urban particulate matter regulates tight junction proteins by inducing oxidative stress via the Akt signal pathway in human nasal epithelial cells. *Toxicol. Lett.* **333**, 33–41 (2020).
76. Won, H. *et al.* Effect of Urban Particulate Matter on Vocal Fold Fibrosis through the MAPK/NF- κ B Signaling Pathway. *Int. J. Environ. Res. Public Health* **21**, 6643 (2020).
77. Fujii, T., Hayashi, S., Hogg, J. C., Vincent, R. & Van Eeden, S. F. Particulate Matter Induces Cytokine Expression in Human Bronchial Epithelial Cells. *Am. J. Respir. Cell Mol. Biol.* **25**, 265–271 (2001).
78. Clark, A. R. The use of laser diffraction for the evaluation of the aerosol clouds generated by medical nebulizers. *Int. J. Pharm.* **115**, 69–78 (1995).
79. Thibeault, S. L., Rees, L., Pazmany, L. & Birchall, M. A. At the crossroads: mucosal immunology of the larynx. *Mucosal Immunol.* **2**, 122–128 (2009).
80. World Health Organization. Ambient (outdoor) air pollution. (2022).
81. Synvivo. SynALI 3D Lung Model Using Idealized Microvascular Network. *Technical protocol* www.synvivobio.com.
82. Park, S. & Young, E. W. K. E-FLOAT: Extractable Floating Liquid Gel-Based Organ-on-a-Chip for Airway Tissue Modeling under Airflow. *Adv. Mater. Technol.* **6**, 2100828 (2021).
83. Na, K., Lee, M., Shin, H.-W. & Chung, S. In vitro nasal mucosa gland-like structure

- formation on a chip. *Lab Chip* **17**, 1578–1584 (2017).
84. Zhang, M., Xu, C., Jiang, L. & Qin, J. A 3D human lung-on-a-chip model for nanotoxicity testing. *Toxicol. Res. (Camb)*. **7**, 1048–1060 (2018).
 85. Huh, D. *et al.* Microfabrication of human organs-on-chips. *Nat. Protoc.* **8**, 2135–2157 (2013).
 86. Singh, A. V. *et al.* Emerging Technologies for In Vitro Inhalation Toxicology. *Adv. Healthc. Mater.* **10**, 1–13 (2021).
 87. Fröhlich, E. *et al.* Comparison of two in vitro systems to assess cellular effects of nanoparticles-containing aerosols. *Toxicol. Vitro*. **27**, 409–417 (2013).
 88. Polk, W. W., Sharma, M., Sayes, C. M., Hotchkiss, J. A. & Clippinger, A. J. Aerosol generation and characterization of multi-walled carbon nanotubes exposed to cells cultured at the air-liquid interface. *Part. Fibre Toxicol.* **13**, 1–12 (2016).
 89. Lungova, V., Wendt, K. & Thibeault, S. L. Exposure to e-cigarette vapor extract induces vocal fold epithelial injury and triggers intense mucosal remodeling. *Dis. Model. Mech.* **15**, (2022).
 90. Raty, S. *et al.* Embryonic development in the mouse is enhanced via microchannel culture. *Lab Chip* **4**, 186–190 (2004).
 91. Azzi, S., Hebda, J. K. & Gavard, J. Vascular Permeability and Drug Delivery in Cancers. *Front. Oncol.* **3**, 1–14 (2013).
 92. Khalil, A. S., Jaenisch, R. & Mooney, D. J. Engineered tissues and strategies to overcome challenges in drug development. *Adv. Drug Deliv. Rev.* **158**, 116–139 (2020).
 93. Sato, K. Blood Vessels of the Larynx and Vocal Fold. in *Functional Histoanatomy of the Human Larynx* 287–303 (Springer Singapore, 2018).
 94. Wang, T. *et al.* Particulate matter air pollution disrupts endothelial cell barrier via calpain-mediated tight junction protein degradation. *Part. Fibre Toxicol.* **9**, 1–12 (2012).
 95. Deinhardt-Emmer, S. *et al.* SARS-CoV-2 Causes Severe Epithelial Inflammation and Barrier Dysfunction. *J. Virol.* **95**, (2021).
 96. Benam, K. H. *et al.* Small airway-on-a-chip enables analysis of human lung inflammation and drug responses in vitro. *Nat. Methods* **13**, 151–157 (2016).
 97. Deinhardt-Emmer, S. *et al.* Co-infection with *Staphylococcus aureus* after primary influenza virus infection leads to damage of the endothelium in a human alveolus-on-a-chip model. *Biofabrication* **12**, 025012 (2020).
 98. Si, L. *et al.* A human-airway-on-a-chip for the rapid identification of candidate antiviral therapeutics and prophylactics. *Nat. Biomed. Eng.* **5**, 815–829 (2021).
 99. Huh, D. *et al.* Reconstituting Organ-Level Lung Functions on a Chip. *Science (80-.)*. **328**, 1662–1669 (2010).
 100. Wilmer, M. J. *et al.* Kidney-on-a-Chip Technology for Drug-Induced Nephrotoxicity Screening. *Trends Biotechnol.* **34**, 156–170 (2016).
 101. Ronaldson-Bouchard, K. & Vunjak-Novakovic, G. Organs-on-a-Chip: A Fast Track for Engineered Human Tissues in Drug Development. *Cell Stem Cell* **22**, 310–324 (2018).
 102. Ramme, A. P. *et al.* Autologous induced pluripotent stem cell-derived four-organ-chip. *Futur. Sci. OA* **5**, (2019).
 103. Chang, S.-Y. *et al.* Human liver-kidney model elucidates the mechanisms of aristolochic acid nephrotoxicity. *JCI Insight* **2**, 1–14 (2017).

104. Choi, H. & Kim, C. S. Polycyclic Aromatic Hydrocarbons from Fine Particulate Matter Induce Oxidative Stress and the Inflammatory Response in Human Vocal Fold Fibroblast Cells. *Oxid. Med. Cell. Longev.* **2021**, 1–10 (2021).
105. Mizuta, M. *et al.* Expression of Reactive Oxygen Species during Wound Healing of Vocal Folds in a Rat Model. *SAGE*, **121**, 804–810 (2012).